Universität Augsburg
Institut für Geographie

The influence of proglacial lakes on climate and surface mass balance of retreating ice sheets: A study of the North American and Scandinavian ice sheets at 13 ka BP

Master Thesis

University of Augsburg
Chair of Physical Geography and Climate Science

Supervisors:
Prof. Dr. Wolfgang Buermann
Dr. Uta Krebs-Kanzow, Alfred Wegener Institute, Bremerhaven

Lianne Sijbrandij

Matrikel-Nr.: 1405860

Climate and Environmental Sciences, M.Sc.

Submitted: 14.03.2022

Abstract

This study investigates the effect of proglacial lakes in direct contact with large ice sheets on regional climate and surface mass balance (SMB). A novel subroutine was implemented for this purpose, enabling the atmospheric general circulation model ECHAM6 to incorporate proglacial lakes and their specific characteristics. Other lakes can still freely evolve according to a mixed layer scheme. As a first application the impact of proglacial lakes during the Allerød interstadial 13 ka BP (ka is thousand years before present) was studied for the Laurentide (LIS) and Fennoscandian (FIS) ice sheets. This was achieved using three atmosphere stand-alone experiments:

1. with 13 ka BP land surface boundary conditions (GLAC-1D, Ivanovic et al., 2016) and a modern lake configuration
2. same as (1) but with additional lakes around LIS and FIS
3. same as (2) but additional lakes are treated with to new proglacial lake approach.

All three simulations were evaluated with respect to the regional climate response, while ice sheet specific parameters like SMB were analysed using the diurnal Energy Balance Model (dEBM, Krebs-Kanzow et al., 2021). Even though the desired equilibrium state of the climate was not achieved during this study, the results still look promising and are indicating a considerable positive effect of proglacial lakes. Lake area seems to be primary factor in these changes, followed then by colder lake surface temperatures.

Contents

List of Figures

List of Tables

1 Introduction

The largest extent of areas covered in ice throughout the year was reached during the last glacial maximum (LGM), which was between 26 and 20 thousand years ago (Clark et al., 2009). Since then, climate has changed during various phases, causing the ice sheets to melt and the sea level to rise about 120m (Peltier and Fairbanks, 2006) to the current level. Many of the processes impacting this deglaciation are not yet fully comprehended. One of these is the exact role proglacial lakes play at altering regional climate and surface mass balance of retreating ice sheets.

In the framework of this study, paleoclimatological information was provided on the climatic drivers that played a role during the last deglaciation, specifically during the Allerød interstadial, which was a warm phase preceding the Younger Dryas where a dynamic re-advance of the ice-sheets happened. During this time period, conditions for the evolution of large proglacial lakes were highly favourable. Yet, proglacial lakes are not implemented in ECHAM6, a general atmospheric circulation model. During this study a realization of proglacial lakes (`plake`) has been developed and its functionality tested. All preparatory work and experiments are introduced and the final experiment design presented. The approach here is to investigate the effect of proglacial lakes by means of a sensitivity study with three scenarios:

1. `alakeGLAC`: a reference simulation with boundary conditions according to a 13 ka BP land surface reconstruction (GLAC-1D: Ivanovic et al., 2016) which only accounts for modern lakes configuration
2. `alake13ka`: same as `alakeGLAC` but with the addition of lakes along the Laurentide and Fennoscandian ice sheets
3. `plake`: same as `alake13ka` but with additional lakes marked and recognized as proglacial lakes, so that lake surface temperatures will be calculated by the new proglacial lake enabled version of ECHAM6.

While further studies must be conducted, most importantly with a prolonged run time as the results showed, this new implementation makes a thorough research concerning proglacial lakes and their climatic effects possible with ECHAM6.

2 Paleoclimatological background

Climate variability is the result of both dynamic processes and static change parameters. For proper understanding of the conducted studies in this thesis, the most important factors are summarized during the following sections. Furthermore, the basic concepts of proglacial lake dynamics need to be introduced and the choosing of the 13 thousand years before present (short: 13 ka BP) timeslice justified.

2.1 Climate variability

2.1.1 Forced (or external) variability

This section explains the influence of astronomical forcing, including variations of orbital parameters as well as solar luminosity changes, on Earth's climate.
The sun's shortwave radiative output according to Newman and Rood (1977) has increased at a rate of about 68 x 10^{-9} $W/m^2/y$. Derived from this comes the solar constant (S), which quantifies the energy flux normal to the outer limit of the planetary atmosphere (Saltzman, 2002). However, this 'constant' can also change on a smaller time scale, when so-called sunspots alter the sun's emitted energy, or when *solar winds* interact with the Earth's magnetic field (Saltzman, 2002).

Concerning this study, orbital variations are of higher significance. They often pose the starting point of changes on the scale of ice ages by modifying the energy budget or its distribution around this planet (Saltzman, 2002). Saltzman (2002) summarizes the following three perturbations extracted from several studies:

1. **Eccentricity (e)** describes the variations caused by interactions between Earth, Sun, Moon and other planets and basically tells, if the orbit has rather the shape of an ellipse or that of a circle. Pronounced phases seem to repeat at a rate of about 100 and 400 thousand years (ky).

$$e = \frac{\sqrt{r_1^2 - r_2^2}}{r_2} \tag{2.1}$$

with r_1 and r_2 being semi major and minor axes of the planet's orbit

2. **Obliquity**, ε, represents the angular tilt of the planet's axis in relation to its elliptic plane. Its dominant phase is split and varies approx. every 41 ky.

3. **Precession** is given as an index, (e sin Λ), with Λ being the longitude of perihelion measured from a fixed point along the orbit (called *vernal equinox*). Here, the dominant phase is also split, its periodicity ranges from 19 to 25 ky depending on the current eccentricity period.

These three have different impacts on the energy distribution around the planet, first quantified by Milankovic (Milanković, 1930, 1941). While the eccentricity varies between 0 and 0.7 and has an effect on the net annual solar radiation received, obliquity and precession modify seasonal contrasts. Obliquity varies between 22.1 and 24.5 degrees and increases summer and winter extremes one both hemispheres, whereas precession is mostly affecting the dates of perihelion (closest approach) and aphelion (furthest departure), thus increasing the seasonal contrast in one hemisphere and decreasing it in the other one (EarthObservatory, 2000). For better understanding, Fig. 2.1 shows a schematic drawing of the above mentioned processes. Because of the significance of Milankovic' work, these cycles of radiative variation are commonly referred to as "Milankovic cycles".

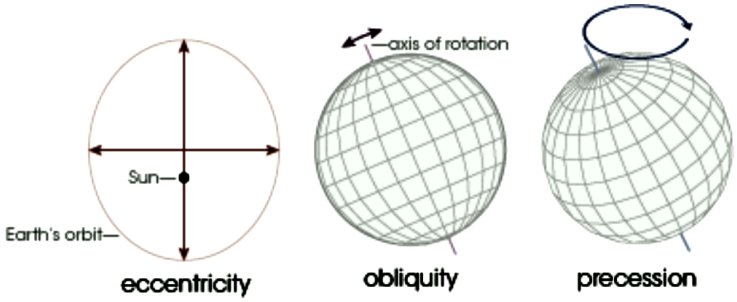

Figure 2.1: Orbital Parameters. Source: Riebeek and Simmon (2006).

Since this study focuses heavily on ice ages, the so-called *ice-age problem* will be shortly explained. Basically, this problem is about discrepancies concerning "the main variations

of planetary ice mass [not representing] a linear response to the known orbitally induced radiative forcing" (Saltzman, 2002). Regarding this, Saltzman (2002) emphasizes the role of non-steady rates of change for ice growth and decline. He points out that (considering studies of Berger and Loutre (1991), Berger et al. (1993) and Hays et al. (1976)) the orbital forcing is not enough to account for the whole spectrum of ice mass variation. Keeping this in mind, temperature variations have to be controlled by other processes, too. These processes, capable of amplifying changes started by astronomical forcing are the topic of the next section and should cast some light on this issue.

Astronomical forcing is counted as an external forcing as climate does not affect the Earth's orbit. Other climate independent forcings such as tectonics, geothermal heat or volcanic activity are neglected in this study.

2.1.2 Free (or internal) variability

Since the Earth has characteristics of a non-linear, non-equilibrium system, driving mechanisms can be found in both, externally forced, as well as internally free effects, which furthermore contain positive and negative feedbacks (Saltzman, 2002). In this context, some studies suggest that the relevance of internal forcing exceeds that of external, thus making it the main source of climate variations (e.g. Wunsch (2003)).

One of the most influential internal forcings is greenhouse gas (GHG) forcing. By modifying greenhouse gas concentrations (e.g. CO_2, CH_4, NO_x), the solar radiation reaching the Earth's surface can increase or decrease and through absorption the energy budget can be altered in the according layers of the atmosphere.

An interesting phenomenon, highlighting that not only GHGs have an effect on climate but also that climate has an impact on GHG concentrations can be found in the Deep Water's carbon storage. Yu et al. (2020) suggest, that an expansion of Pacific deep water in a cooler climate caused significant sequestering of atmospheric CO_2, adding another factor for reaching the last glacial maximum. During deglaciation Rae et al. (2014) point out, that if stratification of deep water breaks down it starts releasing carbon dioxide. This hypothesis was also shortly described by Skinner et al. (2010) among other factors like a changing ice sheet and wind forcing. Yet, several studies also point out that there

are large uncertainties concerning past ocean circulations and its interaction with the atmosphere, despite huge research interest.

Apart from the ocean, vegetation plays a significant role in altering climate parameters, too. Changes in vegetation can be followed by changes in albedo, as addressed in e.g. Thompson et al. (2009) but also release water vapour that become clouds as well as the fact, that large amounts of carbon can be storaged in forests. All of these factors are in constant motion and often influence each other directly or indirectly, which is why modelling and understanding the climate is such a complex task.

Another principal large scale effect is in regard to albedo. The amount of incoming solar radiation being reflected is changing with the extent of ice covered areas. When an ice sheet is retreating, it thus exposes more surface with lower albedo and amplifies warming which then again has a negative effect on the ice sheets. In this specific context the ice-albedo-feedback should be mentioned, too, which is a so-called positive feedback. This means it is self-reinforcing and therefore of destabilizing character, whereas negative feedbacks can have a stabilizing effect. The ice-albedo-feedback is (in short) the following process: A big (and maybe even growing) ice sheet has a higher surface albedo due to its 'whiter' appearance. If the ice sheet starts melting, dark substances accumulate on its surface, this favours the existence of melting pools or even supraglacial lakes. Albedo is then decreased, which means more insolation causing higher melting rates and even lower albedo.

Special significance during the last deglaciation is given to Dansgaard-Oeschger cycles (D/O) and Heinrich events (HE). D/O are dramatic changes in climate occurring in a $\pm$ 1500 year cycle, typically starting with abrupt warming in the Greenland and North Atlantic region by 5-10 K in only a few years or decades (Claussen et al., 2003; Dokken et al., 2013). These were in strong relation to ice sheet fluctuations and had a severe impact on their extent (Marshall and Koutnik, 2006). HE on the other hand occurred irregularly on an interval of $\pm$ 10 000 years (Claussen et al., 2003). Although they were highly relevant during this larger time period, they are not represented in this study. This is based on the fact that this is a pure sensitivity analysis with the conditions of a 13 ka BP time segment.

2.2 The Allerød interstadial

2.2.1 Placement in the geological era

The Allerød interstadial is part of the Bølling-Allerød-Oscillations (B/A) and is one of several warming phases that caused the ice sheet retreat from the LGM to today's levels. This section focuses on the chosen period of interest, which is 13 ka BP and embeds the events of that time into the deglaciation series (before and after) as well as giving a rough summary concerning the state of the Earth at that time. Furthermore, it addresses the problem of sometimes confusing time references and terminology surrounding the Allerød interstadial, Bølling/Allerød oscillations and Younger Dryas in literature (as addressed in Krueger and Damrath (2020)).

To start with, the B/A is part of the Phanerozoic (Eonothem), Cenozoic (Erathem), Quaternary (Period), Pleistocene (Series), lastly and most precisely the Upper Pleistocene (Stage). The Pleistocene in general is characterized by strong cooling of the atmosphere, its beginning can be pinned to several biological as well as geological indicators. The mollusk *Cyprina islandica* for example needs colder temperatures and appeared first in the Mediterranean around 1.6 million years ago. But, the geological boundary is set quite some time before, when the paleomagnetic period switched 2.3-2.4 million years ago (Kelletat, 2005). Not only was this period colder in general, it also displayed high climate variability, altering between warm and cold periods, the latter regularly becoming ice ages (Kelletat, 2005). It ends with gradual warming and a more steady climate towards the beginning of the Holocene.

The Upper Pleistocene stage includes roughly the years 126 ka BP to 11.7 ka (Cohen et al., 2013) and contains a series of D/O and HE that caused frequent changes in the climate system (Elliot et al., 2002; Lisiecki and Stern, 2016). These reoccurring climate fluctuations are commonly associated with episodes of reduced meridional heat transport in the Atlantic due to freshwater induced disruptions of NADW formation (Galbraith et al., 2016). Therein, the onset of the B/A is set at approx. 14.7-14.6 ka BP, when a strong warming trend was observed (Samartin et al., 2012; Yu and Eicher, 2004).

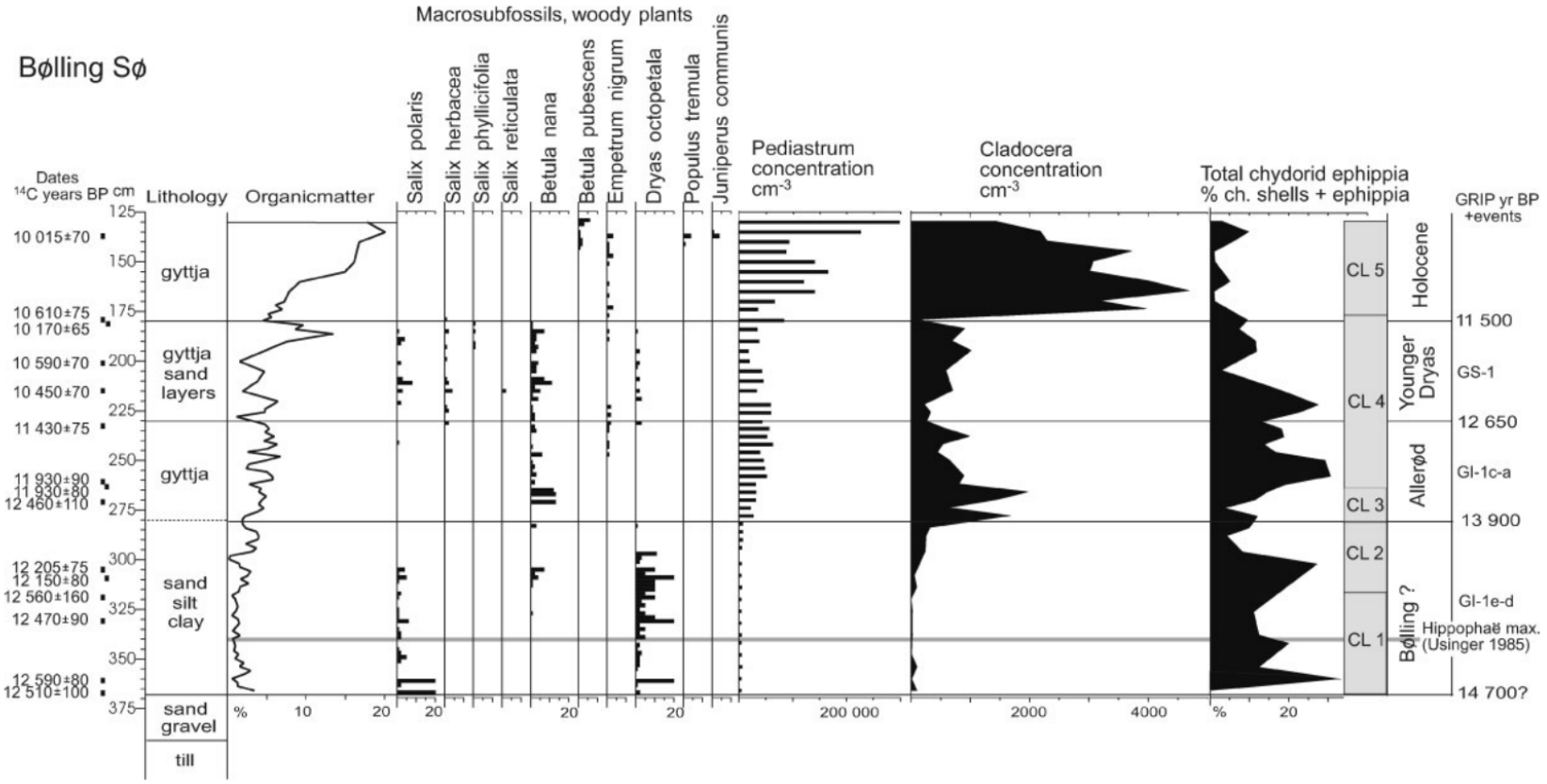

Figure 2.2: Summary diagram showing results of AMS dates, analyses of organic matter (LOI), macrofossils of woody plants and *Pediastrum* algal colonies from Bølling Sø, Denmark. Source: Bennike et al. (2004).

This onset can also be described as Termination 1a and the following period spanning 15 to 13 ka BP as the late-glacial interstadial (Lotter et al., 2012). The B/A oscillations started with the Bølling interstadial, which was followed (at least in some references, e.g. Andersen and Borns (1994); Mangerud et al. (1974)) by the Older Dryas - a shorter cold stage -, which in turn was followed by the Allerød interstadial. The Younger Dryas then marks the end of the Pleistocene, subsequently followed by the Preboreal introducing the beginning of the Holocene.

2.2.2 On the subject of time

As a response to the above mentioned ambiguities, Mangerud et al. (1974) tried to establish a more consistent definition of boundaries in conventional radiocarbon years BP. Although this provisional chronostratigraphic subdivision has not completely prevailed in the majority of literature, it still serves as a good overview. In table 2.1 the subdivision by Mangerud et al. (1974) is compared to the Greenland events by Björck et al. (1998). While Mangerud et al. (1974) state the time periods as Radiocarbon years BP, Björck et al. (1998) concentrate on GRIP (meaning *Greenland Ice Core Project*) ice-core years BP. The important thing to mention here is that for these dates to be comparable, 14C years need to be converted to calendar years (the latter often indicated by the *cal.*, e.g. in 12 000 cal. yr BP).

subdivision	Mangerud (1974)	Greenland Events	Björck (1998)
Preboreal	10 000	Gl-1a	12 900
Younger Dryas	11 000	Gl-1b	13 150
Allerød	11 800	Gl-1c	13 900
Older Dryas	12 000	Gl-1d	14 050
Bølling	13 000	Gl-1e	14 700

Table 2.1: Comparison of method-dependent dates and subdivisions using two examples: Mangerud (1974) and Björck (1998).

Looking at Fairbanks et al. (2005), their calibration curve for calendar and 14C years, shows that 13 ka BP corresponds to roughly 11 ka BP (respectively). For the rest of this study whenever a time is given without further specification, it can be assumed that regular calendar years are meant. A very nice overview concerning the division throughout the period of approx. 10 to 15 ka BP is given in Fig. 2.2.

2.2.3 Key drivers in the climate of Bølling-Allerød

Several climatic processes had been discussed in for the B/A the past. One of the events starting the Bølling-Allerød warm interval seems to have been the Meltwater Pulse 1A (mwp-1a) from Antarctica, which occurred at ± 14.6 ka BP and led to a global sea level rise of about 20 m in less than 500 years (Weaver et al., 2003). When the drastic warming during that time could not be connected to melt water coming only from the Laurentide (LIS) or Fennoscandian (FIS) ice sheets, as was speculated before (Fairbanks, 1989), Weaver et al. (2003) showed that Antarctic' meltwater caused the North Atlantic Deep Water (NADW) formation to increase, thus warming the North Atlantic region. So, while freshwater input from North America or Europe should have led to a reduction of the thermohaline circulation (i.e. the opposite of observations), it was proposed that when the Southern Ocean is warming, there is an increased mass transport (with higher salinity) originating from the Pacific and Indian Ocean, in turn leading to a strengthening of the Atlantic thermohaline circulation (Knorr and Lohmann, 2003). Nevertheless, there are still some doubts if this event preceded or lagged the onset of the B/A (Carlson et al., 2012), and how big the contribution of the specific ice sheets of that time was. A more recent study by Brendryen et al. (2020) e.g. found that the Eurasian Ice Sheet might have contributed up to half of the mwp-1a.

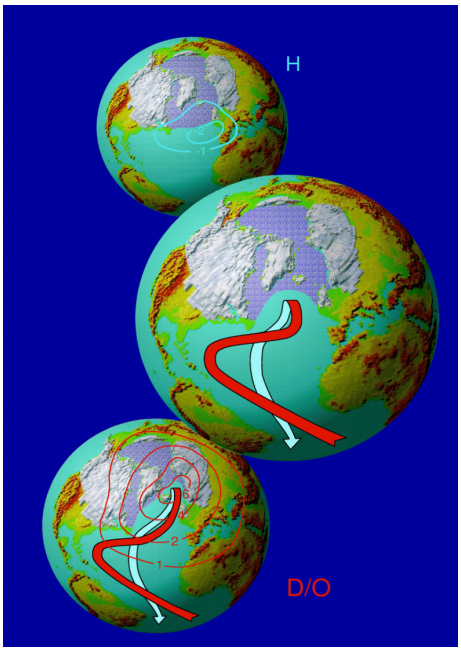

Figure 2.3: Modes of the thermohaline ocean circulation. Upper: *off* mode during HE, center: cold mode, lower: warm mode during D/O. Source: Rahmstorf (2006).

Generally, there are two modes of thermohaline circulation (hereafter THC) - one where NADW is formed ('on') and one without NADW formation ('off'). These modes usually occur with different events/circumstances, the *off* mode mostly coinciding with Heinrich-Events (Paillard and Labeyriet, 1994), stopping the THC due to freshwater input. This

is followed by a rapid restart of the circulation (*on* mode) while freshwater influx to the Northern Atlantic is heavily reduced, thus causing advection of heat from the tropics to increase (Bond et al., 1993). To complete the picture, the *on* mode can be separated into *cold* and *warm* state, the difference being the site of deep water formation (South of Iceland in the Irminger Sea or North of Iceland in the Greenland Sea, respectively) (Rahmstorf, 2006). The three modes of THC are visualized in Fig. 2.3, the red and blue lines indicating temperature anomalies.

2.3 Lake and Glacier Dynamics

2.3.1 Characteristics of proglacial lakes

Proglacial lakes are lakes that are either in direct contact with an ice sheet or indirectly connected to them via melt water fluxes. The term can also be used for lakes which have formed historically under these conditions but still exist today. However, this study focuses exclusively on the first type (i.e. marginal lakes, being lakes in direct contact with an ice sheet). Assumptions made here are thus not always transferable to any other proglacial lake.

Surface temperatures of proglacial lakes (PL) are low due to constant melt water input and glacial calving, which describes loss of ice mass into the lake in form of ice bergs. More specifically, it can be assumed that PL temperatures never exceed +4 °C. This is due to the fact that the lake's surface water, if heated up to this value, reaches its point of highest density and then sinks to the bottom of the lake where it is mixed with cool melt water again (Andersen and Borns, 1994; Vincent et al., 2010). At the same time, PL can act as powerful archives for palaeo-environmental information through sedimentation processes that show patterns of glacier-derived meltwater fluctuation (Carrivick and Tweed, 2013). Proglacial lakes can be of diverse origins. Sometimes they emerge when glaciers are retreating and melt water is caught between the ice sheet and moraines (*moraine-dammed*), other times due to a rise in bedrock topography (*bedrock-dammed*). Two other ways for proglacial lakes to evolve are when the ice sheet itself or a landslide cuts off the drain (*ice-dammed* or *landslide-dammed* respectively) (Fig. 2.4). While proglacial lakes can be

formed by one particular of these processes, it is also possible for them to be caused by a combination, or, for the main cause (i.e. dam type) to change through time (Carrivick and Tweed, 2013). Depending on the stability of its structure, the expansion of those lakes over time can result in large glacial lake outburst floods (GLOFs) (Carrivick and Tweed, 2013). These are - along with volcanically triggered floods and subglacial lakes - counted among the three types of sources for jökulhlaups (also called *glacier outburst floods*) (Björnsson, 2000)). In this context, it is important, not to confuse the terms *glacial lake outburst flood* and *glacier outburst flood*. Jökulhlhaups are generally characterised by "sudden-onset discharges that are far higher than those generated by snowmelt or rainfall in glacier systems", according to Tweed and Carrivick (2015). Through these events, the morphology of the surrounding area can be changed rapidly and severely, transporting high volumes of sediment and causing erosion along the way (Tweed and Carrivick, 2015). However, it is also possible for lakes to separate from the ice mass and outlast their former neighbour (Krivonogov et al., 2005; Pasquini et al., 2008)), as has been the case at the Great Lakes in North America.

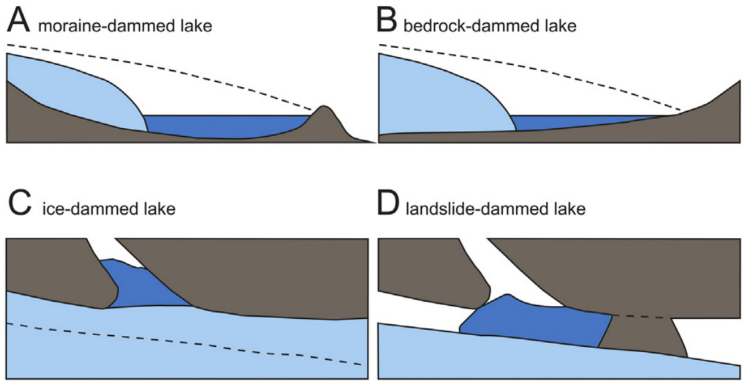

Figure 2.4: Proglacial lake evolution in response to ice advance and retreat, where dashed line indicates a precious ice margin or slope margin in part D. Note that part A and B are in longitudinal view, and parts C and D are in plan view. Source: Carrivick and Tweed (2013).

2.3.2 Dynamics between proglacial lakes and ice sheets

Depending on the exact processes (which in general are not yet completely understood), the following dynamics can cause either rapid disintegration or glacier advance.

Generally, lake water beneath an ice sheet is causing higher tension, supporting fracture and thus turning the ice sheet into an unstable system (Tweed and Carrivick, 2015). If a glacier is shrinking it will at some point reach its over-deepened glacier basin. This in turn supports higher calving rates whereby proglacial lakes can grow, causing more calving and shrinking of the ice sheet (Carrivick and Tweed, 2013; Tweed and Carrivick, 2015). One more important (positive) feedback is the *elevation feedback*, which increases melting of the glacier due to the lowering of the glacier's surface (Raymond et al., 2005). Krinner et al. (2004) states, that large proglacial lakes play a role in cooling regional summer climate. The strength of this effect will be investigated in one of the following pre-experiments. Furthermore, rainfall patterns are altered by mesoscale atmospheric feedbacks, e.g. moisture and snowfall are decreased, though this effect doesn't seem to outweigh the reduced melting during regional summer (e.g. in case of the Barents-Kara ice sheet 90 ka BP) (Krinner et al., 2004).
Water depth at glacier margins is influenced by three factors:

- "distance 'up-ice' that water propagates;
- vertical extension of a glacier's basal hydrological system via basal water pressure;
- ice calving rates" (Tweed and Carrivick, 2015),

accelerating the ice velocity and thus glacier mass loss. Another effect contributing to the reduction of glacial ice is thermally induced melting through the adjacent lake leading to higher calving rates by thermal undercutting (Tweed and Carrivick, 2015).

On a bigger scale, the drainage of ice-dammed lakes in the higher latitudes triggered disturbances of the North Atlantic circulation, e.g. in case of the Baltic Ice Lake at around 11 550 a BP (Andrén et al., 2002), or at Lake Agassiz ± 13 000 a BP (Murton and Murton, 2012). As emphasized by several studies (Carrivick and Tweed, 2013; Mangerud et al., 2004; Murton and Murton, 2012; Teller, 2001), proglacial lakes in general played an im-

portant role during the Quaternary (de)glaciation. According to Patton et al. (2017), two major proglacial lakes of the European region (today's Baltic and White sea) regularly flooded into the Northern Atlantic during B/A. Such processes were of particular importance in the North American region, where e.g. another abrupt drainage of Lake Agassiz at ± 8.2 ka BP led to a mean temperature drop of 5 °C for about 200 years (Clarke et al., 2003). Events like these heavily altered salt concentrations in the Northern Atlantic and thus caused the thermohaline circulation to weaken (Clark et al., 2002), in turn enabling ice sheet growth as was found for the Younger Dryas cold period (Patton et al., 2017).
Since there are still ice sheets and glaciers which can cause either the development or the drainage of proglacial lakes, this topic is also of high interest today. There are several studies stating the importance of glaciers and proglacial lakes for freshwater supply a long way downstream (Glas et al., 2018; Kaltenborn et al., 2010), as well as for agriculture, hydropower generation, recreation and industry (Huss et al., 2017; Bolch et al., 2021; Nabi et al., 2019). On the other hand, glacier lake outbursts can have devastating impact.

3 Methodology

3.1 ECHAM6: Model description and default settings

3.1.1 General information

ECHAM6 is an atmospheric general circulation model (AGCM) developed by the Max-Planck-Institute for Meteorology in Hamburg. Calculations take place for 47 vertical levels, 96 Gaussian latitudes and 192 maximum points on each latitude line, called the T63-truncation (Giorgetta et al., 2013). The following information on ECHAM6 is, if not stated otherwise, extracted from Stevens et al. (2013). Vertical levels are defined by so-called half levels, where pressure is graded vertically depending on temperature and can be seen in Fig. 3.1.

Potential and kinetic energy is conserved throughout every box transition, while conservation of mass unfortunately cannot always be guaranteed due to different treatments of transport for surface pressure and temperature. In the horizontal, diffusion is needed for the model to run stable.

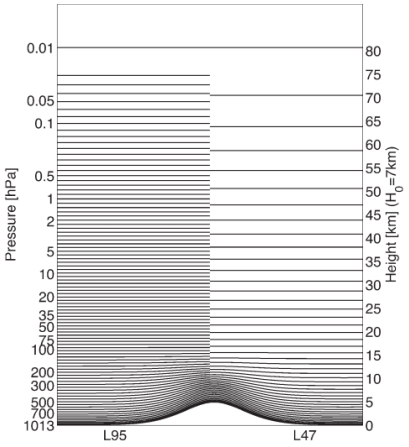

Figure 3.1: L47 and L95 hybrid vertical coordinates in ECHAM6 for the case of a 500 hPa surface pressure variation (e.g. at a large mountain). Source: Stevens et al. (2013).

Generally, the model has a dry spectral-transform dynamical core, which is the part of the code that describes model dynamics. Those include large-scale dynamics, movement of air and heat as well as thermodynamics, based on Newton's second law Brunke (2011). This dynamic core uses vorticity and divergence form of equations, while thermodynamic coordinates consist of temperature and surface pressure. Concerning the boundary layer turbulent mixing is implemented according to the eddy diffusivity/viscosity approach, where eddy viscosity is the product of a velocity and length scale and the

boundary layer is limited at 150 m.

The output is afterwards provided in monthly resolution, including 141 variables in 1D, 3D and 4D. Equilibrium climate sensitivity is only given for the T63L95 resolution as between 2.9 and 3.4 K and stated as "somewhat larger for the 47 level model" (Stevens et al., 2013, page 167).

In case of this study, the atmosphere model was coupled with JSBACH3.2, the land component of the MPI-M. This name is the short form for Jena Scheme for Biosphere-Atmosphere Coupling in Hamburg. JSBACH was originally part of ECHAM5 and was then separated to include all land processes, it is accessed each time step through a subroutine. Some characteristics have been changed since then, e.g. the concept of bucket hydrology towards a diffusive transport model for soil water and the description of LAI and albedo by state dependent models (Reick et al., 2021). This model is primarily used to enhance understanding of the coupled climate-carbon dynamics, including processes like the absorption of solar radiation in vegetation canopies, leaf photosynthesis, allocation and turnover of carbon in vegetation and soils. While it can be also used to study anthropogenic forces on nature and climate thoroughly, in this study JSBACH3.2 output was not analyzed in further detail, but only relevant variables were modified to fit the study. Diversity per grid point is implemented by providing a sub-structure which contains information on diversity of land cover types. All of the information on JSBACH3.2 can be found in the documentation released recently by Reick et al. (2021).

3.1.2 General setup procedure

For a better understanding of the main part in this thesis, the workflow related to setting up numerical models shall be described. As a starter, the following list gives an impression and shows the usual procedure when preparing simulations. Steps mentioned here will be described in more detail below the list.

1. Compile model
2. Prepare input
3. Adjust runscript
4. Submit runscript
5. (Optional) Bug fixing
6. Analyze the outdata

To set up a simulation, the model code first has to be compiled to make sure the right version is used.

Modified boundary conditions can be implemented via several input files, the ones most relevant in this study being `jansurf` (the ECHAM6 input file) and `jsbach` (the JSBACH3.2 input file). With these, surface parameters are prescribed to the model, which makes them also highly important if simulations should be run for earlier time periods, where topography, forest cover, lake configuration and other parameters might be quite different. This of course is also the case for this study, where 13 ka BP surface information was needed for the setup.

The runscript specifies all the settings you need for running your specific simulation. Here, basic information like compute time, location of the boundary conditions, model directory, run directory, experiment name and namelist parameters (see below) are entered. The run time setting usually considers the spin up period, which is in easier words the time the model needs to adjust to new settings and builds up the experiment. Additionally, more complex settings, e.g. if a restart is used (then adding a restart directory), how many processing nodes should be used for parallel computing and namelist changes can be modified to your need. If compiled successfully, the model needs to access the namelist.echam, where settings can be adjusted, without having to access and recompile the model code. It contains radiation control settings (described in more detail below), prescribes output format, controls submodules as well as many other parameters. To ensure that the runscript contains all experiment specific information, these namelist parameters are also modified via an interface within the runscript (recommended procedure). Lastly, the runscript is also the place where settings are adjusted if coupled simulations are done, e.g. coupling ECHAM6 with FESOM, a high resolution ocean model. In summary, if all input files are located as specified, the runscript should enable any user to rerun or continue the experiment.

When all this is done, the runscript can be submitted with a single line command to the job queue of the computing envionment, for the experiments here this was the CRAY CS400, internally called "Ollie" (regarding this naming: originally there was also a machine called Stan, which had a smarter architecture but was not so big with respect to its computing power). After some waiting time in the queue, the runscript will be executed

and (if everything is perfect) the experiment will enter a loop: run for a certain timeperiod, produce output- and restart files and after that will be resubmitted to the queue, wait and then restart again-this time starting from the last restart file which was produced. This processing ends when the specified simulation years in the run time settings are covered. ECHAM6 stand-alone runs (for clarification: JSBACH3.2 is used nevertheless) usually take about 20 minutes for one simulated year. Due to waiting times in the queue it is typically possible to simulate about 50 years per day on Ollie, but this also strongly depends on the workload in the job queue.
Initially experiments are submitted only for one or two model years, as usually some problems will appear. If bug fixing is needed, a look into the log file pays out most of the times. Here, the settings for the namelist, submodules, used model versions as well as error messages can be found. Typically problems are caused by bugs in the (modified) ECHAM code, wrong path names or inconsistent boundary conditions.
Afterwards, the output has to be processed and converted to netCDF for further investigations. Specific changes to these "tools" are referred to for each simulation that follows. Still, to avoid a too technical description, the focus is laid on the main modifications.

3.1.3 Specific default settings for the model version used

In this study, simulations were run on Ollie (the supercomputer at Alfred Wegener Institute in Bremerhaven) on 24x24 nodes. The overall model version used for all of the simulation is called `echam-6.3.05p2-concurrent_radiation-paleodyn`. The concurrent radiation part was described by Heidari et al. (2021) and a specification was added for paleoclimate studies with stable oxygen isotopes and dynamic ice sheets (GitLab: Gierz, 2022). Radiation per default is controlled by the settings listed in Tab. 3.1. Where "`iaero = 3`" refers to the aerosol climatology compiled by Kinne et al. (2013), "`io3 = 4`" means that climatological O_3 volume mixing rations provided by the IPCC are used for radiation calculation, "`isolrad = 6`" controls the choice of solar constant (CMIP6 pre-industrial), "`ich4 = 3`" tells that in the troposphere a volume mixing ratio `ch4vmr` with a decay in the layers above the troposphere is used in the radiation computation, the same is said for the volume mixing ratio `n2ovmr` by "`in2o = 3`". CO_2, CH_4 and N_2O volume mixing ratios are given by `co2vmr`, `ch4vmr` and `n2ovmr` respectively. This volume mixing ratio

describes the amount of molecules of a specific gas in relation to the total gas molecule count. Lastly, `yr_perp` describes the perpetual year for the orbit, while `lrad_async = .false.` forces the model to call the synchronous radiation scheme. The meaning to most of the parameters above is explained in more detail by Rast et al. (2013). For the later simulations, some of these had to be adjusted to the 13 ka BP time slice and will be mentioned in due time.

parameter	value	parameter	value
iaero	3	co2vmr	284.3169860840e-06
io3	4	ch4vmr	808.2490234375e-09
isolrad	6	n2ovmr	273.0210571289e-09
ich4	3	yr_perp	1850
in2o	3	lrad_async	.false.

Table 3.1: `radctl`-settings for running a preindustrial simulation with ECHAM6.

These settings, as well as the following can all be modified in the namelist. Resolution is set at T63 (subsection 3.1.1) and a short one-year test run was executed using the `PI-CTRL` (pi control) scenario and a submodule called `use_dynveg`, which is a module that supports dynamic evolution of vegetation patterns.

3.2 Boundary Conditions

3.2.1 Test run: Great Lake simulation in PI settings

The goal of this test run was to get familiar with the handling of new boundary conditions in ECHAM6 and to get a general idea of how the model works. In order to achieve this, a new big lake (in the following called *Great Lake*, extending from 60-85 °N and 45-60 °E), should be introduced to the middle of Eurasia. To begin with, the steps listed in subsection 3.1.2 will be shown for this simulation.

1. **Compile model**: A pre-industrial (PI) setup for ECHAM6 is used without any code changes.

2. **Prepare input**: The goal was the introduction of a new lake, so the boundary conditions had to be changed. In ECHAM6, a lake surface is recognized by a combination of the lake mask being ≥ 0.5, the sea land mask being 0 and sea land fraction being ≤ 0.5 in one grid cell. So in this case, it was necessary to set the values of *lake* (lake mask) to 1 and the values of *slm* (land sea mask) and *slf* (fractional land sea mask) to 0 in the selected box using CDOs (Schulzweida, 2021). This was done for the JSBACH input file as well as for the ECHAM6 input file respectively adjusting *ALAKE*, *SLF* and *SLM*.

3. **Adjust runscript:** Run time was set to 20 years, the input sources were added (short: the newly created `jansurf` and `jsbach` files). Only changes to the namelist were made to `default_output` as a reaction to a bug. Again, `use_dynveg` was set to `True`, so that vegetation is allowed to change throughout time.

4. **Submit runscript**: Runscripts are submitted using the ESM-Tools described in Andrés-Martínez et al. (2020)

5. **Optional Bug fixing**: The simulation was stopped repeatedly in February, until the `default_output` was switched off in the namelist.

6. **Analyze the outdata**: This was again done using CDOs (Schulzweida, 2021), as in all following experiments

This experiment was deliberately executed in a reliably working Pre-industrial control run and not yet with the later aimed 13 ka BP boundary conditions, risking unnecessary problems. The results shown in Fig. 3.2 depict May as well as November multi-year monthly mean (also: *ymonmean*) anomaly towards the reference simulation without this new lake.

Results of Great Lake experiment. The results quite accurately reflect the expected behaviour and are taken as confirmation of a successful implementation of this new water body to the model. While late spring temperatures are widely decreased due to the higher specific heat capacity (c_p) of water compared to land mass, late autumn temperatures

show clear warming over wide parts. May and November were chosen, because changes were most prominent during these months.

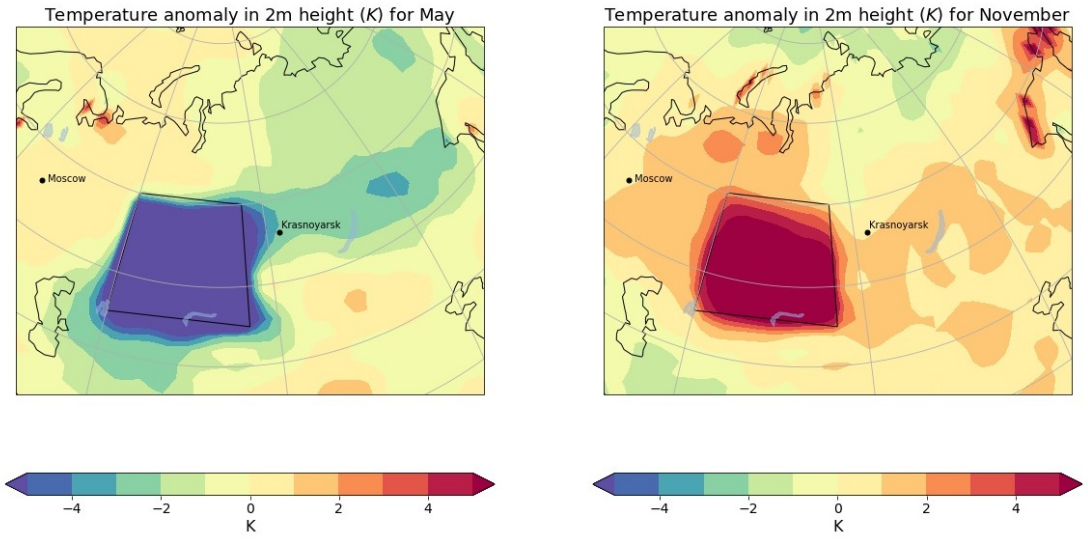

Figure 3.2: Multi-year monthly mean temperature anomaly in 2m height, box indicates location and size of GL.

When looking at the mean 2m temperature (*temp2*) anomaly of roughly the extent shown in Fig. 3.2, a warming signal between 0.2 and 1.1 °C is detected for the months October to January, while the rest consistently shows cooling between -0.2 and -2.59 °C (June). Concentrating at the surface temperatures of the lake (*tsw*), they are low during the whole simulation, staying at 0 °C as long as the lake is frozen. During this time, temperature above the ice is calculated, while the water temperature stays at 273.104 K. The averaged annual temperature range is about 16 °C, which seems reasonable. To further evaluate the quality of the model's output, *surface albedo* was inspected. It showed that high values were reached during boreal winter due to freezing of the lake. This starts at the northeastern boundaries and progresses towards the southeastern tip, while the lake is completely free of ice during most of July to November. The melting of the ice, saved in the variable *ahfres* [(W/m^2], shows the same pattern of melting throughout one year. Large scale precipitation (*aprl*) anomalies are negative during January to May and become positive during the rest of the year. The 2m relative humidity (*rh2m*) difference shows positive values most of the year, with highest values occurring in September, around the

time when also lake surface temperatures are highest. As a conclusion, ECHAM6 seemed to be properly set up for the further experiments.

The Boundary Conditions Generator. To test the compatibility with ECHAM6, the previous experiment was re-arranged using output masks from the *boundary conditions generator* (BCG, a tool to modify the default boundary conditions according to land surface reconstruction), which ultimately should also be used for the final simulation setups. Taking up the described steps again, this list shows what has been done:

1. **Compile model**: Same as above
2. **Prepare input**: This time, only the `jansurf`-input file used before was fed to the BCG and two new input files were received.
3. **Adjust runscript**: Same as above, but with input files out of the BCG
4. **Submit runscript**: Same as above
5. **(Optional) Bug fixing**
6. **Analyze the outdata**: Same as above

The BGC operates by taking manually modified input files and calculating all other variables over again, thus produces inherently consistent boundary conditions. In this case, major differences between those two input files are in the variables *alb* (albedo), *az0* (surface roughness length), *forest* (vegetation type), *orothe* (orographic angle), *sn* (snow depth), *wsmx* (field capacity of soil), *ws* (soil wetness) and in *FAO* (FAO data set). The adapted *jsbach*-file from the BCG changed accordingly and showed similar differences in albedo, vegetation cover, snow as well as extended modifications in leaf area index and mainly soil parameters (e.g. saturated hydraulic conductivity, maximum soil water capacity and heat capacity of dry soil).
Using this strategy it is also ensured more easily, that the JSBACH3.2 and ECHAM6 input files do not interfere with each other. In summary, all these changes were made in order to ensure that boundary conditions for the land surface and vegetation remain consistent after implementation of the Great Lake. Fig. 3.3 shows the multi-year monthly

mean temperature difference in 2m height (*temp2)*, positive values suggest that the results of the BCG-input files are higher than the ones from the manually modified input files, while negative values imply decreased temperatures.

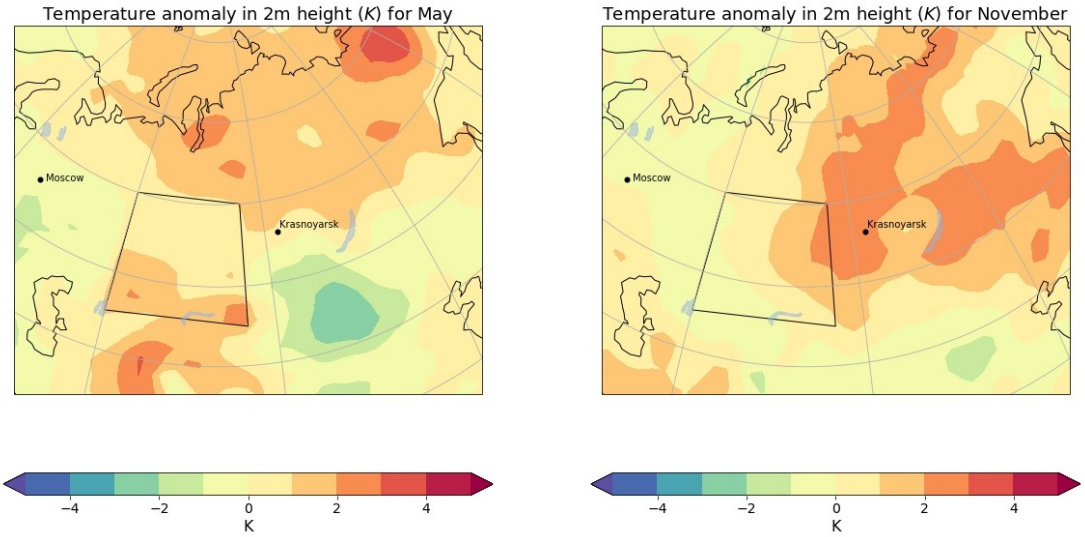

Figure 3.3: Multi-year monthly mean temperature anomaly in 2m height, box indicates location and size of GL. BGC values are subtracted from first experiment.

As can be seen, rather high differences have resulted from the new input files. Since the BCG adjusted all the other parameters accordingly, it can be assumed, that these results are of higher quality, which is why the BCG was in fact used for all following simulations. Another main advantage is a more ”harmonious” calculation of the variables, so that some errors occurring when modified manually can be easily avoided. Based on the knowledge attained during this chapter, the variables that needed to be changed could be identified. This helped to create the proglacial lake mask for the final simulations, as described in subsection 3.2.2.

3.2.2 Creating a proglacial lake mask *plake* for 13 ka BP

One of the major goals was to obtain a realistic proglacial lake mask. To select the suitable regions for this approach, the GLAC-1D reconstruction for topography and ice cover was used. Meters above sea level are abbreviated by *masl*. This reconstruction contains information about GLAC contemporary elevation [*masl*] (*HDC*), GLAC contemporary el-

evation [*masl*]: bathymetry for floating ice (*HDCB*) and the GLAC ice mask [fraction] (*ICEM*) for a time period reaching back 122 thousand years with 100 years resolution. The Eurasian and North American parts of the GLAC-1D reconstruction are taken from Tarasov et al. (2012), whereas the Greenland part has been developed in Tarasov and Peltier (2002). As described by Ivanovic et al. (2016), these components employ dynamical ice sheet models that have been constrained with relative sea-level data. Furthermore, geologically inferred deglacial ice margin chronologies, proglacial lake levels, ice-core temperature profiles, present-day vertical velocities, past ice thickness and present-day ice configuration were taken into account (Ivanovic et al., 2016) and used to derive a more realistic representation of past surface conditions. Since the single parts of GLAC-1D focus on different locations (Antarctica, Eurasia, North America, Greenland), they had to be combined under glacial isostatic adjustment (GIA) post-processing using the gravitationally self-consistent theory after Peltier (1998). Lastly, it should be mentioned that "GLAC-1D [is] subject to as yet unquantified uncertainties, such as the impact of lateral inhomogeneity in the viscous structure of the Earth" (Ivanovic et al., 2016, page 2574). The areas of interest were extracted from the existing GLAC-1D dataset, supporting a better view on the evolution of ice sheets and topography. This selection aimed at North America for the inspection of the Laurentide ice sheet as well as Europe for the inspection of the Fennoscandian ice sheet. The dataset was then cropped to a selected relevant time period, including 16 ka BP to 10 ka BP and thoroughly studied to find the best time slice for the introduction of proglacial lakes. This time slice was conveniently found to be at 13 ka BP, when ice sheets were retreating during the Allerød interstadial but also before the dynamic re-advance at 12.9 ka BP (Patton et al., 2017), thus posing best conditions for the production of proglacial lakes. Hence, analyzing the GLAC-1D reconstructions led to choosing the time period described in detail in section 2.2.

Out of the GLAC-1D reconstruction, PISM-lakeCC simulations were performed by Hinck et al. (2020) to get potential locations of (proglacial) lakes for several time steps during the last deglaciation. The results of this study for 13 ka BP were then used to choose some of the lakes as proglacial lakes, including the Baltic Ice Lake in Europe, as well as Lake Agassiz, and the predecessors of the Great Lakes, Great Slave Lake and Great Bear

Lake in northern America. The base for this can be seen in 3.4, where possible lake basins identified by the lakeCC tool are shown. The ice mask was then used to manually choose the lakes that are in direct contact with ice sheets.

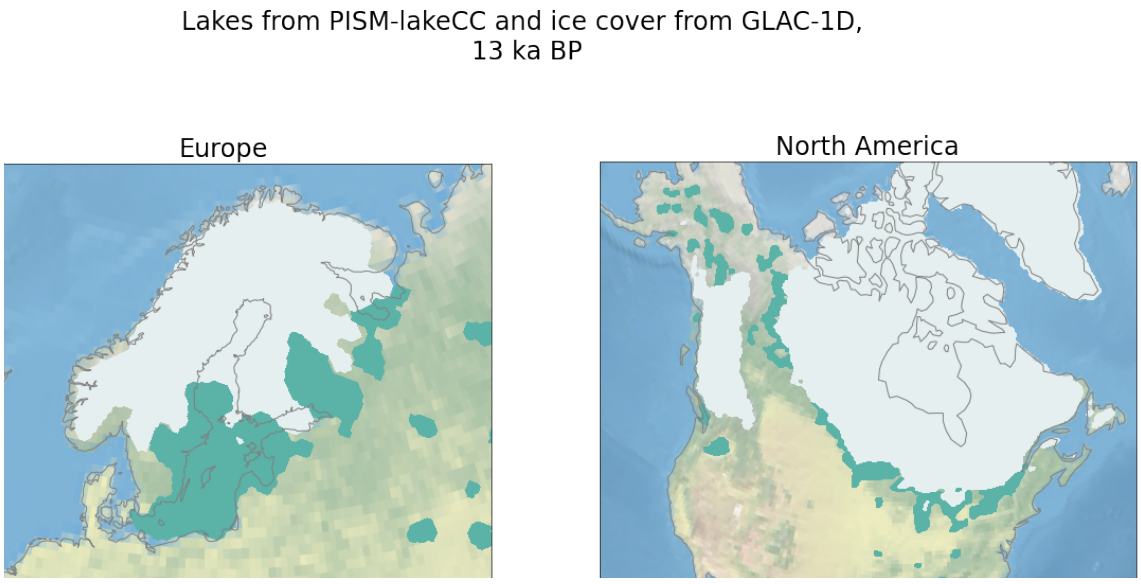

Figure 3.4: The origin for the choice of lakes in this study, derived from lakeCC output. Green areas are possible lake basins for the selected time period, white is ice cover. Source: data from Hinck et al. (2020).

The extracted plake mask had to be remapped bilinearly to fit the T63 grid of the input `jansurf`-file and to represent the structure of the original data best. After the remap, *ALAKE* as well as *SLM* and *SLF* were adjusted before submitting them to the BCG. Here, some lake area was lost, when 15 ka BP ocean boundary conditions were added, since there is a tool embedded which prevents lakes from forming in coastal areas (personal communication, Dr. Uta Krebs-Kanzow 16.11.2021). However, this loss was accepted, since the lakeCC tool tends to overestimate lake formation when applied to Lev Tarasov's reconstruction (personal communication, Dr. Sebastian Hinck 27.07.2021). The final boundary conditions can be seen in section 3.5.

3.3 Model Physics: Modifying lake temperature calculation

3.3.1 An introduction to surface temperature calculation over water in ECHAM6

For the next part, the assumption was made that the mixed layer temperature of proglacial lakes in reality never exceeds 4 °C due to constant melt water input and glacial calving, as explained in section 2.3. This temperature threshold was chosen based on several studies concerning behaviour and characteristics of ice-dammed and proglacial lakes (Carrivick et al., 2017; Richards et al., 2012; Vincent et al., 2010). Since ECHAM6 itself does not account for glacial calving or melt water input, a special subroutine is needed so that lake surface temperatures do not overstep the 4 °C limit.

The following section along with the before mentioned introduction of the new input variable to ECHAM6 were the main part of this study. Thus, this thesis makes its own contribution to the technical development of ECHAM6 by adding a novel calculation for proglacial lake related characteristics. In contrast to the version missing the *plake* section, this should lead to a better understanding of the influence they have on climate and surface mass balance of retreating ice sheets. A detailed description of what has been changed for the calculation of (proglacial) lakes follows.

In ECHAM6, surface temperature (*zts*) is defined by:

$$zts = ptsw + zdthcap * (zfluxw + pfluxres) \tag{3.1}$$

where *ptsw* = surface temperature over water, *zdthcap* = delta time / heat capacity of mixed layer (mixed layer depth for lakes is 10m), *zfluxw* = latent heat flux + sensible heat flux + surface net longwave + surface net shortwave and flux residuum (*pfluxres*). As long as *zts* is greater or equal than *tmelt* (*tmelt* is set in ECHAM6 to 273.15K), the following applies: *ptsw* = *zts*. To initialize freezing of the lake and significant ice formation, *zts* has to fall below *tmelt*, which is defined at 273.15K. If that's the case, then *ptsw* = *tmelt* and further calculations in regard to ice depth are initiated.

3.3.2 Test run: Global Plake experiment in PI settings

As mentioned above, one of the goals during this thesis was to cap proglacial lake temperatures at 4 °C in the code part where surface temperature is defined, i.e. no proglacial lake reaches surface temperatures above this threshold. For simplicity reasons, this temperature calculation was first tested globally on all lakes (independently of being proglacial or not) to check if the logic itself is working (without adding an extra *plake* mask yet) and to evaluate the model's reaction. These changes can not be coordinated using a namelist, so the physics had to be adjusted in the model code, which is why an additional step is added to the general workflow.

1. **Modify model code**: Changes were applied to the ECHAM6 source code, more specifically in a module (`mo_surface_ocean.f90`) that regulates most of the processes related to water surface. To clearly state the changes in an easy understandable manner, they are described in more detail below.

2. **Compile model**: Modifications were executed in an extra branch of ECHAM6 (called `global_ plake`) to ensure that the original branch stays untouched.

3. **Prepare input**: No input had to be prepared, default PI settings were used.

4. **Adjust runscript**: runtime was set to 50 years, while the rest of the settings - apart from a new model directory and left out input-files - are the same as in subsection 3.2.1. In parallel, a reference simulation was done using the unchanged model directory with the rest of its runscript being the same as in the `global_plake` simulation.

5. **Submit runscript**

6. **(Optional) Bug fixing**

7. **Analyze the outdata**

Since these changes are already the basis for the later adaptations in the model code, it was considered important to list them again in a clear form. To begin with, lake physics

were modified for this experiment in ECHAM6's source code, more exactly in the module `mo_surface_ocean.f90` and yet more exactly in the `s_lake`-subroutine as follows:

1. **Adding *tpmax***: A constant was added for the maximum surface temperature of (proglacial) lakes, this constant was set to 4 °C (277.15 K)

2. **Cutting temperatures at *tpmax***: If temperatures exceed 4 °C, they are set to *tpmax*

3. **Open temperature between *tmelt* and *tpmax***: Temperatures are free to range between 0 and 4 °C

Global effects. The results from the *global_plake*-simulation in comparison to the reference simulation can be seen in Fig. 3.5. A strong cooling of the surface temperature over lakes is visible, an indication that the new temperature calculation has taken place. While temperatures met the expectations, sea ice depth (*siced*) showed results somewhat unexpected. While not every variable can be depicted due to limited space, a short summary of the most important findings should be given. Although anomalies are mostly positive, indicating an earlier and more intense freezing of lakes, slight negative values were found locally throughout the months February to May. While those values of the ymonmean are quite small (on the order of mm) and might be insignificant, it should be pointed out that this is a specific behaviour of the Great Bear Lake, which is one of the northernmost lakes. When looking at precipitation during this time period, that lake gets less precipitation as well as snow fall than in the reference simulation. Yet overall, the global annual and field mean of *siced* showed a slight increase in comparison to the reference simulation. Albedo values increased in the early NH winter season although differences were rather small. More interestingly, cloud cover in the near vicinity of Lake Victoria was generally reduced, which seemed rather odd, while the Northern Sahara experienced higher cloud cover. Large scale precipitation decreased over central Africa, while Southern Africa had higher precipitation values. Evaporation increased on time average and globally showed - as expected - high values above the newly calculated lakes (not shown).

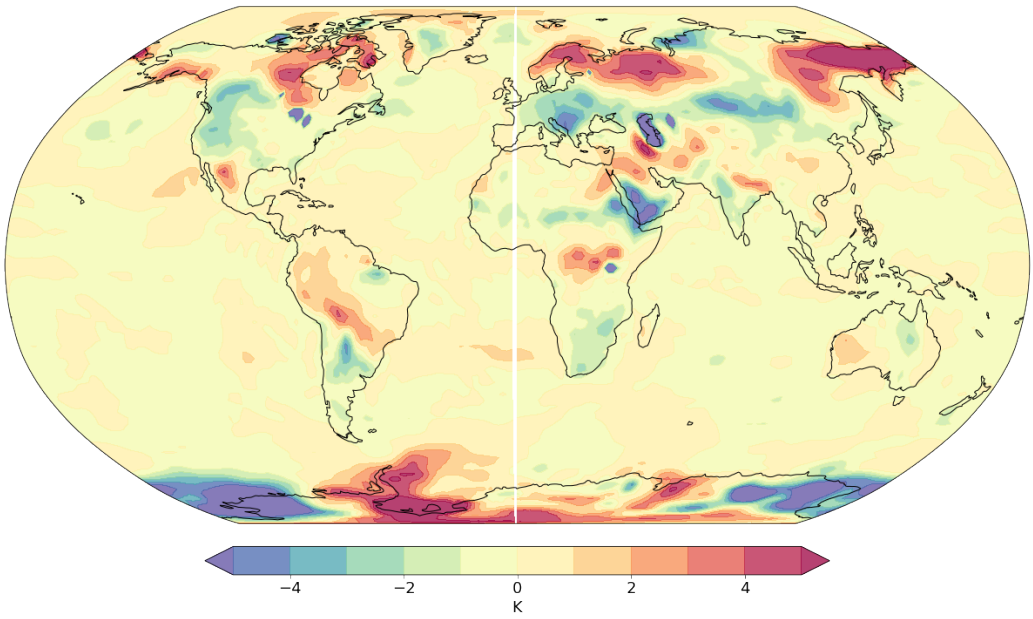

Figure 3.5: Anomaly in multi-year monthly mean surface temperature between the *global_plake* and the *reference*-simulation (gplake-ref, 50 years runtime).

North American Lakes. Next, a more specific look was taken at the effect on the Great lakes area in North America. This was done out of general interest and because these lakes are subject to higher seasonal changes. As said before, modifications were only made to the lake surface temperature calculation, making the variable *tsw* the most important for checking if the routine works. The results of a 50-year run can be seen in Fig. 3.6, which shows only water surface temperatures while surface temperatures above land are always set to 273.106 K in a PI run. A clear warming can be seen in the reference simulation, while this is completely absent in the modified version. This was taken as a first sign, that modifications were adapted successfully by ECHAM6.

Furthermore, seasonal mean of total precipitation (*aprt=aprc+aprl*) showed quite a similar picture for the months December - February (DJF), with higher precipitation south of the lakes and decreasing values towards the Northwest, indicating a more continental climate. For the months March - May (MAM), rainfall increased regionally, having a bigger impact south of the lakes than towards the north. In June - August (JJA), pattern changes were most prominent with lower values right above the lakes, surrounded by higher values

towards south and east. September - November (SON), a drier climate is experienced, with the reference simulation showing wetter cells above the lakes, missing in the *global plake* simulation (figures not included).

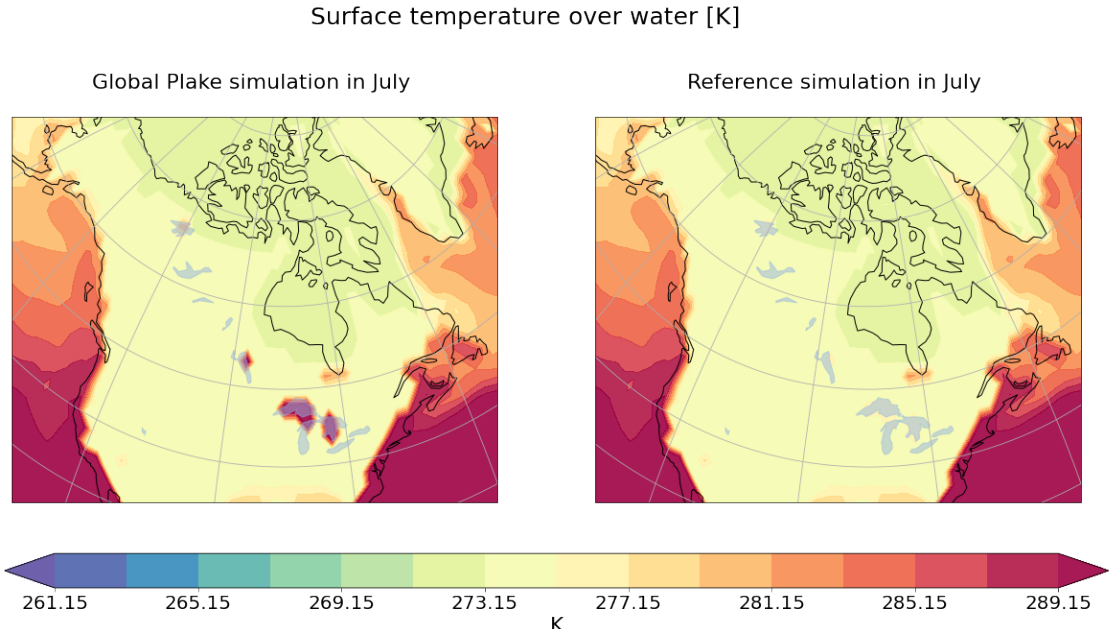

Figure 3.6: Multi-year averaged July water surface temperatures for the reference and global plake simulations.

When looking at the seasonal cloud cover, changes are rather small during NH winter. In spring, the pattern of higher cloud cover in the surrounding area and lower above the lake area, is more pronounced. During boreal summer, cloud cover seems to decrease generally with the areal patterns again staying mostly the same. For the months SON, values right above the lake are higher than in the *global plake* simulation, while the patterns are found to stay similar again. Humidity is staying quite the same for both simulations throughout DJF, but shows cells of lower values above the lake area for the rest of the year, peaking in a $\pm$ 60 percent decrease during JJA.

When looking at seasonal mean temperature in 2m height, the simulations showed nearly identical results in DJF and MAM, with only a slight temperature decrease above the lakes in spring. Strong changes can be seen in JJA indicated by highly decreased values above the lakes due to the new temperature calculation, with fall still showing generally

decreased temperatures. Since values for specific humidity are temperature dependent, the patterns of specific humidity in 2m height are thus very similar. Air parcels of higher temperatures are able to hold more water vapour, thus allowing higher values of specific humidity. Precipitation patterns are strongly bound to orographic features, making the Appalachian Mountains one of the main courses for precipitation. Most of it seems to come down from the northwestern borders of this mountain range, indicating that air transport is mainly occurring in this direction. Only during JJA, precipitation on the SE borders of the Appalachians. During this time, humidity originating from the Atlantic ocean seem to peak.

3.4 Key experiment preparation

3.4.1 Namelist switch: `lplake`

Namelist switches, as shortly indicated in subsection 3.1.2, are basically tools to simplify making changes to the model settings. The main advantage is the following: Instead of having to modify and compile the model code every time before running simulations, the namelist switch tells the model which modules/submodules/etc. should be switched on/off.

Knowing this, it seemed obvious that such a switch would also simplify the handling of a new `plake` routine. In ECHAM6, switches can be accessed via a control module `mo_control.f90`. In case of `lplake`, it was implemented in a file containing many different namelist switches (`mo_submodel.f90`). First, it had to be made `public` to allow access by the other parts of the code. Then the default for `namelist.echam` was set to `false` (and can be switched to `true` in the runscript). Lastly, its status should be shown in the `log`-file, so that it can be easily checked if it's on.

After a quick test-run it was clear that the *lplake*-switch was successfully implemented when the log-file showed "`LS Proglacial Lake:  active`". Although this only meant that it worked without any "content" added yet.

3.4.2 *plake*: Introducing a new Variable to ECHAM6 and making it globally accessible

This was the most challenging part of this study and made clear how already rather small physical changes made to the code have a wide impact. Since ECHAM6 up to now had no way of recognizing proglacial lakes as a special lake type, it was decided to introduce this ability via an extra surface input variable.

As a start, the existing *ALAKE* variable was followed through all of the modules, to see where it appears and where it is changed towards any specific purpose. This lead to the point where it was first introduced, the `ioinitial.f90` module. Here, ECHAM6 gets its (per default 12) input variables for surface calculations via the `jansurf`-input file. Among others, it contains familiar variables like *ALAKE* and *SLM*, which at the point of reading become their lower case equivalent. Now that it was clear where to start, the further way down the road had to be examined.

After studying the complex ways the *alake* variable takes through the model code (sometimes travelling incognito using different names), it was also clear that not every location of *alake* also needed *plake* to be assigned. For example, modules used for the coupling could be neglected as long as ECHAM6 is run as stand-alone. Coupling the atmosphere model with an ocean part can be subject to later studies. The *plake* variable was thus only entered in the following modules:

1. `ioinitial.f90`
2. `mo_memory_g3b.f90`
3. `mo_physc.f90`
4. `vdiff.f90`
5. `mo_surface.f90`
6. `mo_surface_ocean.f90`

In ECHAM6, processes are run simultaneously on several nodes, given by the runscript. This means, that a variable given to the model code is needed in several places at the same time. While the `ioinitial` module first reads *plake*, the `memory_g3b` module makes it globally available. The following modules mostly "transport" the variable towards its destination in `mo_surface_ocean.f90`, where lake temperatures are calculated. Throughout this modification process, a big problem was ultimately fixed by correct parameter

positioning of *plake* in the submodules `mo_surface.90`, `mo_physc.f90` and `vdiff.f90`. After those big changes, ECHAM6 was able to read and process an additional input variable (*plake*) successfully via the `jansurf`-file.

3.4.3 `temp_plake`: New temperature routine

The temperature calculation draft out of *Global Plake* (subsection 3.3.2) was now modified heavily to fit the new needs. This required changes in the existing subroutine as well as a new one called `temp_plake` in the `mo_surface_ocean.f90` file of ECHAM6.

```
1     ELSEWHERE (palake(:).GE.0.5_wp .AND. pplake(:).GE.0.5_wp)
2        WHERE (pseaice(:) .LT. 0.5_wp)                    ! open water
3           zfluxw(:)   = pahflw(:) + pahfsw(:) + ptrflw(:) + psoflw(:)
4
5           !------------ Lake temperature -----------------!
6           zts(:)      = ptsw(:) + zdthcap * (zfluxw(:) + pfluxres(:))  ! zts is surface temp
7           tplake(:)   = zts(:)                                         ! proglacial lake temperature
8                                                                        ! is now zts
9           ptsi(:)     = tmelt                                          ! ice surface temp is 0C
10          pfluxres(:) = 0._wp                                          ! No flux residuum
11          psiced(:)   = 0._wp                                          ! No ice
12          WHERE (tplake(:) .GE. tpmax)                                 ! Temp can't be above 4C
13             ptsw(:)  = tpmax
14          ELSEWHERE (tplake(:).LT.tpmax .AND. tplake(:).GE.tmelt)      ! Temp between 0 and 4C
15             ptsw(:)  = tplake(:)
16          ELSEWHERE                                                    ! check ice formation
17             ptsw(:)  = tmelt
18             zfres    = (zts(:) - tmelt) * zhcapdt                    ! zts can be used again for
19             WHERE (zts(:) .LE. tmelt - tfreez)                       ! ice formation
20                psiced(:)   = hcaprilf * (tmelt - zts(:))             ! >= dice
21                pseaice(:)  = 1._wp
22             ELSEWHERE
23                pfluxres(:)    = zfres(:)
24             END WHERE
25          END WHERE
26       ELSEWHERE (psiced(:) .GE. dice)
```

Figure 3.7: Most important part of new `temp_plake` subroutine as part of `mo_surface_ocean.f90`.

The process starts in the `s_lake` subroutine, where lake temperatures are usually calculated. By switching `lplake` on, it automatically skips the old routine and starts the newly implemented `temp_plake` routine. Here, all of the required variables are listed and a new constant is declared to limit proglacial lake surface temperatures to 4 °C ($tpmax = 277.15$ [K]). The next step was to check whether the current lake is a common lake or a proglacial lake. For this, the arguments $alake \geq 0.5$ and $plake < 0.5$ are checked. In Fig. 3.7, variable names have been altered slightly by the model, indicating them being "**p**ublic)" by an additional **p** in front of their conventional name. If these two arguments are true, the "old" lake surface temperature routine is executed. If not, it skips this part

and gets to check, if *alake* ≥ 0.5 and *plake* ≥ 0.5. If this is true, proglacial lake surface temperature is executed. This includes limiting surface temperature over water (*tsw*) to 4 °C, but allowing it to range freely between 0 and 4 °C. If temperatures fall below this threshold, and this is valid for both parts - proglacial lake or not, ice formation is started and its depth calculated. The complete new subroutine can be found in the Appendix A, while all other changes can be found at GitLab (Sijbrandij, 2022).
Lastly, it should be emphasized once more, that ECHAM6 had no possibility to recognize proglacial lakes and their behaviour before and instead calculated every lake consistently with a free range of temperature, making this special type of lakes basically absent. This part is therefore a novel contribution to the technical development of this model.

3.4.4 Test run: Running `plake` in PI setting

To test the changes described in this chapter, a simulation was set up for a PI setting. Since all of these changes were rather severe, this was done on purpose to exclude further sources of error which might have come from additional adaptations to the 13 ka BP time period. The main goal during this section was to see, if the model is able to accept the new input variable and to check, if the temperature calculation makes sense. It is similar to the `GreatLake` experiment in subsection 3.2.1, but now the great lake should be a great proglacial lake.

1. **Modify model code**: Changes included the additional namelist switch `lplake`, parameter positioning of *plake* throughout several modules of the ECHAM6 source code to make it globally accessible, new lake surface temperature calculation `temp_plake`.

2. **Compile model**: Modifications were executed in an extra branch of ECHAM6 (with the suffix `plake`) to ensure that the original branch stays untouched.

3. **Prepare input**: Boundary conditions were used from the BCG and were the same as in subsection 3.2.1, but the ECHAM6 input file included a new variable *plake*, while this variable was not needed in the JSBACH3.2 input file.

4. **Adjust runscript**: The runtime was set to 30 years, the model directory was adjusted to the `plake` branch of ECHAM6. The `jansurf`-file needed to be updated, while `jsbach` stayed the same. Lastly, the namelist switch `lplake` was set to `True`.

5. **Submit runscript**

6. **(Optional) Bug fixing**: Several major errors occurred throughout the preparation of this experiment but were fixed.

7. **Analyze the outdata**

After fixing all the bugs that occurred during this process and receiving the outdata for a 30 year simulation, it was analyzed in further detail. First, the `log`-file was checked for several points. Here, it could be seen that this simulation took place on the `plake` branch of the ECHAM6 version and that `lplake` was successfully switched on. Further settings concerning the PI scenario were shown to be the same as in all the other experiments. The boundary conditions used in this simulation can be seen in Fig. 3.8 and show the new proglacial lake mask, as well as sea land mask and ice mask which are fields of zeros and ones (one indicating a proglacial lake, land and ice surface respectively). The lake fraction provides values ranging from zero to one, values being higher than 0.5 indicate the existence of a lake.

The results were promising. Regional summer temperatures in general were reduced heavily, but when looking at the surface temperature above water, it did not exceed the 277.15 K as anticipated, while other lakes along the same latitude showed values up to 295 K, e.g. the Great Lakes. Unless stated differently, the following statements only consider regional summer months, since the biggest changes were detected during this period. Now taking a specific look at the values above the proglacial lake surface, evaporation was reduced on average. The same accounts for specific humidity in 2m height while relative humidity in 2m height stays roughly the same. This is a result of cold temperatures, that can hold less water in vaporized form. Cloud cover is higher in comparison to the `GreatLake` experiment, which is used as a reference.

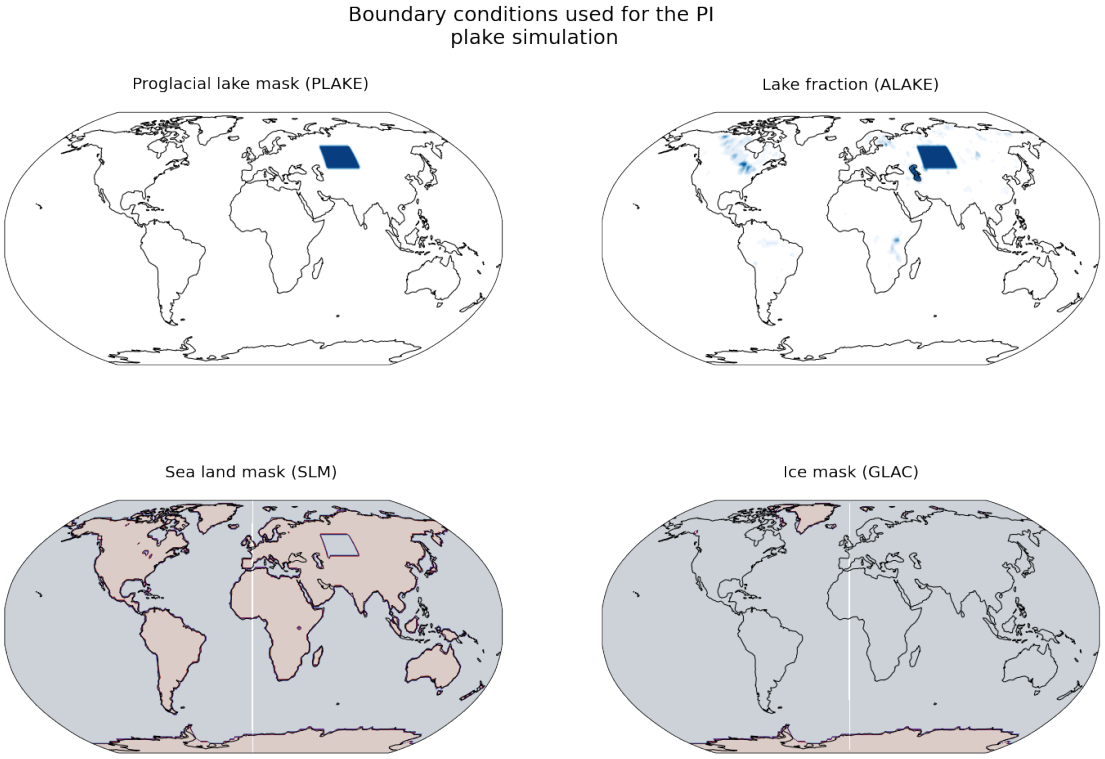

Figure 3.8: Boundary conditions for `PI_plake` experiment setup.

Looking at the greater area (roughly the extent shown in Fig. 3.3), cloud cover stays quite the same for both scenarios. Evaporation is still reduced, though less than in the lake extent. The same accounts for specific humidity, while relative humidity again is changed only slightly. 2m temperature is only altered by $\pm$ 1 °C, which is a rather small anomaly. Still, these climate reactions were a positive sign for the implementation of the new `temp_plake` subroutine.

3.5 Final simulation setup

After all the pre-experiments were done, three final experiments with 100 years runtime were prepared for the evaluation of the influence of proglacial lakes on the climate and the surface mass balance of retreating ice sheets. The settings for these simulations are described in the following. It was by intention, that only lake fraction, sea land mask and ice mask are shown in a total of 19 ECHAM6 surface input variables, since the other

variables are mostly the same in all three scenarios. Only slight adaptations were made by the BCG to fit the new surface parameters better. The bigger exception is for the `plake` scenario, where the additional PLAKE variable enables the model to recognize this as a special lake type.

3.5.1 alakeGLAC: 15.2 ka BP base with 13 ka BP *glac* and PI *alake*

This simulation was performed primarily to make the experiments conducted in this study comparable to experiments from the PalMod Project (PalMod, 2022). An overview to the workflow for this experiment is shown here, while a more detailed description follows behind.

1. **Compile model**: This simulation was executed on the original branch of ECHAM6.
2. **Prepare input**
    - Boundary conditions: The BCG provided the adjusted input files. This was a hybrid simulation, uniting 15 ka BP surface variables and sea land distribution with 13 ka ice and PI lakes
    - Forcing files: A FESOM2.0 equilibrium run provided forcing files for the oceanic state at 15.2 ka BP. These had to be adjusted to the specified format of ECHAM6.
    - The bootstrap was executed by AWI-ESM using the `jansurf_alakeGLAC`-file
3. **Adjust runscript**
    - The runtime was set to 100 years, the model directory was adjusted to the original branch of ECHAM6, `lplake` is switched off.
    - The restart block: Basically gives the model the possibility of a slow adaptation to new settings in contrary to a ”cold start”, possibly posing extra problems. This had to be done for the `echam` section as well as for the `jsbach` section
    - Orbital parameters were adjusted
    - Forcing sources were added

4. **Submit runscript**

5. **(Optional) Bug fixing**: Solved `wind speed` and `digest_evapotrans` error

6. **Analyze the outdata**: See chapter 4

Concerning boundary conditions, the hybrid setting mentioned in the list might seem rather "wild". The assumption here - and in the following experiments - is that the sea-land distribution has no influence on the effects of proglacial lakes. Because there already were equilibrium simulations for the 15.2 ka BP ocean, these were taken as forcing input for the ECHAM6 stand-alone run. In this context it can be emphasized again that this study's main purpose is a sensitivity analysis. Thus, there is no claim to completely represent reality. In reference to the PalMod project, the `alakeGLAC` scenario uses a PI lake mask, which can be seen in ensemble in Fig. 3.9. The most relevant variables for `alakeGLAC` are shown in the `jansurf_alakeGLAC`-file, where lake fraction and sea land mask differ from `alake13ka` and `plake`, while the ice mask stays the same. Masks (as in SLM, GLAC and PLAKE) contain values of 0 or 1, while fraction can additionally be anything between.

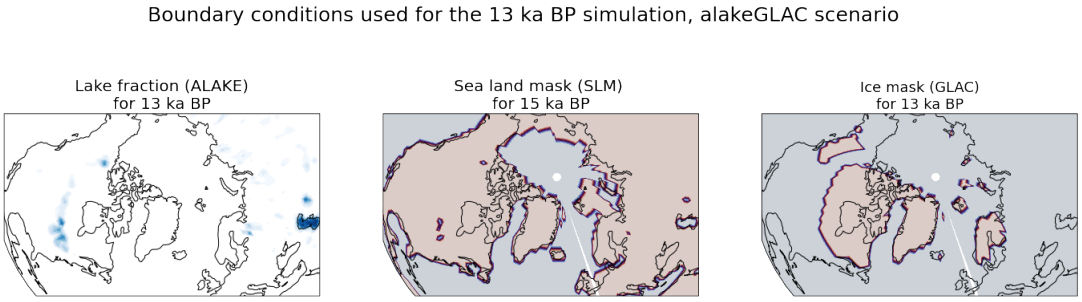

Figure 3.9: Final boundary conditions for `alakeGLAC` experiment setup.

The forcing files extracted from FESOM2.0 included sea surface temperature (*sst*) and sea ice cover (*sic*), which are accessed via the forcing files `unit.20` and `unit.96` after adjusting them to the required format. This was done to avoid the `wind speed` error, which evolves when temperature differences, e.g. between hot land surfaces and cold ocean surface (or vice versa), provoke extremely high wind speeds to compensate. These high wind speeds as a result, cannot be solved numerically anymore and the calculation crashes. Another bug encountered was one related to a JSBACH3.2 routine, the `digest_evapotrans`, where

soil water content was too high. As a response, all 5 soil layers of the variable *layer_moist* were set to zero. This did not affect later data quality, since the model achieves to reasonably refill these layers during the first ten years of the spin-up. The reason why these bugs are explained here, is because they led to modifications in the input and forcing files for all three simulations.

The restart files were created as follows: In order to initialise the model with a different topographic boundary condition, a so-called bootstrap procedure is employed. In this approach, a target orographic field describing the geopotential height as well as variables relevant for the gravity wave drag parameterisation are read. These fields are then linearly approached beginning from a standard Pre-Industrial topography over the course of one simulated year such that the change in orography between two time steps remains small (on the order of millimetres). Numerical stability can be ensured by this procedure. The overall setting for it (not including surface information) was the same for all final simulations. (personal communication, Dr. Paul Gierz 12.03.2022).

Next, the orbital parameters and greenhouse gas forcing had to be adjusted to the respective time slice in the runscript. These values were respectively taken from Berger and Loutre (1991) and Köhler et al. (2017). They apply to all scenarios as follows:

- Obliquity: 24.093
- Eccentricity: 0.02018
- Omega: 244.71
- CO_2: 234.52e-6
- CH_4: 0.64226e-6
- N_2O: 0.26069e-6

Concerning JSBACH3.2 settings, the `dynveg` component was set to *true*, enabling geographical shifts of vegetation and deserts shown in potential vegetation. For this study, potential vegetation is also actual vegetation, due to the absence of anthropogenic land-use (and cover) change. With processes like vegetation fires and windbreak simulated by `dynveg`, natural biogeographical changes can be better understood (Reick et al., 2021). Apart from the specific surface changes, settings concerning the calculation of vegetation processes by the land component stay the same in all three scenarios.

3.5.2 alake13ka: 15.2 ka BP base with 13 ka BP *glac* and *alake*

This simulation should serve as kind of a reference simulation to `plake`. It holds 15.2 ka BP boundaries derived from GLAC-1D reconstructions for most of the variables, including SLM and SLF as depicted in Fig. 3.10. Additionally, 13 ka BP glaciation and lakes are chosen, because of the severe retreat of ice sheets between 15 - 13 ka BP, enabling the evolution of large proglacial lakes.

1. **Compile model**: This simulation was executed on the original branch of ECHAM6.
2. **Prepare input**
    - Boundary conditions: The BCG provided the adjusted input files. This was a hybrid simulation, uniting 15.2 ka BP surface variables and sea land distribution with 13 ka BP ice and lakes
    - Forcing files: Same as in `alakeGLAC`.
    - Restart files: The bootstrap was executed by AWI-ESM using the `jansurf_alake13ka`-file
3. **Adjust runscript**
    - The runtime was set to 100 years, the model directory was adjusted to the original branch of ECHAM6, `lplake` is switched off.
    - The restart block: Settings for the restart are the same as in `alakeGLAC` but with the correct 13 ka BP lake surface, thus a different directory is used
    - Orbital parameters: Same as in `alakeGLAC`
    - Forcing sources: Same as in `alakeGLAC`
4. **Submit runscript**
5. **(Optional) Bug fixing**
6. **Analyze the outdata**: See chapter 4

No changes were needed in the model code, which is why the original branch of ECHAM6-concurrent radiation could be used.

The following part gets slightly complicated but is important to understand in which aspects `alake13ka` and `plake` are the same and where the differences lie. To start with, the `jansurf`-file was modified manually, adding to *ALAKE* the lakes derived from the lakeCC-tool Hinck et al. (2020), but also creating the *plake* mask including only these specific lakes. To create an internally consistent setup for all of the `jansurf`-variables, this file then was given to the BCG creating the `jansurf_plake`-file. Now, for `alake13ka` of course, the *PLAKE* variable is unnecessary and even causes problems, since the original ECHAM6 does not know how to handle this additional variable. So, *PLAKE* was then again excluded from the now called `jansurf_alake13ka`-file, which then can be used in the input section of the runscript. An overview to the used boundary conditions can be seen in Fig. 3.10. Here again, the correct implementation of the namelist switch would simplify the handling in the future.

The bootstrap used the `jansurf_alake13ka` file among other to couple ECHAM6 with the 15.2 ka BP oceanic state calculated by FESOM2.0 to produce the corresponding restart files.

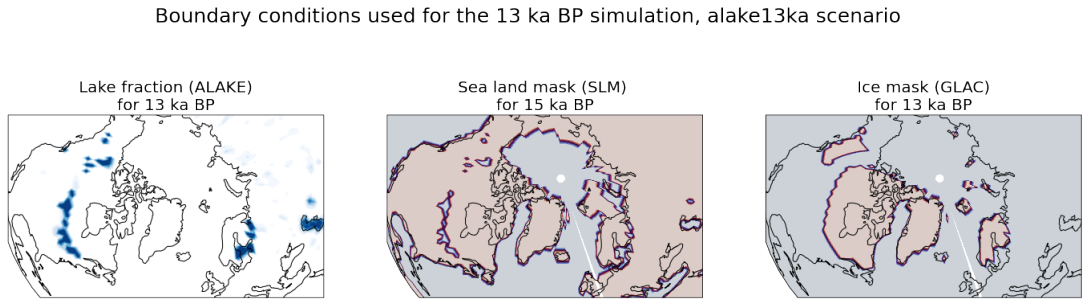

Figure 3.10: Final boundary conditions for `alake13ka` experiment setup.

3.5.3 plake: 15 ka BP base with 13 ka BP *glac*, *alake* and *plake*

This simulation is the key experiment for testing the effects of proglacial lakes with surface temperature limited to 4 °C on the regional climate and surface mass balance of ice sheets. Most of the changes predating the submit of this simulation can be found in detail in the Methodology section (chapter 3) and shall be only quickly summarized here if necessary.

1. **Compile model**: This simulation was executed on the `plake` branch of ECHAM6.

2. **Prepare input**

   - Boundary conditions: The BCG provided the adjusted input files. This was a hybrid simulation, uniting 15.2 ka BP surface variables and sea land distribution with 13 ka BP ice and lakes, additionally including the proglacial lake mask
   - Forcing files: Same as in `alakeGLAC`.
   - Restart files: The bootstrap directory from `alake13ka` was copied and its `jansurf`-file modified to contain *plake*

3. **Adjust runscript**

   - The runtime was set to 100 years, the model directory was adjusted to the `plake` branch of ECHAM6, `lplake` is switched on.
   - The restart block: The path to the new restart directory had to be aligned
   - Orbital parameters: Same as in `alakeGLAC`
   - Forcing sources: Same as in `alakeGLAC`

4. **Submit runscript**

5. **(Optional) Bug fixing**:

6. **Analyze the outdata**: See chapter 4

The adaptations shown during the methodology part (chapter 3) are accessed by setting `lplake: True` and using the `plake` model version, where `temp_lake` is run for all the lake surface calculations. This experiment is performed with 15 ka BP boundary conditions, except for the 13 ka BP glaciation and lakes. It is consistent with the `alake13ka` simulation, but includes *PLAKE* as an additional variable. Thus, every PLAKE is also ALAKE, but not vice versa, providing a criterion for the model code to determine how surface temperature should be computed. Boundary conditions for this scenario can be seen in Fig. 3.11.
Settings for the restart are the same as in `alake13ka`. The restart directory was copied to add a proglacial lake to its `jansurf`-file, without harming the original directory.

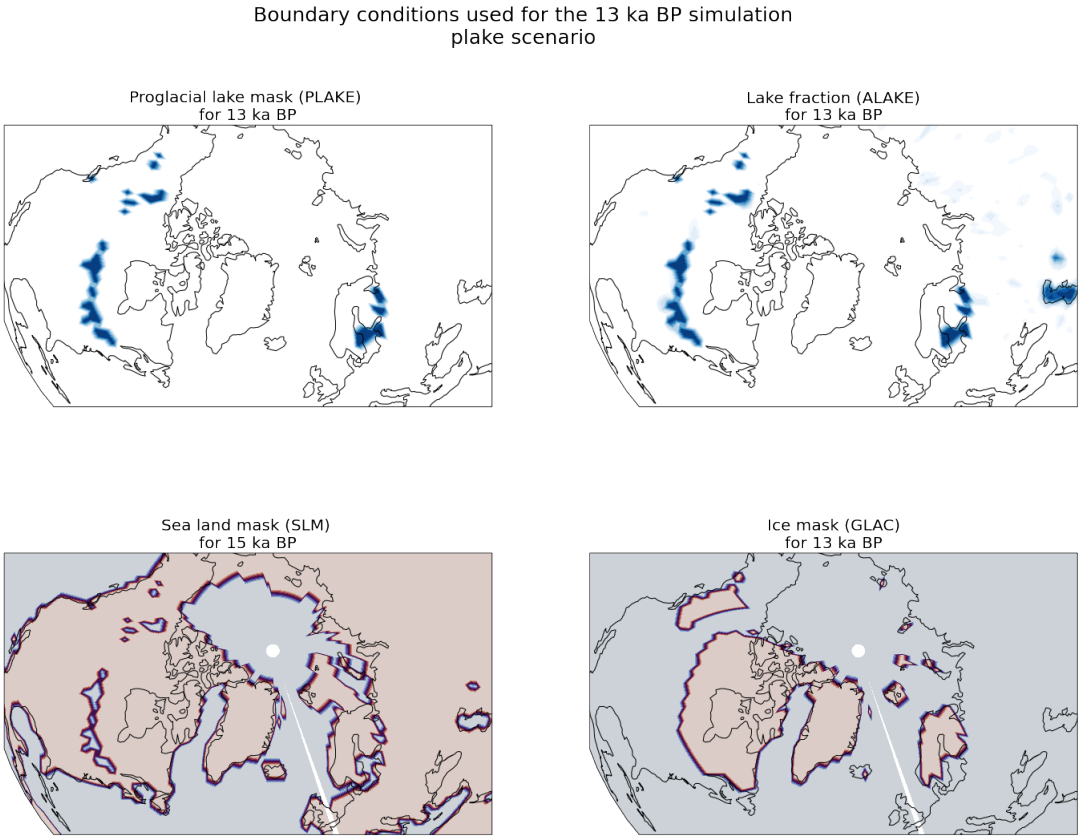

Figure 3.11: Final boundary conditions for `plake` experiment setup.

While the namelist switch exists and should simplify controlling the `plake` procedure massively, it was not yet possible to implement this completely as intended. The correct implementation of the namelist switch shall be subject to later work. Nevertheless, this model branch only differs in regard to the *plake* variable not being checked and thus carries out the usual lake temperature calculation.

As a summary: For `alake13ka` and `plake` PLAKE, ALAKE and GLAC are derived from the 13 ka BP GLAC-1D reconstruction, while SLM shows 15 ka BP sea land mask in all three scenarios. This is due to the combination of the 13 ka boundary conditions with a 15.2 ka BP equilibrium state of the ocean model, which is taken as input for the oceanic state. Since this study's focus is primarily on performing a sensitivity analysis, this "inconsistency" was considered not to distort the influence of proglacial lakes on glaciers and climate significantly.

4 Results

This chapter presents general results obtained during this study. The implementation of the novel `plake` routine was considered successful, but it was also shown that a longer run time would have been needed. Furthermore, it is worth mentioning that not all figures could be included in this chapter, so further information can be found in the Appendix.

4.1 Variability

To get a general idea of the climate of the past and anomalies between the three scenarios, it was chosen to look at the variability. It was clear rather soon that there was still considerably high (multidecadal) variability - a first hint that the climate model did not reach an equilibrium state in this period of time. Reasons for this will be mostly discussed in chapter 5.

4.1.1 Global

This section concentrates on the global variability. The graphs in Fig. 4.1 show global 2m temperature, the area including land as well as sea surface. It was additionally chosen to calculate the 30-year running mean in relation to the climate normal period. Global 2m temperatures are between 10.35 and 10.40 °C, the results can be seen in Fig. 4.1. Even though global variability took place as expected on quite a small scale, it nevertheless showed interesting results. While `alake13ka` and `plake` share a rather similar temperature trend, `alakeGLAC` increases during the second half and seems to settle at higher temperatures.

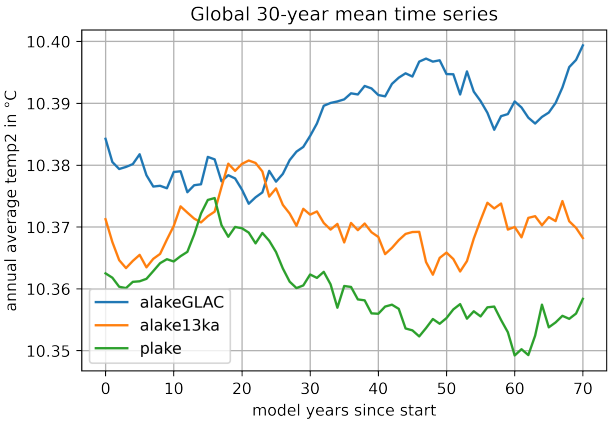

Figure 4.1: Variability during 100 years run time. Global mean near surface temperature filtered.

The simulation with default GLAC-1D lake settings has the highest temperatures on average, while `alake13ka` comes next and the `plake` scenario is the coldest one. It is quite interesting to see that the extent of a lake plays such a crucial role in altering the climate, confirmed by this being the only difference between `alakeGLAC` and `alake13ka`. To validate the course of the temperature lines, the standard deviation (*std*) was taken in into account. It was highest for `alakeGLAC` with 0.007 °C, followed by the `plake` simulation with 0.006 °C, while `alake13ka` had the smallest value of 0.004 °C.
One more note on the labelling of the x-axis: This graph shows the running mean calculated by the following equation (Schulzweida, 2021):

$$o(t + (nts - 1)/2, x) = mean\{i(t, x), i(t + 1, x), ..., i(t + nts - 1, x)\} \tag{4.1}$$

where *nts* is the number of timesteps given as `integer` (here: 30). Thus, on the timeline the x-value 0 is the 30 year average around the 15th year of the simulation, while 70 is the 30 year average around the 85th year of the simulation.

4.1.2 Northern America

In case of North American land surface 2m temperatures range from -14.2 to -14.9 °C in a 30 year running mean, as can be seen in Fig. 4.2. The area of interest spans roughly from 145 °W to 60 °W and 30 °N to 80 °N, which is roughly the extent shown in Fig. 3.4 (right). The figure shows once more, how cool the regional climate during the 13 ka BP time slice is, even though this was considered an interstadial, i.e. a warm period.

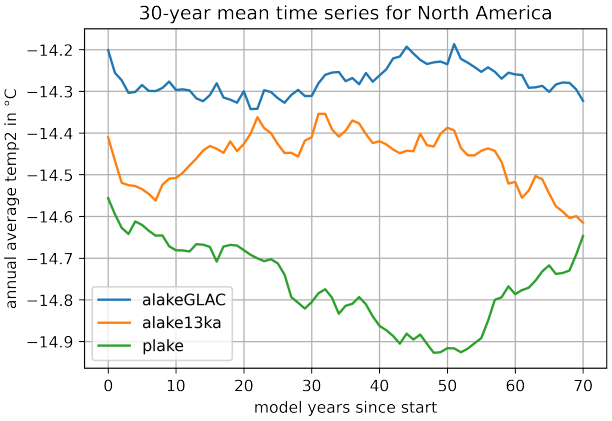

Figure 4.2: Variability during 100 years run time. North American near surface temperature filtered.

Calculating the standard deviation for this data, `alakeGLAC` had the smallest value (0.036 °C), followed by `alake13ka` with

0.063 °C and the `plake` scenario showing the highest *std* with 0.097 °C, thus a 30% decrease from the first to the latter. This is in accordance with the curves in the figure, where `plake` shows the highest range. While the `alake13ka` and `alakeGLAC` simulations have a slightly similar *temp2* course, both indicating a drop towards the end, the `plake` simulation drops during the second half and increases steeply towards the end of the runtime. Highly interesting is the large difference between `alake13ka` and `plake` during most of the century, while they start and end quite similar. At this point it would be particularly interesting to look at the development of the curves in a longer simulation.

4.1.3 Northern Europe

The three scenarios show a 2m temperature ranging from -5.2 to -6.3 °C during a time span of 100 years above the land surface of northern Europe. The respective study domain reaches its outer limits at 2 and 45 °E and 50 and 80 °N, which corresponds to roughly the area shown in Fig. 3.4. These values are computed from a 30 year running mean on the 100 years of run time and can be seen in Fig. 4.3. In this case, `alake13ka` and `plake` share a rather similar temperature curve, decreasing towards the second half of the century, though `alake13ka` in a strongly less pronounced way. On the contrary, `alakeGLAC` increases strongly towards the end of the period indicating a further rise, if run time was longer. This again is a strong sign, that the time period chosen here, might be too short to reliably achieve an equilibrium state for all three simulations and shall be discussed in chapter 5.

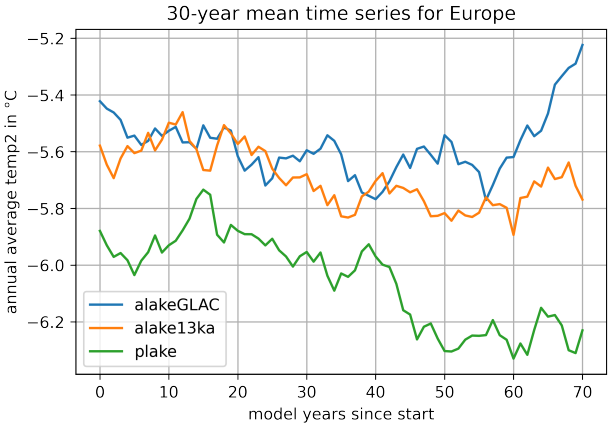

Figure 4.3: Variability during 100 years run time. North European mean near surface temperature filtered

Concerning the standard deviation for this data, it is significantly higher than for the northern America region. Values are lowest for `alakeGLAC` and `alake13ka` (0.108 and

0.101 °C respectively), while `plake` - as it's the case for northern America, has highest values with a standard deviation of 0.163 °C.

4.2 Global changes

Before we dive in deeper, a glance will be taken at significant changes between the three scenarios on a global level. This was done using standard significance test, the t-test that works on temporal variation (Decremer et al., 2014). The period chosen for the analysis from now on contains the last 30 years (climate normal period) of each simulations unless stated otherwise. This period is called 2070-2099 in several parts of this thesis and is not a prediction, but just the period extracted from a run that has a default initial year of 2000, thus counting from there on. This is done even though the equilibrium state as mentioned above has not been reached. Still, it was assumed that climate trends during this time, already give some kind of a hint at the possible outcome. In the same context, the spin up obviously takes longer than anticipated, which is why including earlier years was avoided for the analysis. Uncertainties concerning this topic were knowingly accepted, but with a clear focus on repeating the simulations with a longer run time.

Annual *temp2* changes for `alake13ka` and `alakeGLAC` are only significant in a few places, showing a slight increase on the order of 0.5 °C for the central part of the Amazon rainforest and a slight decrease of -0.5 °C for the southern parts of Democratic Republic of Congo, as well as for Vietnam and Cambodia. This is a quite stunning result, since it underlines the wide reaching effect, land surface changes in higher latitudes can have on the tropics, as well as it highlights the sensitivity of tropical rainforest to slight climate changes. Looking at the months DJF, global changes paint a more chaotic picture, negative anomalies can be found in southeastern Sahara, as well as parts of the Himalaya and Southeast Asia. A kind of a dipole pattern is seen for northern South America (+0.5 °C) and central South America (-0.5 °C) as well as for Northern Australia (+0.5 °C) and Southern Australia (-0.5 °C) and Bellingshausen Sea (+1 °C) vs. Amundsen Sea (-1 °C). A noticeable increase in *temp2* of up to +2 °C is detected across wide parts of Siberia. These results can be seen in Appendix A. During JJA, *temp2* generally is decreasing across the Northern hemisphere and increasing in most parts of Antarctica, most drastic changes occurring near the new

lakes ($\lesssim$ -4 °C) and in the Bellingshausen Sea (+1.5 °C), while the Weddell Sea experiences a decrease of -1 °C as can be seen in Fig. 4.4a).

When looking at the significant changes between `plake` and `alake13ka`, the annually averaged *temp2* shows negative anomalies above the new lake surfaces, the only positive anomaly can be found in Myanmar. Again, we get a more interesting picture when looking at seasonal changes. For DJF, positive anomalies are found in large parts of the higher northern latitudes, increasing from the Labrador Sea (+1 °C), to Alaska and Canada (+1.5 °C) and reaching values of up to +2 °C in the Arctic Ocean. Furthermore, positive anomalies are seen in region spanning from southern Mali, to Chad, to Georgia. Negative anomalies are found in the northeastern parts of the USA, in Norway, Northern Siberia, parts of the Himalaya and Arabian Peninsula. During JJA highest negative anomalies in *temp2* are above the proglacial lake surfaces and their surrounding regions as can be seen in Fig. 4.4b). In return, large parts of central South America show positive anomalies of up to +1.5 °C. Two regions of positive changes (roughly Turkmenistan and northeast Asia) are separated by a large region with negative anomalies of up to 1 °C. Australia shows a slight decrease in *temp2* at the northern tips and an increase in the central western parts. Antarctica mostly experiences negative anomalies throughout both seasons.

Between `plake` and `alakeGLAC`, annual changes are not significant except for the newly calculated proglacial lake surfaces and - as above mentioned - some tropical regions, but missing the Amazon anomaly. For DJF, positive anomalies can be found in eastern Alaska ($\geq$ +3.5 °C), as well as central Eurasia (+1.5 °C). Slight positive anomalies ($\leq$ +0.5 °C) are calculated above the African Mediterranean Coast and North Korea, as well as Morocco. Negative anomalies can be found in South Australia, at the Amundsen Sea and Central South America. For Europe, proglacial lake temperatures consistently lead to a cooler climate, even affecting Iceland with changes of -2 °C, while North American climate seems to react differently. During JJA, high negative anomalies are found surrounding the new proglacial lakes. Furthermore, central Asia and the southern parts of the Arabian peninsula experience a cooler climate, while southern Sahara, Ural mountains and the southeastern tip of Russia see higher temperatures. In Antarctica, positive and negative anomalies are alternating - Arctic ocean temperatures are cooler during the `plake` scenario, which can be seen in Fig. 4.4c).

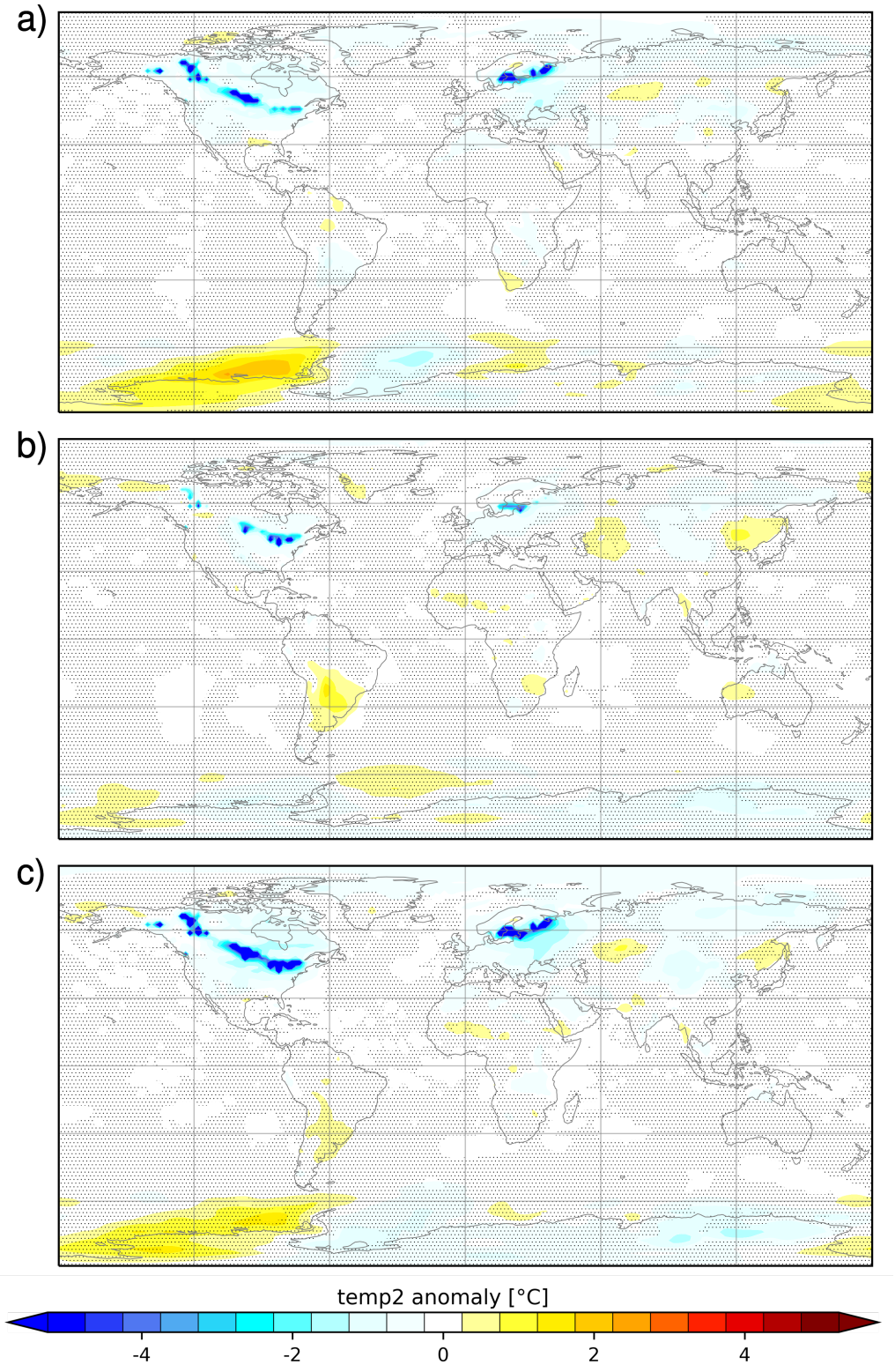

Figure 4.4: Global map of changes in seasonal 2m temperature (JJA) between a) `alake13ka` and `alakeGLAC`, b) `plake` and `alake13ka`, c) `plake` and `alakeGLAC`. Stippled areas indicate where changes are not significant, while unstippled regions mean significant changes according to a t-test.

Generally, the global and time averaged change for temperature in 2m height is -0.0098 °C when comparing *plake-alake13ka*, is -0.0410 °C in case of *plake-alakeGLAC* and -0.0311 °C for *alake13ka-alakeGLAC*. For global glacier depth values - again - increase from `alakeGLAC` towards the `alake13ka` with `plake` having the highest glacier depth in a time averaged observation, as well as looking at seasonal values. This could be a first hint that nearby lakes and in specific proglacial lakes support the growth of ice sheets. On the other hand, this calculation includes Antarctica which is why tele-connections could be a possible reason for higher glacier depth and shall be discussed in more detail after looking at the results provided by the dEBM.
Since the most pronounced changes can be found during JJA, only these were included at this point. This is also when the new temperature calculation has the biggest impact, limiting summer temperatures in `plake` significantly. Appendix A contains further figures concerning the annual (Fig. A.1) and DJF (Fig. A.2) maps of significant changes.

4.3 The diurnal Energy Balance Model

To analyse the ECHAM6 output in regard to ice sheet dynamics, the diurnal Energy Balance Model (dEBM, Krebs-Kanzow et al., 2021) was used. This is a novel interface between atmosphere and land ice and considers changes in the Earth's orbit and atmospheric composition. It needs precipitation, cloud cover, near surface air temperature, downward shortwave and longwave radiation at the surface and downward shortwave radiation at the top of the atmosphere in monthly resolution as input (Krebs-Kanzow et al., 2021). After it has finished, the output provides the following variables: *SNH* (snow height, also used for the restart), *ME* (surface melt rate), *SMB* (total surface mass balance), *RZ* (refreezing rate), *A* (albedo), *RF* (rain fall) and *SF* (snow fall). which are again in monthly resolution. dEBM focuses primarily on the ablation zone, where snow fall is the key driver for accumulation as long as melting is absent (Krebs-Kanzow et al., 2021). Even though it is computationally inexpensive, it takes into account e.g. the cloudiness of days for surface energy balance calculation and the ice-albedo feedback as a result of snow type. For this, GLAC-1D boundary conditions as well as the ECHAM6 outdata were interpolated on a PISM grid for higher resolution and variables relevant to surface

mass balance calculation were processed. Unfortunately the ECHAM6 output, spanning 100 years of monthly data, was too large to be fed to the dEBM in one piece so it had to be split into two periods (period one: 2000-01-01 to 2049-12-31, period two: 2050-01-01 to 2099-12-31). Thus, a restart was used to continue calculations where they stopped in time period one. In the `namelist.debm`, the input file had to be changed accordingly and obliquity was updated to 13 ka BP. The namelist for the dEBM serves basically the same purpose than in ECHAM6. Coordinates and time information had to be added again when they were altered during the process, the 30 year period was selected and projected onto the ice mask, cutting off all other values concerning land and sea surface and thus enabling specific ice sheet calculation. Since this still included the Greenland Ice Sheet, two boxes were selected for both areas of interest. One includes the Laurentide and Cordilleran ice sheet for investigations in the North American part and the other one is showing the Fennoscandian ice sheet.

4.4 Laurentide ice sheet

Here the greater area near the Laurentide ice sheet shall be analysed. As far as ECHAM6 is concerned, calculations take place for land/sea surface as a total but also for land surface exclusively as indicated when necessary. The study domain is quite the same as depicted in Fig. 3.4. dEBM results consider calculations made specifically for the surface of the ice sheet.

4.4.1 Results from ECHAM6

Considering land and sea surface surrounding the Laurentide ice sheet, *temp2* anomalies are highest between `plake` and `alakeGLAC` and reach values of -0.32 °C in annual mean. This followed by `alake13ka` and `alakeGLAC` showing a value of -0.29, while the anomaly in annual mean is by far smallest between `alake13ka` `plake`. This already indicates, that the existence of extensive lake surface in the near vicinity of the ice sheet highly moderates climate.

When looking at seasonal changes, these are highest when comparing `plake` to `alakeGLAC` during regional summer months, reaching a *temp2* difference of -1.16 °C. Smallest dif-

ferences when comparing all simulations have been calculated for boreal autumn, where `plake` and `alakeGLAC` interestingly show mostly similar values. These numbers can also be found in Appendix A, Tab. A.5 showing all the anomalies and Tab. A.4 showing absolute values.

Concerning land surface only, the broader pattern seems to be the same as when including sea surface, but more pronounced. This is interpreted as a result of the ocean having a more moderate temperature change and thus dampening the effects on land. The biggest change in annual 2m temperature is detected again when comparing `plake` and `alakeGLAC` reaching a value of -0.32 °C, while `plake` and `alake13ka` are roughly on the same order of magnitude. Seasonal changes in 2m temperature are highest again for boreal summer months and can be found when comparing `plake` to `alakeGLAC`. During regional winter, `alake13ka` and `alakeGLAC` show roughly the same and `plake` a ± 0.3 °C higher temperature. These numbers can also be found in Appendix A, Tab. A.6.

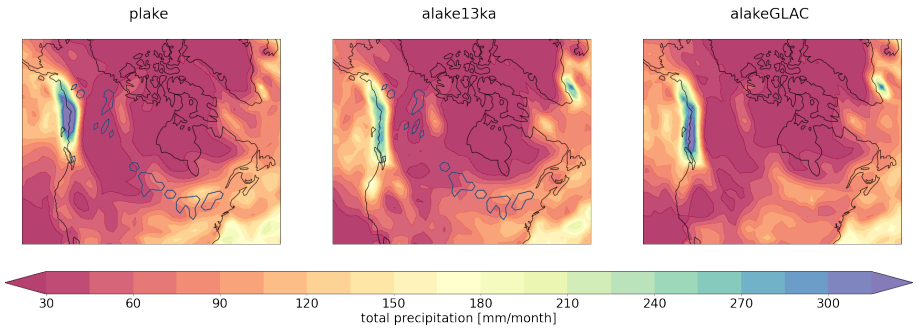

Figure 4.5: Mean monthly precipitation for summer months in northern America. Blue lines indicate the location of lakes.

Precipitation patterns are mostly the same for all scenarios, but with different ranges as can be seen in Fig. 4.5. `plake` shows the widest area of high seasonal (JJA) precipitation along the Cordilleran ice sheet when compared to the others, while the borders of the Laurentide ice sheet is indicated by higher precipitation values. In this regard, orographically induced precipitation can be safely assumed to play a role. During 13 ka BP the Laurentide ice sheet reached up to around 2000 metres above sea level, while the surrounding area in its southwestern margins lies significantly lower. Here, it can be seen that in the `plake` scenario, the western borders lag behind when precipitation is considered, while along the

eastern borders it is higher than for `alake13ka` and `alakeGLAC`. This figure and additional ones for *temp2* and evaporation (*evap*) can be found in Appendix A, Fig. A.3.
When looking at annual significant changes, as was done in section 4.2, highest anomalies can be found above proglacial lake surfaces in a comparison of `plake` and `alakeGLAC`, but these are also relevant for `plake` and `alake13ka` - only `alake13ka` and `alakeGLAC` don't show significant changes in the t-test, when annual *temp2* is considered. During boreal summer, *temp2* is significantly reduced in `plake` when compared to `alake13ka` as well as `alakeGLAC`. It also shows quite drastic changes between `alake13ka` and `alakeGLAC` with reduced temperatures above most of northern America's land surface, due to the large extent of newly implemented lakes. In regional winter months, significant changes are mostly absent, but there is a slight increase indicated when comparing `plake` to `alake13ka` as well as `alakeGLAC`. The figures described in this part can be seen in Appendix A, Fig. A.1 and A.2.

4.4.2 Results from the dEBM

First of all, it should be clarified that the analysis here not only includes the original Laurentide ice sheet in calculations, but also takes into account the Cordilleran Ice Sheet (CIS) and part of the Innuitian Ice Sheet (IIS), as their location and extent was depicted in Stokes (2017).
The main variable of interest here is the *SMB*, which is depicted in Fig. 4.6. This figure shows similar patterns for annual *SMB* (on the left) with varying degrees of end values. In terms of regional patterns, LIS experiences positive values throughout a large region in the center of the ice sheet. Negative values can be seen mostly along the edges, being more pronounced at specific topography characteristics. Also, the ice sheet seems to lose more ice towards continental regions, while regions more exposed to the coasts show smaller losses. This is probably due to higher accumulation, when moist air from the ocean reaches the ice surface. Sites of higher losses are as expected more pronounced during boreal summer months (JJA), showing negative values in an area being largest for the `alakeGLAC` scenario, but also indicating higher losses for `plake` when compared to its reference simulation `alake13ka`. These results can also be seen in Appendix A.

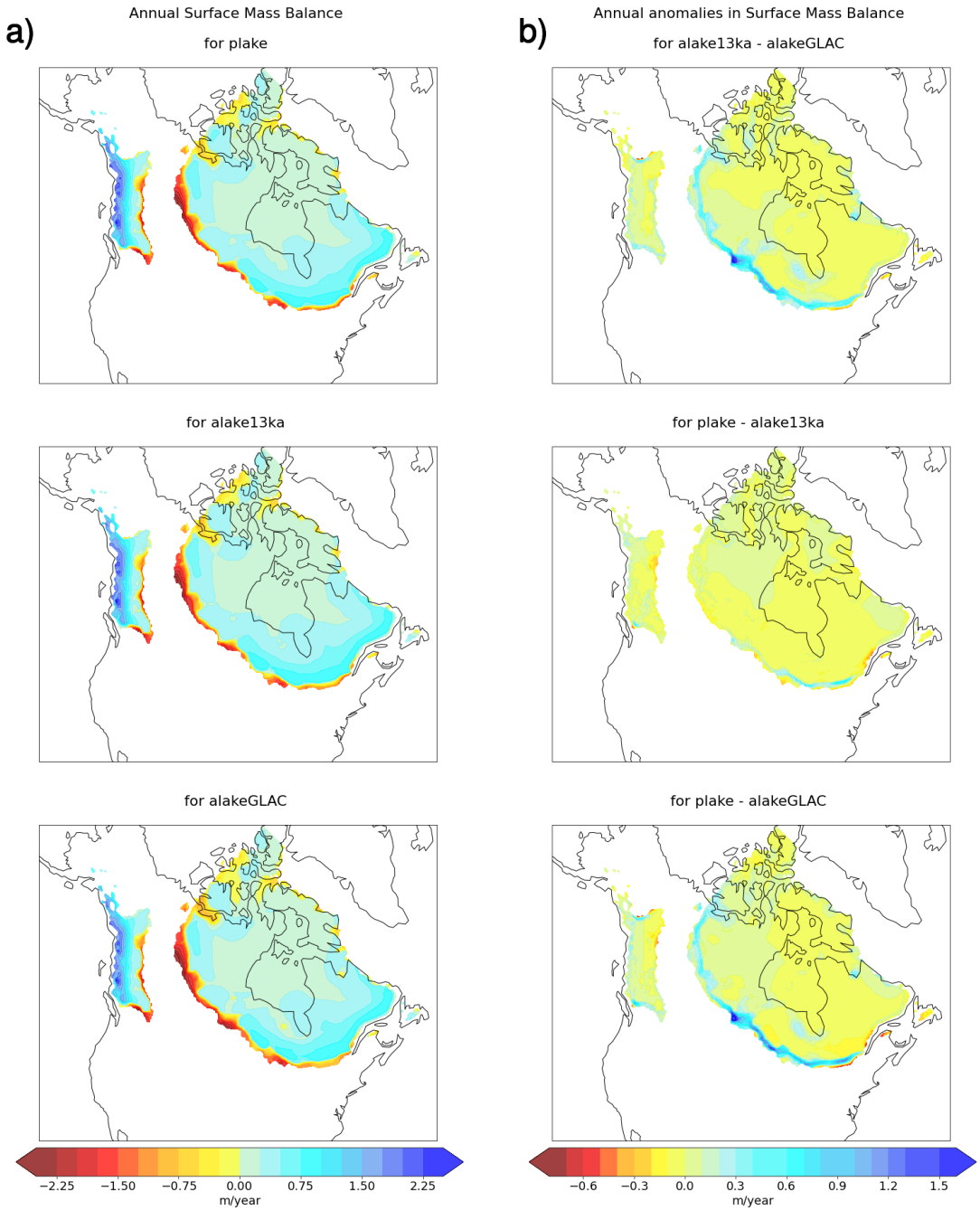

Figure 4.6: Surface mass balance for the Laurentide ice sheet showing a) annual mean and b) annual anomaly. Output from dEBM.

While not only losses are higher during these months, regions gaining surface mass are also more pronounced. This can be seen specifically along the eastern coast, where the above mentioned processes seem to have a high positive effect on *SMB* values, even showing highest values in the `alakeGLAC` scenario. One peculiar detail should be adressed for CIS, where `plake` along the western coast seems to have higher accumulation throughout regional summer months.

These values can also be seen in Tab. 4.1, nevertheless they should be emphasized explicitly here to give a sense of the order of magnitude indicated in Fig. 4.6. Given a time period of one year, LIS grows by 2151 Gigatons (Gt) in an `alake13ka` setting, by 2089 Gt in a `plake` setting and by 1764 Gt in an `alakeGLAC` setting. To put these numbers into perspective: with today's ocean area the difference between the two most distinct scenarios could lead to a global sea level rise of 1.1 mm per year (Sea level equivalent calculated with ocean area value from Zemp et al., 2019, being 362.5 x 10^6 km^2).

More results provided by dEBM are summarized in Tab. 4.1. These values represent only data above the ice sheet, that means e.g. no temperature above land surface and ocean is included. To begin with, cloud cover is highest in the `alake13ka` scenario, which makes sense since lakes in the `plake` scenario are cooler and probably provide less evaporation, while lakes in `alakeGLAC` are either absent or a lot smaller, hence not being a significant evaporation source. Mean precipitation is highest in `alakeGLAC`, standing somewhat in contrast to cloud cover values at first sight. This might be due to higher mean temperatures, which enable air parcels to hold more water. Specifically during boreal spring and summer months this seems to be a relevant factor, `alakeGLAC` showing highest values in comparison. During boreal autumn and winter months `alakeGLAC` has lower values, which again might be due to absent or smaller water bodies that are able to moderate winter temperatures in `alake13ka` as well as in `plake`.

Surface mass balance is highest in the `alake13ka` scenario, indicating that the overall combination of higher temperatures and bigger water bodies in near vicinity of the ice sheet is mainly favorable to glacier growth in the North American region. Next, `plake` shows high values, possibly a response to lower melt rates with altered NH summer temperatures among other factors. An odd detail is the higher temperature of `plake` in mean annual temperature above the ice sheet, which should be discussed later on.

	alakeGLAC	alake13ka	plake
Cloud cover [%]	62.70978	62.8455	62.75255
Seasonal cloud cover [%]			
DJF	65.20771	65.15827	65.30963
MAM	57.7013	57.63952	57.77017
JJA	65.64347	65.42807	65.30796
SON	62.28667	63.15616	62.62245
Precipitation [kg/m^2/s]	0.4369121	0.4326698	0.4224184
Seasonal precipitation [kg/m^2/s]			
DJF	0.2804239	0.2849095	0.2826315
MAM	0.3433198	0.3356398	0.3275201
JJA	0.6101605	0.5873298	0.5717195
SON	0.5137442	0.5228001	0.5078023
2m temperature [K]	251.0488	250.826	250.9711
Seasonal 2m temperature [K]			
DJF	236.4305	236.4916	236.8745
MAM	248.4279	247.8948	248.0548
JJA	266.8886	266.292	266.1626
SON	252.4482	252.6257	252.7926
Surface mass balance [Gt/years]	1764.248	2150.75	2089.41

Table 4.1: Climate parameters and surface mass balance for all simulations over 30 years above the Laurentide ice sheet. Except from SMB, numbers represent mean values.

To better understand the two sides of the *SMB*, a specific look will be taken at runoff and accumulation variables. Runoff and accumulation in this case are defined as follows:

$$ACC = SF + RZ \tag{4.2}$$

$$ROF = ME - RZ + RF \tag{4.3}$$

Accumulation patterns are similar for all three simulations. This text describes Fig. A.7, which is attached to Appendix A. Highest accumulation takes place at CIS as a response to moist air from the ocean meeting the mountain range and thus leading to high precipitation. Also, higher values can be found in the southeastern borders of LIS due to the same reasons. Accumulation is lowest in the central ice sheet and towards more continental conditions. Runoff takes place only in ice sheet margins, increasing towards the edges independently of continental and marine conditions, instead reacting primarily to topography. Most of the ice sheet remains unaffected by runoff, this area being smallest

in the alakeGLAC scenario. One of the oddities is a small area in the plake simulation, which shows negative runoff values in the center of LIS.
Accumulation is highest in the alakeGLAC scenario which supports the theory that higher temperatures have led to higher water content per air parcel. In this context it should also be pointed out that this scenario had the highest mean precipitation values in ECHAM6. It is followed by the alake13ka and plake simulations, the latter posing coldest temperatures and lowest accumulation (confirmed as well by lowest precipitation values in ECHAM6). In contrast, runoff is severely higher in alakeGLAC than in the other two scenarios, the latter ones behaving rather similar. These values result in the alake13ka scenario gaining most in mass, followed by plake and lastly alakeGLAC.
Lastly, since the Laurentide ice sheet gains slightly (compared to the overall mass) in all three scenarios, this supports the theory that the settings of this experiment encourage ice growth or at least provide a stabilizing effect. All further figures and tables concerning this topic can be seen in the Appendix A.

4.5 Fennoscandian ice sheet

In this section, the focus is laid on the broader region around FIS. While results from ECHAM6 include sea and land surface as indicated at the relevant points, dEBM results focus solely on calculations concerning the surface of ice sheets.

4.5.1 Results from ECHAM6

Including surrounding sea surface, a multi-year mean temperature difference in 2m height of -0.38 °C can be detected between the plake simulation and the alake13ka simulation. This difference is even higher when comparing plake with alakeGLAC, reaching values of -0.84 °C, while the *temp2* anomaly between the alake13ka and alakeGLAC is -0.46 °C. Interestingly, highest seasonal differences are not exclusively limited to regional summer, but peak during MAM in case of alake13ka - alakeGLAC, during boreal winter in case of plake - alake13ka and during summer when calculation plake - alakeGLAC.
The general patterns of anomalies stays the same when reducing calculations to land surface only, but anomalies are more pronounced in comparison. Highest anomalies in mean

2m temperature are reached again for `plake-alakeGLAC`, where temperature is lower by 1 °C. During MAM, comparing `alake13ka` as well as `plake` to `alakeGLAC` shows even quite the same difference (1.30 and 1.29 °C respecively), indicating that lakes are behaving similarly during this time independent of the new temperature routine. Winter temperatures are in contrast quite different when comparing `plake` to the other two scenarios. The strongly reduced 2m temperature in the latter scenario might cause a reduced ice loss during regional winter.

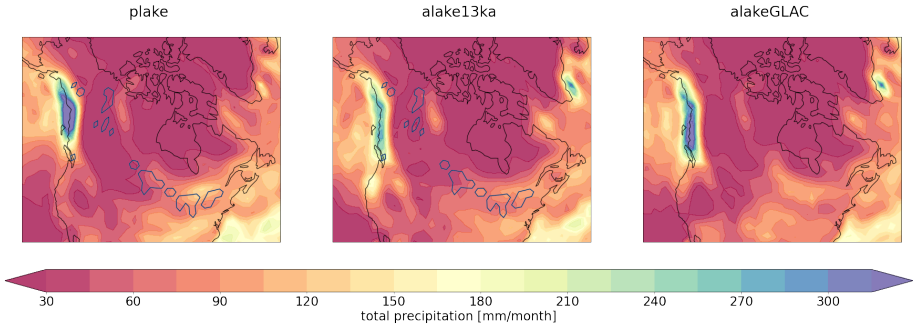

Figure 4.7: Mean monthly precipitation for summer months in northern Europe. Blue lines indicate location of lakes.

As far as seasonal (JJA) precipitation is considered, *plake* as well as `alakeGLAC` show high values in the southwestern tip of Norway, while all scenarios share a region of lower precipitation in the northeastern margins of Scandinavia (as depicted in 4.7). They also show higher precipitation in general along the coast, which is again a result of moist air coming from the Atlantic ocean and reaching a steep mountainous region even higher due to its ice cover. Precipitation is higher above the lakes that are calculated with freely evolving temperatures as in `alake13ka`, while these areas receive less rainfall in case of `plake`. Further figures including evaporation and temperature in 2m height can be seen in Appendix A.

When looking at significance, as was done in section 4.2, anomalies in annual 2m temperature can only be found above the new lake centre for `alake13ka-alakeGLAC`. This is not a surprise, since lake surface was the only parameter changed here. Staying with these two scenarios, significant anomalies can be found in the southwestern UK and neighbouring French coast, while high anomalies of up to -2 °C are indicated for Iceland and parts of

the Arctic Sea, along the Greenland coast during DJF. This could be either linked to the BIL in Europe or to the extensive lakes in northern America. Most pronounced negative changes take place in boreal summer months, with a relevant significance throughout big parts of northeastern Europe, extending even to the Ural mountains. Interestingly, there is also a slight increase in *temp2* north of the new lakes.

Significant anomalies in this region are mostly absent for `plake` and `alake13ka` when concentrating on annual 2m temperature, only showing negative anomalies for the proglacial lakes - confirming the correct implementation of the new temperature routine. Boreal winter season is more interesting, showing a high negative temperature difference (-1.5 °C) for southern Norway, while the Seas bordering northeastern Greenland and Svalbard show high positive anomalies of up to 2 °C. Also, there's an indication for a dipole pattern, posing cooler temperatures around the new proglacial lakes as well as the eastern side of the Ural mountains, opposed by higher temperatures in the Arctic Sea. Boreal summer months show a slight cooling (-1 °C) for most parts of central and northern Europe, temperatures decreasing severely (<-4 °C) towards the centre of the proglacial lakes.

For the `plake` and `alakeGLAC` anomalies are most pronounced above the new lake surfaces, that are land in the latter. there is no significant anomaly indicated by the t-test when looking at annual 2m temperature. Also, boreal winter months come with significant reductions in 2m temperature, these changes being highest above the southern tip of Norway and also including drops in temperature for Iceland. Furthermore, large parts of Europe are affected. Most pronounced are these effects during JJA, spanning a still wider region that is affected by lower 2m temperatures, peaking above the new lake surfaces, but also showing one slight positive anomaly north of the new lake which shall be discussed later. Again, additional figures depicting the results of the significance-testing for DJF and annually can be seen in Appendix A.

Glacier depth in this region - as derived from ECHAM6 - also is highest towards the `plake` scenario, supporting the claim once more, that proglacial lakes have a positive effect on glacier growth. Still, the truth to this should be discussed in more detail using the dEBM output in the next section.

4.5.2 Results from the dEBM

Output from the dEBM is quite different for FIS when compared to LIS. Again, it should be mentioned that these values represent only data above the ice sheets without including any land or sea surface.

Patterns for annual *SMB* and the anomalies between the simulations can be seen in Fig. 4.8. They are similar throughout all scenarios, but with changes in the range of losses. In contrast to LIS, FIS generally looses mass pointing towards a highly unstable state of the ice sheet during the 13 ka BP timeslice. It can be seen, that annual surface mass balance (as a mean over 30 years) is highest in a `plake` setting and lowest in `alakeGLAC`. The ice sheet shows massive losses towards the continental margins in all three simulations, while positive *SMB* values are only found in a smaller area of the very center, not being able to compensate the other regions. Particularly high values are reached during regional summer months, where up to nine meters are lost in height per year. The exact same figure but for JJA can be seen in Appendix A. These severe reductions take place mainly in one spot at the middle of the continental side of the ice sheet, meeting in case of `plake` and `alake13` the Baltic Ice Lake, while `alakeGLAC` treats this region mainly as land. The extent of losses becomes clear when pointing towards the yearly mean accumulation, where *alakeGLAC* has highest values of -544 Gt followed by `alake13ka` with -333 Gt and lastly `plake`, only loosing -254 Gt (negative values indicate overall losses) per year. This difference in lost ice makes up for a global sea level rise of 0.8 mm per year between the two most distinct ones (Zemp et al., 2019).

Cloud cover generally is higher in case of FIS, probably owning to a rather large exposure to water surfaces. In `alake13ka` and `plake` the ice sheet is flanked in the Northwest by the ocean, the Southeast is neighbour to the Baltic Ice Lake (BIL), while in `alakeGLAC` this water body is not existent. This might be the reason for a slightly smaller cloud cover, most pronounced during boreal summer months when evaporation off the BIL is a big factor. Mean precipitation is still higher in `alakeGLAC` than in `plake`, which is probably again due to generally higher temperatures in the first scenario.

While for LIS, mean *temp2* above the ice sheet is higher in `plake` than in `alake13ka`, in case of FIS, `plake` continually shows lowest temperatures except during SON. These val-

ues can be seen in Tab. 4.2. Surface mass balance is negative throughout all simulations but highest for `alakeGLAC`, where FIS looses more than twice the volume compared to `plake`. This indicated an overall positive effect of proglacial lakes on glacier growth.
Runoff and accumulation patters in general seem to be quite similar throughout all simulations. Highest accumulation values are found in the northern parts of FIS, while gradually less accumulation takes place toward the southeastern tip. In `alakeGLAC`, accumulation is again slightly higher than in the other two scenarios. Biggest differences can be found in runoff, where FIS looses most during the `alakeGLAC` scenario and least during in case of `plake`. More on this topic can be found in the Appendix A. Patterns, as stated before in case of LIS, are similar in all three simulations, showing no runoff at the central ice sheet and an increase towards margins. Generally, FIS seems to be more stable toward the northwestern borders than towards its continental side. In contrast to the findings regarding the North American ice sheets, the Fennoscandian seems to be highly unstable in this climate setting.

	alakeGLAC	alake13ka	plake
Cloud cover [%]	67.16658	68.25315	68.38377
Seasonal cloud cover [%]			
DJF	71.77724	71.48821	70.51737
MAM	64.55079	63.60298	63.66415
JJA	62.45673	67.1532	67.66633
SON	69.88159	70.7682	71.68722
Precipitation [kg/m^2/s]	0.6236766	0.6265686	0.6122497
Seasonal precipitation [kg/m^2/s]			
DJF	0.5004489	0.5041388	0.444308
MAM	0.553794,	0.5156256	0.5145339
JJA	0.7244149	0.7371764	0.7402261
SON	0.7160486	0.7493335	0.749931
2m temperature [K]	259.8155	259.4994	259.2247
Seasonal 2m temperature [K]			
DJF	248.3979	248.3605	247.2168
MAM	258.4352	257.2766	257.2241
JJA	271.5979	271.2904	271.1637
SON	260.8311	261.0701	261.2941
Surface mass balance [Gt/year]	-543.5422	-332.6989	-253.9887

Table 4.2: Climate parameters and surface mass balance for all simulations over 30 years above the Fennoscandian ice sheet. Except from SMB, numbers represent mean values.

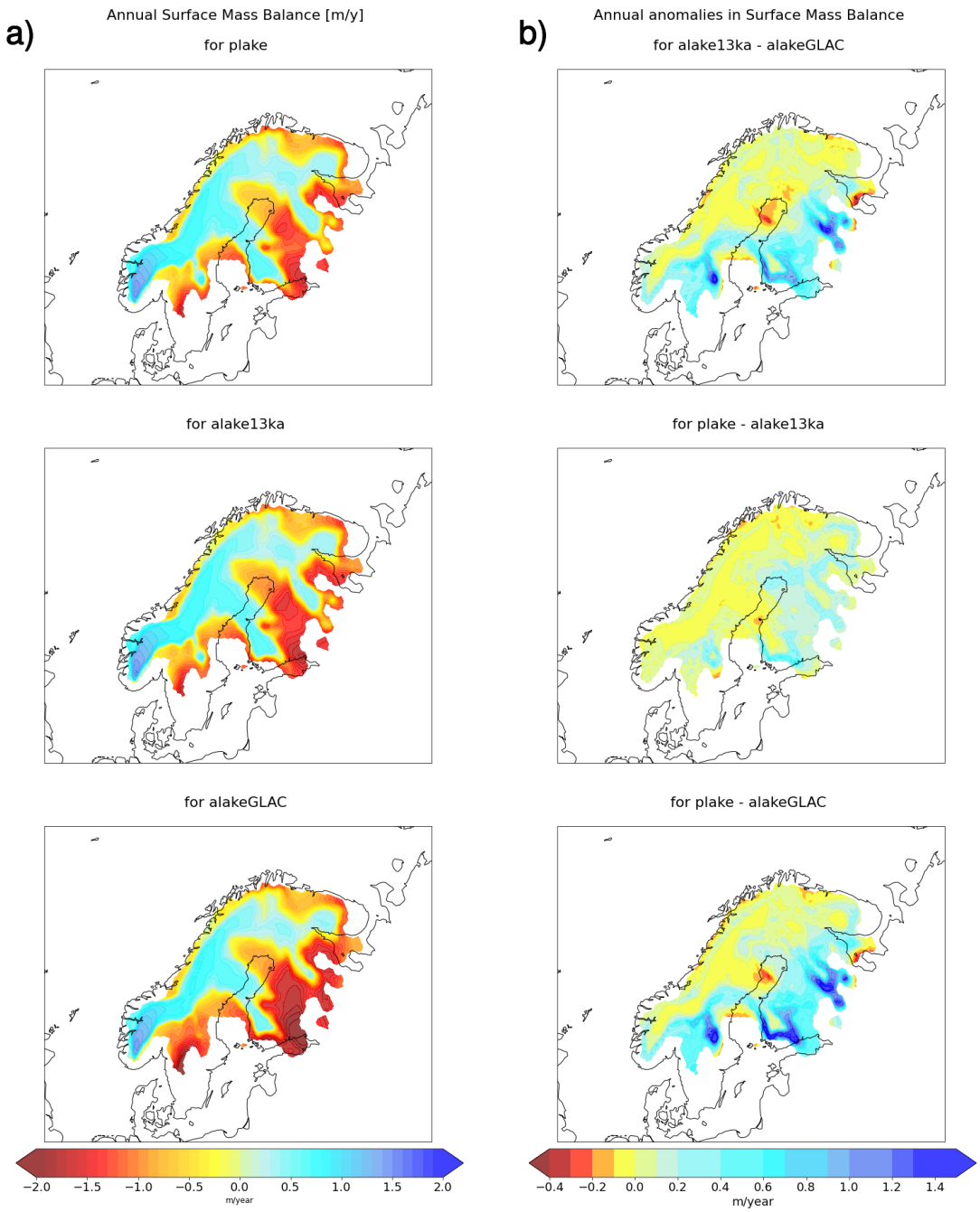

Figure 4.8: Surface mass balance for the Fennoscandian ice sheet showing a) annual mean and b) annual anomaly. Output from dEBM.

5 Discussion

The conducted experiment is aimed to help understand the effect of proglacial lakes on the climate and surface mass balance in an equilibrium state during the Bølling-Allerød interstadial at 13 ka BP. The hypothesis was that the presence of proglacial lakes results in cooler summers and a delay of ice sheet retreat through modified regional conditions, as stated by Tweed and Carrivick (2015) among others. Even though the relevance of proglacial lakes for (regional and large scale) climate is stated in several studies (Carrivick and Tweed, 2013; Pasquini et al., 2008; Teller, 2003), ECHAM6 lacked the ability to calculate these lakes with their proper characteristics, therefore posing uncertainties to this subject in model calculations. This study successfully provides a way for ECHAM6 to fill this gap and account for proglacial lakes in a climate simulation using the novel implementation of `plake`.

It was found that the climatic effect of proglacial lakes on the retreating Northern Hemisphere ice sheets will primarily increase their surface mass balance and, thus, eventually slow their retreat. The simulations indicate that the effect of proglacial lakes may cause an increase in SMB by approximately 20% and 50% for the Laurentide and Fennoscandian ice sheets respectively. Accumulation decreases by 2% and 4% for LIS and FIS, while runoff decreases by approx. 20 % in both domains. Furthermore, evidence points to the fact that the stabilizing effect is primarily caused by the additional lake surface while the cold surface of proglacial lakes slightly decreases (further increases) the SMB of the LIS (FIS). The reduced summer ablation noted here was also in accordance with findings in Peyaud et al. (2007). Mean seasonal 2m temperature was reduced by 1 to 1.5 °C when it comes to FIS, and slightly more than 0.5 °C in case of LIS, using the `alakeGLAC` as reference. Though this might seem like only a slight change, it can have a considerable effect on evaporation and specific humidity in near surface layers. These findings are in accordance with literature (Krinner et al., 2004; Mangerud et al., 2004).

In general, the two ice sheets displayed a completely different behaviour in this study. The first idea is that continentality plays a crucial role in this regard, though this should be

answered with another experiment, where a stable climate state can be reached. When looking at lake surface temperatures in a setting that has free temperature range (as in `alake13ka`), lakes are completely frozen during the months December to June for norther Europe, while in case of northern America melting starts earlier in May and complete ice coverage returns in January. This can be seen in Appendix A, Tab. A.10. Surface temperature above the European lakes while they're not frozen is 5.7 °C on average, while 5.8 °C is the value for north American lakes. This is not the biggest change and therefore was looked at in more detail. When looked at the specific months, lakes in front of LIS show consistently higher surface temperature than lakes at FIS (the anomaly peaking in September with 3 °C) while melting starts sooner and freezing later. This means, that LIS generally is exposed a longer time period to open water surface while FIS is in contact with an ice lake for half of the year. Nevertheless, there must be done further investigations to understand the exact differences for these two study domains.

Since in reality the climate during this period was anything but stable (as mentioned in section 2.2), several assumptions had to be made for this anticipated stable-state experiment. The aim behind this was to be able to evaluate the specific effect of proglacial lakes without the interference of other large-scale processes (such as a proglacial lake drainage events for example). In this context, it must be said that the aim of an equilibrium state turned out not to be reached during a run time of 100 years. It was shown hereby that the period, although optimistically thought to suffice at first, was unfortunately not enough for the model to get to this state. As will be explained below, most likely the vegetation component JSBACH3.2 did not have enough time to react to new surface and climate conditions. At the end of this experiment, as stated shortly in section 4.1, there was persistent variability on a multi-decadal scale. In an optimal scenario there would only be inner-decadal variability left. This can also be seen in high standard deviation values, which - to give an example - in case of mean 2m temperature was approx. 12 °C for north American land surface and only a little lower (approx. 10 °C) northern Europe, probably due to the higher exposure to marine conditions. However, it is still assumed that the changes so far are generally robust and provide a good insight into the expected climate response.

As mentioned before, possible sources for this continuing high variability were assumed to be related to vegetation dynamics. Through the `dynveg` module, vegetation is allowed to migrate into spaces opened by a reduction in coverage of the former vegetation type. The other possibility for vegetation to occupy uncolonized land is when regions inhospitable are shrinking. Grasses can migrate easier, while wooden vegetation types are somewhat slower. As a result, woody types dominate under low disturbance rates (Reick et al., 2021). In this study, it's possible that forests were evolving around the new lakes where at the start there was uncolonized land, thus leading to the absence of an equilibrium state and instead still showing ongoing developments. One interesting detail is, that vegetation can only be hindered by unfavorable conditions to grow in the first place. It will continue existing, when conditions change to non-bearable for the vegetation type (Reick et al., 2021).

Another uncertainty in this experiments is due to systematic biases in ECHAM6. The following statements concerning this topic can be found in Stevens et al. (2013). Clouds and convection remain limited in their correct representation and pose one of the bigger uncertainties. Low and mid level clouds in particular are simulated too few and at the same time appear too bright, leading to possible regional biases on the order of many tens of W/m_2. In the same context, systematic shifts in major precipitation features, the partitioning of precipitation between land and sea as well as midlatitude jets are counted among the biases in ECHAM6. Improvements in ECHAM6 which are relevant in this study include a more accurate description of albedo, specifically in regard to melt ponds on sea ice. But, on the other, side biases remain over continents when it comes to reflected shortwave irradiance at the top of the atmosphere. One of the bigger regions affected by this is the study domain of the Laurentide ice sheet, which as a consequence tends to be overestimated in shortwave absorption and heats more than appropriate. Tropical changes, which are mentioned in section 4.2, might also result from several biases concerning the tropics (e.g. regarding tropical cloudiness and marine boundary layer - cloud simulation). Regarding this topic, ECHAM6 seems to slightly overestimate precipitation in general, but in specific for large parts of the tropics. Another relevant point is that there is no glacial calving resolved in ECHAM6. In this context, a more realistic scenario would also involve

a transiently evolving ocean which apart from this process also reacts to changes in the SMB an. The mass balance of ice sheets is defined to similar extent by the SMB and the effect of calving, so the analysis of SMB here can only provide one side of a medal. While climate response in the individual experiments might be affected by these shortcomings, the sensitivity to proglacial lakes remains mostly robust.
Lastly, another small point is that interesting insights could be provided by looking at general wind direction. Unfortunately this was not included in this study but should definitely be part of the analysis when the equilibrium state simulation is set up.

While the work conducted in this study contributes to a better representation of our climate system in ECHAM6, it was also showed that the run time used here was not sufficient to reach a stable climate state. This is why it should be repeated with a longer time period (approx. 400 years) to enhance the quality of this study's results. Another important aspect is the further development of the namelist switch in such a way that no additional model branch is needed. By this, the handling of the `plake`-subroutine would be highly simplified.
Lastly, the main subject for future work is to make `plake` compatible for coupled runs with AWI-ESM. This could considerably enhance the understanding of proglacial lake related dynamics in a more complex system.

6 Conclusion

The incentive for this project was to improve understanding in regard to the influence of proglacial lakes on SMB and climate of retreating ice sheets. This concerned climate parameters like temperature and precipitation as key descriptors, as well as ice related parameters like the SMB. The answer to the initially asked question, if and to what extent proglacial lakes influence these, was answered for two ice sheets (LIS and FIS) during the Allerød interstadial. It was shown, that large proglacial lakes had a stabilizing effect on retreating ice sheets of northern America and Europe during the last deglaciation.

A way to account for proglacial lakes and their specific characteristics was created by the novel implementation of the `plake` subroutine to ECHAM6's source code. Even though this first implementation was considered successful in a way that the subroutine is working, it will be interesting to expand this to a longer time period as well as extend its use to coupled experiments in the future.

While the `plake` subroutine can be used for paleoclimatic studies when there were more extensive proglacial lakes than today, they also play a role in the current setting with a globally warming climate. Here, proglacial lakes evolve as a result to glacier retreat and even though they do not reach the extent of those large historical lakes, their local impact can be assessed using the `plake` subroutine. This additionally highlights the relevance and future potential of this study's work.

Bibliography

Andersen, B. and Borns, H. (1994). *The Ice Age world: an introduction to Quaternary history and research with emphasis on North America and northern Europe during the last 2.5 million years*. Number 551.33 AND.

Andrén, T., Lindeberg, G., and Andrén, E. (2002). Evidence of the final drainage of the baltic ice lake and the brackish phase of the yoldia sea in glacial varves from the baltic sea. *Boreas*, 31(3):226–238.

Andrés-Martínez, M., Barbi, D., Cristini, L., Gierz, P., Ural, D., and Wieters, N. (2020). Esm-tools version 5.0: A modular infrastructure for stand-alone and coupled earth system modelling.

Bennike, O., Sarmaja-Korjonen, K., and Seppänen, A. (2004). Reinvestigation of the classic late-glacial bølling sø sequence, denmark: chronology, macrofossils, cladocera and chydorid ephippia. *Journal of Quaternary Science*, 19(5):465–478.

Berger, A. and Loutre, M. (1991). Insolation values for the climate of the last 10 million years. *Quaternary Science Reviews*, 10(4):297–317.

Berger, W., Bickert, T., Schmidt, H., and Wefer, G. (1993). 22. quaternary oxygen isotope record of pelagic foraminifers: site 806, ontong java plateau. In *Proceedings ODP: Scientific Results*, volume 130, pages 381–395.

Björck, S., Walker, M., Cwynar, L., Johnsen, S., Knudsen, K., Lowe, J., and Wohlfarth, B. (1998). An event stratigraphy for the last termination in the north atlantic region based on the greenland ice-core record: a proposal by the intimate group. *Journal of Quaternary Science*, 13(4):283–292.

Björnsson, H. (2000). Jökulhaups in iceland: Characteristics and impact. In *Second International Conference on Mars Polar Science and Exploration*, number 1057, page 8.

Bolch, T., Duethmann, D., Wortmann, M., Liu, S., and Disse, M. (2021). Declining glaciers

endanger sustainable development of the oases along the aksu-tarim river (central asia). *International Journal of Sustainable Development & World Ecology*, pages 1–10.

Bond, G., Broecker, W., Johnsen, S., McManus, J., Labeyrie, L., Jouzel, J., and Bonani, G. (1993). Correlations between climate records from north atlantic sediments and greenland ice. *Nature*, 365(6442):143–147.

Brendryen, J., Haflidason, H., Yokoyama, Y., Haaga, K., and Hannisdal, B. (2020). Eurasian ice sheet collapse was a major source of meltwater pulse 1a 14,600 years ago. *Nature Geoscience*, 13(5):363–368.

Brunke, M. (2011). The components of a climate model. `http://www.u.arizona.edu/~brunke/modeling/model-components.html`. [Online; accessed 04-March-2022].

Carlson, A. E., Ullman, D. J., Anslow, F. S., He, F., Clark, P. U., Liu, Z., and Otto-Bliesner, B. L. (2012). Modeling the surface mass-balance response of the laurentide ice sheet to bølling warming and its contribution to meltwater pulse 1a. *Earth and Planetary Science Letters*, 315:24–29.

Carrivick, J. and Tweed, F. (2013). Proglacial lakes: character, behaviour and geological importance. *Quaternary Science Reviews*, 78:34–52.

Carrivick, J., Tweed, F., Ng, F., Quincey, D., Mallalieu, J., Ingeman-Nielsen, T., Mikkelsen, A., Palmer, S., Yde, J., Homer, R., et al. (2017). Ice-dammed lake drainage evolution at russell glacier, west greenland. *Frontiers in Earth Science*, 5:100.

Clark, P., Dyke, A., Shakun, J., Carlson, A., Clark, J., Wohlfarth, B., Mitrovica, J., Hostetler, S., and McCabe, A. (2009). The last glacial maximum. *science*, 325(5941):710–714.

Clark, P., Pisias, N., Stocker, T., and Weaver, A. (2002). The role of the thermohaline circulation in abrupt climate change. *Nature*, 415(6874):863–869.

Clarke, G., Leverington, D., Teller, J., and Dyke, A. (2003). Superlakes, megafloods, and abrupt climate change. *Science*, 301(5635):922–923.

Claussen, M., Ganopolski, A., Brovkin, V., Gerstengarbe, F., and Werner, P. (2003). Simulated global-scale response of the climate system to dansgaard/oeschger and heinrich events. *Climate Dynamics*, 21(5):361–370.

Cohen, K., Finney, S., and Gibbard, P. (2013). The ics international chronostratigraphic chart. `http://www.stratigraphy.org/ICSchart/ChronostratChart2015-01.pdf`. [Online; accessed 15-November-2021].

Decremer, D., Chung, C. E., Ekman, A. M. L., and Brandefelt, J. (2014). Which significance test performs the best in climate simulations? *Tellus A: Dynamic Meteorology and Oceanography*, 66(1):23139.

Dokken, T., Nisancioglu, K., Li, C., Battisti, D., and Kissel, C. (2013). Dansgaard-oeschger cycles: Interactions between ocean and sea ice intrinsic to the nordic seas. *Paleoceanography*, 28(3):491–502.

EarthObservatory (2000). Milutin milankovitch (1879-1958). `https://earthobservatory.nasa.gov/features/Milankovitch/milankovitch_2.php`. [Online; accessed 02-March-2022].

Elliot, M., Labeyrie, L., and Duplessy, J. (2002). Changes in north atlantic deep-water formation associated with the dansgaard–oeschger temperature oscillations (60–10 ka). *Quaternary Science Reviews*, 21(10):1153–1165.

Fairbanks, R. (1989). A 17,000-year glacio-eustatic sea level record: influence of glacial melting rates on the younger dryas event and deep-ocean circulation. *Nature*, 342(6250):637–642.

Fairbanks, R., Mortlock, R., Chiu, T., Cao, L., Kaplan, A., Guilderson, T., Fairbanks, T., Bloom, A., Grootes, P., and Nadeau, M. (2005). Radiocarbon calibration curve spanning 0 to 50,000 years bp based on paired 230th/234u/238u and 14c dates on pristine corals. *Quaternary Science Reviews*, 24(16-17):1781–1796.

Galbraith, E., Merlis, T., and Palter, J. (2016). Destabilization of glacial climate by the radiative impact of atlantic meridional overturning circulation disruptions. *Geophysical Research Letters*, 43(15):8214–8221.

Gierz, P. (2022). Echam6. `https://gitlab.awi.de/pgierz/echam6`. [Online; accessed 08-March-2022].

Giorgetta, M., Roeckner, E., Mauritsen, T., Bader, J., Crueger, T., Esch, M., Rast, S., Kornblueh, L., Schmidt, H., Kinne, S., et al. (2013). The atmospheric general circulation model echam6-model description.

Glas, R., Lautz, L., McKenzie, J., Mark, B., Baraer, M., Chavez, D., and Maharaj, L. (2018). A review of the current state of knowledge of proglacial hydrogeology in the cordillera blanca, peru. *Wiley Interdisciplinary Reviews: Water*, 5(5):e1299.

Hays, J., Imbrie, J., Shackleton, N., et al. (1976). Variations in the earth's orbit: pacemaker of the ice ages. American Association for the Advancement of Science Washington, DC.

Heidari, M., Song, Z., Degregori, E., Behrens, J., and Bockelmann, H. (2021). Concurrent calculation of radiative transfer in the atmospheric simulation in echam-6.3.05p2. *Geoscientific Model Development*, 14(12):7439–7457.

Hinck, S., Gowan, E., Zhang, X., and Lohmann, G. (2020). Pism-lakecc: Implementing an adaptive proglacial lake boundary into an ice sheet model. *The Cryosphere Discussions*, 2020:1–36.

Huss, M., Bookhagen, B., Huggel, C., Jacobsen, D., Bradley, R., Clague, J., Vuille, M., Buytaert, W., Cayan, D., Greenwood, G., et al. (2017). Toward mountains without permanent snow and ice. *Earth's Future*, 5(5):418–435.

Ivanovic, R., Gregoire, L., Kageyama, M., Roche, D., Valdes, P., Burke, A., Drummond, R., Peltier, W., and Tarasov, L. (2016). Transient climate simulations of the deglaciation 21–9 thousand years before present (version 1)–pmip4 core experiment design and boundary conditions. *Geoscientific Model Development*, 9(7):2563–2587.

Kaltenborn, B., Nellemann, C., and Vistnes, I. (2010). *High mountain glaciers and climate change: challenges to human livelihoods and adaptation*. UNEP, GRID-Arendal.

Kelletat, D. (2005). *Pleistocene Epoch*, pages 772–773. Springer Netherlands, Dordrecht.

Kinne, S., O'Donnel, D., Stier, P., Kloster, S., Zhang, K., Schmidt, H., Rast, S., Giorgetta, M., Eck, T., and Stevens, B. (2013). Mac-v1: A new global aerosol climatology for climate studies. *Journal of Advances in Modeling Earth Systems*, 5(4):704–740.

Knorr, G. and Lohmann, G. (2003). Southern ocean origin for the resumption of atlantic thermohaline circulation during deglaciation. *Nature*, 424(6948):532–536.

Köhler, P., Nehrbass-Ahles, C., Schmitt, J., Stocker, T., and Fischer, H. (2017). A 156 kyr smoothed history of the atmospheric greenhouse gases co 2, ch 4, and n 2 o and their radiative forcing. *Earth System Science Data*, 9(1):363–387.

Krebs-Kanzow, U., Gierz, P., Rodehacke, C., Xu, S., Yang, H., and Lohmann, G. (2021). The diurnal energy balance model (debm): a convenient surface mass balance solution for ice sheets in earth system modeling. *The Cryosphere*, 15(5):2295–2313.

Krinner, G., Mangerud, J., Jakobsson, M., Crucifix, M., Ritz, C., and Svendsen, J. (2004). Enhanced ice sheet growth in eurasia owing to adjacent ice-dammed lakes. *Nature*, 427(6973):429–432.

Krivonogov, S., Sheinkman, V., and Mistruykov, A. (2005). Stages in the development of the darhad dammed lake (northern mongolia) during the late pleistocene and holocene. *Quaternary International*, 136(1):83–94.

Krueger, S. and Damrath, M. (2020). In search of the Bolling-Oscillation: a new high resolution pollen record from the locus classicus Lake Bolling, Denmark. *VEGETATION HISTORY AND ARCHAEOBOTANY*, 29(2):189–211.

Lisiecki, L. and Stern, J. (2016). Regional and global benthic δ18o stacks for the last glacial cycle. *Paleoceanography*, 31(10):1368–1394.

Lotter, A., Heiri, O., Brooks, S., van Leeuwen, J., Eicher, U., and Ammann, B. (2012). Rapid summer temperature changes during termination 1a: high-resolution multi-proxy climate reconstructions from gerzensee (switzerland). *Quaternary Science Reviews*, 36:103–113. The INTegration of Ice core, Marine and TErrestrial records of the last termination (INTIMATE) 60,000 to 8000 BP.

Mangerud, J., Andersen, S., Berglund, B., and Donner, J. (1974). Quaternary stratigraphy of norden, a proposal for terminology and classification. *Boreas*, 3:109–126.

Mangerud, J., Jakobsson, M., Alexanderson, H., Astakhov, V., Clarke, G., Henriksen, M., Hjort, C., Krinner, G., Lunkka, J., Möller, P., Murray, A., Nikolskaya, O., Saarnisto, M., and Svendsen, J. (2004). Ice-dammed lakes and rerouting of the drainage of northern eurasia during the last glaciation. *Quaternary Science Reviews*, 23(11):1313–1332. Quaternary Environments of the Eurasian North (QUEEN).

Marshall, S. and Koutnik, M. (2006). Ice sheet action versus reaction: Distinguishing between heinrich events and dansgaard-oeschger cycles in the north atlantic. *Paleoceanography*, 21(2).

Milanković, M. (1930). Mathematische klimalehre und astronomische theorie der klimaschwankungen, handbuch der klimatologie, bdi, teil a, hrg. *Koppen/Geiger, Berlin*.

Milanković, M. (1941). *Kanon der Erdbestrahlung und seine Anwendung auf das Eiszeitenproblem: Königlich Serbische Akademie*. Königl. Serbische Akademie.

Murton, D. and Murton, J. (2012). Middle and late pleistocene glacial lakes of lowland britain and the southern north sea basin. *Quaternary International*, 260:115–142. Commemorative Volume in Honour of Jim Teller.

Nabi, G., Ali, M., Khan, S., and Kumar, S. (2019). The crisis of water shortage and pollution in pakistan: Risk to public health, biodiversity, and ecosystem. *Environmental science and pollution research*, 26(11):10443–10445.

Newman, M. and Rood, R. (1977). Implications of solar evolution for the earth's early atmosphere. *Science*, 198(4321):1035–1037.

Paillard, D. and Labeyriet, L. (1994). Role of the thermohaline circulation in the abrupt warming after heinrich events. *Nature*, 372(6502):162–164.

PalMod (2022). PalMod german climate modeling initiative. `https://www.palmod.de/de/home`. [Online; accessed 26-January-2022].

Pasquini, A., Lecomte, K., and Depetris, P. (2008). Climate change and recent water level variability in patagonian proglacial lakes, argentina. *Global and Planetary Change*, 63(4):290–298.

Patton, H., Hubbard, A., Andreassen, K., Auriac, A., Whitehouse, P., Stroeven, A., Shackleton, C., Winsborrow, M., Heyman, J., and Hall, A. (2017). Deglaciation of the eurasian ice sheet complex. *Quaternary Science Reviews*, 169:148–172.

Peltier, W. (1998). Postglacial variations in the level of the sea: Implications for climate dynamics and solid-earth geophysics. *Reviews of geophysics*, 36(4):603–689.

Peltier, W. and Fairbanks, R. (2006). Global glacial ice volume and last glacial maximum duration from an extended barbados sea level record. *Quaternary Science Reviews*, 25(23-24):3322–3337.

Peyaud, V., Ritz, C., and Krinner, G. (2007). Modelling the early weichselian eurasian ice sheets: role of ice shelves and influence of ice-dammed lakes. *Climate of the Past*, 3(3):375–386.

Rae, J., Sarnthein, M., Foster, G., Ridgwell, A., Grootes, P., and Elliott, T. (2014). Deep water formation in the north pacific and deglacial co2 rise. *Paleoceanography*, 29(6):645–667.

Rahmstorf, S. (2006). Thermohaline ocean circulation. *Encyclopedia of quaternary sciences*, 5.

Rast, S., Brokopf, R., Cheedela, S., Esch, M., Gayler, V., Kirchner, I., Kornblüh, L., Rhodin, A., Schmidt, H., Schulzweida, U., et al. (2013). User manual for echam6-june 21, 2013,(2013-02-26), version echam-6.1. 06p3-guide-1.3.

Raymond, C., Neumann, T., Rignot, E., Echelmeyer, K., Rivera, A., and Casassa, G. (2005). Retreat of glaciar tyndall, patagonia, over the last half-century. *Journal of Glaciology*, 51(173):239–247.

Reick, C., Gayler, V., Goll, D., Hagemann, S., Heidkamp, M., Nabel, J., Raddatz, T., Roeckner, E., Schnur, R., and Wilkenskjeld, S. (2021). Jsbach 3-the land component of the mpi earth system model: documentation of version 3.2.

Richards, J., Moore, R., and Forrest, A. (2012). Late-summer thermal regime of a small proglacial lake. *Hydrological Processes*, 26(18):2687–2695.

Riebeek, H. and Simmon, R. (2006). Paleoclimatology: Explaining the evidence. `https://earthobservatory.nasa.gov/features/Paleoclimatology_Evidence`. [Online; accessed 02-March-2022].

Saltzman, B. (2002). *Dynamical paleoclimatology generalized theory of global climate change*. Volume 80 in the International geophysics series. Academic Press, San Diego.

Samartin, S., Heiri, O., Lotter, A., and Tinner, W. (2012). Climate warming and vegetation response after Heinrich event 1 (16 700-16 000 cal yr BP) in Europe south of the Alps. *CLIMATE OF THE PAST*, 8(6):1913–1927.

Schulzweida, U. (2021). Cdo user guide.

Sijbrandij, L. (2022). Climate feedbacks: Proglacial lakes. `https://gitlab.awi.de/paleodyn/Students/lianne-sijbrandij/climate-feedbacks-proglacial-lakes`. [Online; accessed 08-March-2022].

Skinner, L., Fallon, S., Waelbroeck, C., Michel, E., and Barker, S. (2010). Ventilation of the deep southern ocean and deglacial co¡sub¿2¡/sub¿ rise. *Science*, 328(5982):1147–1151.

Stevens, B., Giorgetta, M., Esch, M., Mauritsen, T., Crueger, T., Rast, S., Salzmann, M., Schmidt, H., Bader, J., Block, K., Brokopf, R., Fast, I., Kinne, S., Kornblueh, L., Lohmann, U., Pincus, R., Reichler, T., and Roeckner, E. (2013). Atmospheric component of the mpi-m earth system model: Echam6. *Journal of Advances in Modeling Earth Systems*, 5(2):146–172.

Stokes, C. (2017). Deglaciation of the laurentide ice sheet from the last glacial maximum. *Cuadernos de investigación geográfica.*, 43(2):377–428.

Tarasov, L., Dyke, A., Neal, R., and Peltier, W. (2012). A data-calibrated distribution of deglacial chronologies for the north american ice complex from glaciological modeling. *Earth and Planetary Science Letters*, 315:30–40.

Tarasov, L. and Peltier, W. (2002). Greenland glacial history and local geodynamic consequences. *Geophysical Journal International*, 150(1):198–229.

Teller, J. (2001). Formation of large beaches in an area of rapid differential isostatic rebound: the three-outlet control of lake agassiz. *Quaternary Science Reviews*, 20:1649–1659.

Teller, J. (2003). Controls, history, outbursts, and impact of large late-quaternary proglacial lakes in north america. *Developments in quaternary sciences*, 1:45–61.

Thompson, M., Adams, D., and Johnson, K. N. (2009). The albedo effect and forest carbon offset design. *Journal of Forestry*, 107(8):425–431.

Tweed, F. and Carrivick, J. (2015). Deglaciation and proglacial lakes. *Geology Today*, 31(3):96–102.

Vincent, C., Auclair, S., and Le Meur, E. (2010). Outburst flood hazard for glacier-dammed lac de rochemelon, france. *Journal of Glaciology*, 56(195):91–100.

Weaver, A., Saenko, O., Clark, P., and Mitrovica, J. (2003). Meltwater pulse 1a from antarctica as a trigger of the bølling-allerød warm interval. *Science*, 299(5613):1709–1713.

Wunsch, C. (2003). The spectral description of climate change including the 100 ky energy. *Climate Dynamics*, 20(4):353–363.

Yu, J., Menviel, L., Jin, Z., Anderson, R., Jian, Z., Piotrowski, A., Ma, X., Rohling, E., Zhang, F., Marino, G., et al. (2020). Last glacial atmospheric co2 decline due to widespread pacific deep-water expansion. *Nature Geoscience*, 13(9):628–633.

Yu, Z. and Eicher, U. (2004). Three amphi-atlantic century-scale cold events during the bølling-allerød warm period. *Geographie Physique Et Quaternaire*, 55:171–179.

Zemp, M., Huss, M., Thibert, E., Eckert, N., McNabb, R., Huber, J., Barandun, M., Machguth, H., Nussbaumer, S. U., Gärtner-Roer, I., et al. (2019). Global glacier mass changes and their contributions to sea-level rise from 1961 to 2016. *Nature*, 568(7752):382–386.

Eidesstattliche Erklärung

Ich versichere, dass ich die vorliegende Abschlussarbeit ohne fremde Hilfe und ohne Benutzung anderer als der angegebenen Quellen angefertigt habe, und dass die Arbeit in gleicher oder ähnlicher Form noch keiner anderen Prüfungsbehörde vorgelegen hat. Alle Ausführungen der Arbeit, die wörtlich oder sinngemäß übernommen wurden, sind als solche gekennzeichnet.

[Name, Vorname, Unterschrift]

[Ort, Datum]

A Additional figures and tables

A.1 On Variability

As a small hint: Of course, not all variables in all time slices can be depicted, so a selection of the most relevant ones for this study was chosen. This selection can be seen in the following and is only providing supplementary material for the final simulations, since their output is considered the key subject to this thesis.

	alakeGLAC	alake13ka	plake
EU: 2m temp time mean [K]	267.57	267.457	267.094
EU: 2m temp time std [K]	0.108444	0.100977	0.16253
NA: 2m temp time mean [K]	258.875	258.69	258.387
NA: 2m temp time std [K]	0.0359648	0.0634788	0.0974334
GL: 2m temp time mean [K]	283.536	283.52	283.51
GL: 2m temp time std [K]	0.00719756	0.00435948	0.0059704

Table A.1: Mean 2m temperature and standard deviation (std) for a 30y running mean above European (EU) and North American (NA) land surface as well as global surface.

A.2 On Significance

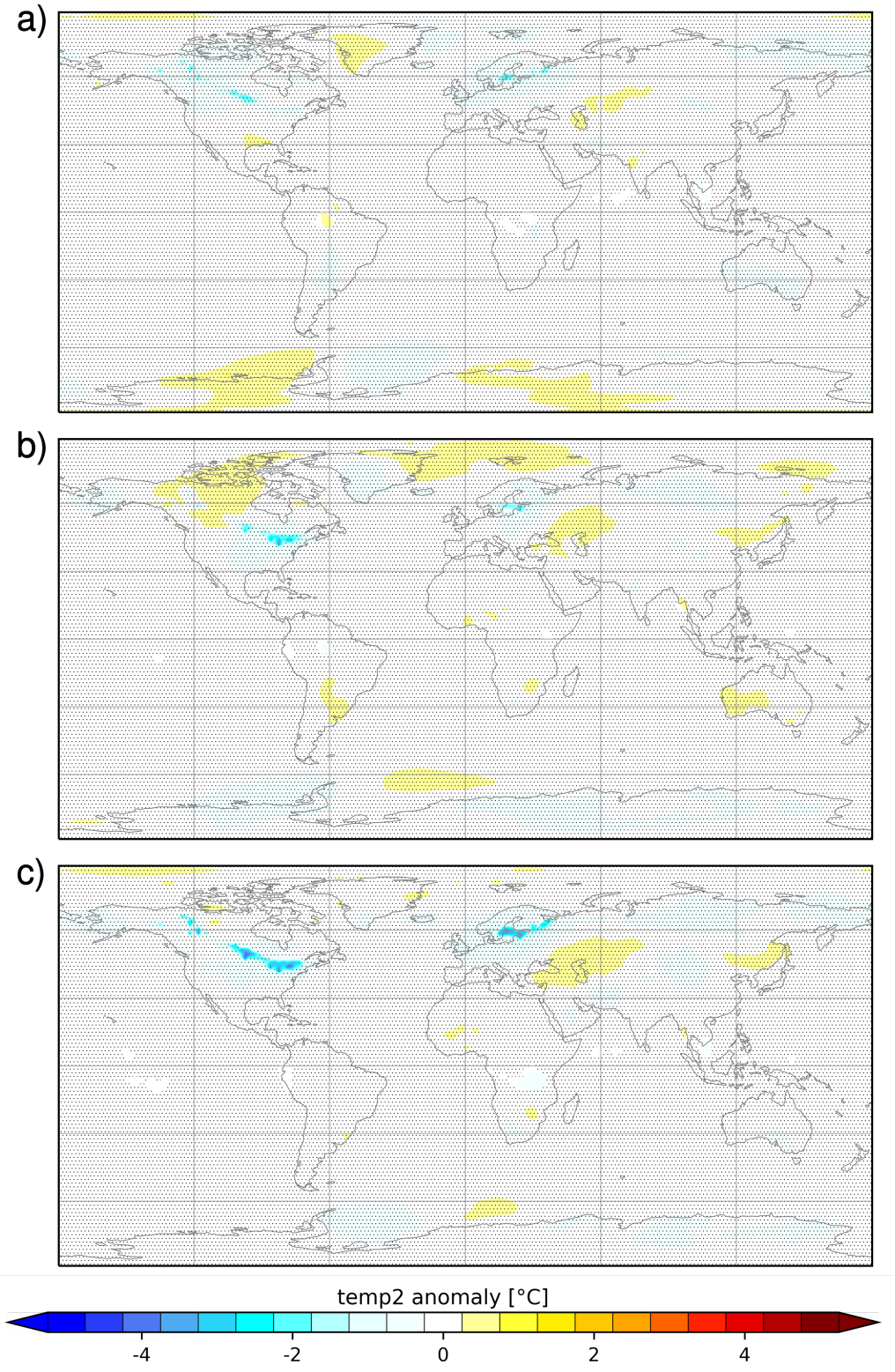

Figure A.1: Global map of changes in annual 2m temperature between a) alake13ka and alakeGLAC, b) plake and alake13ka, c) plake and alakeGLAC. Stippled areas indicate where changes are not significant, while unstippled regions mean significant changes according to a t-test.

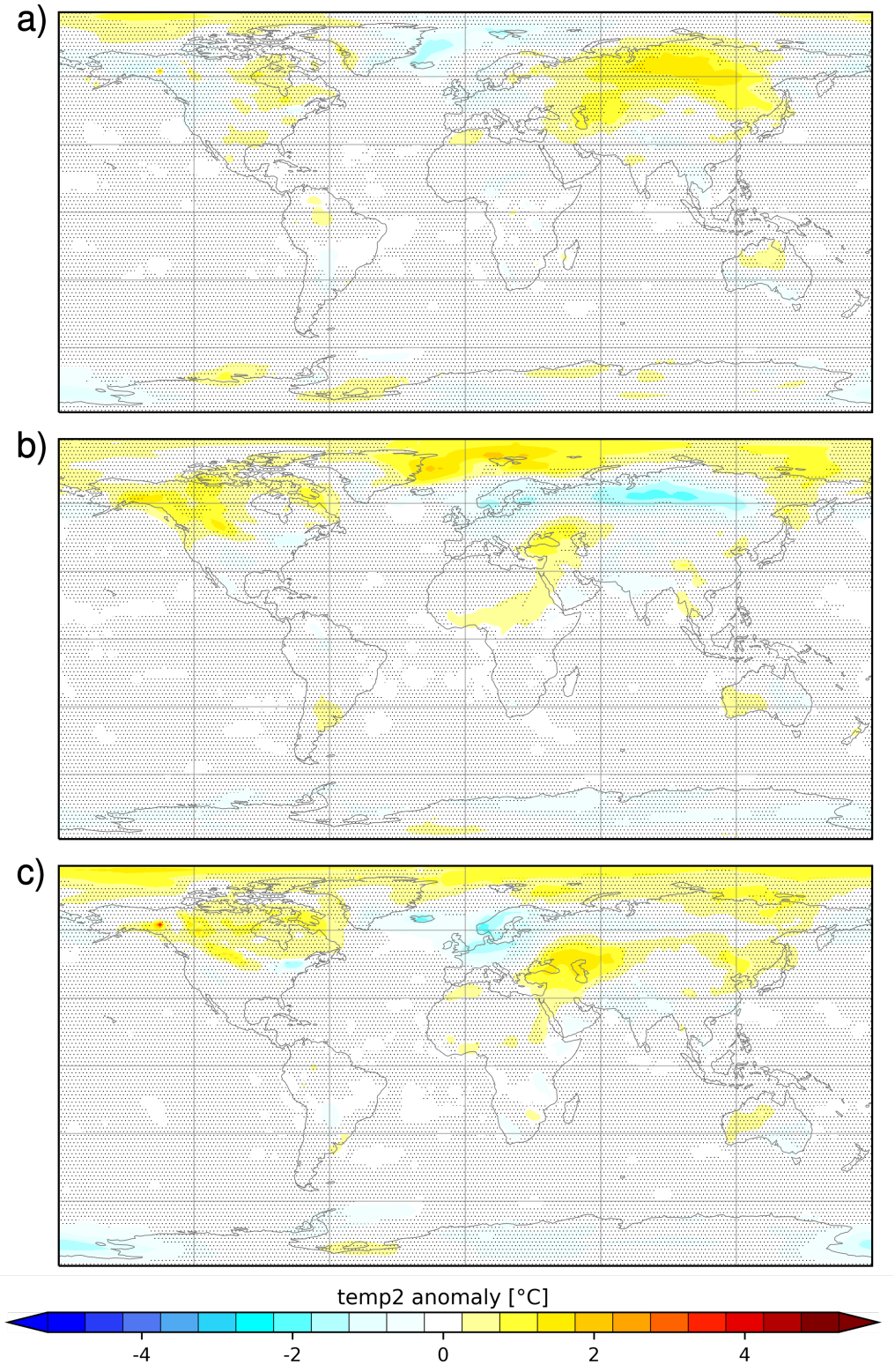

Figure A.2: Global map of changes in seasonal (DJF) 2m temperature between a) alake13ka and alakeGLAC, b) plake and alake13ka, c) plake and alakeGLAC. Stippled areas indicate where changes are not significant, while unstippled regions mean significant changes according to a t-test.

A.3 Further calculations with ECHAM6 output

A.3.1 Globally

	alake13-alakeGL	plake-alake13	plake-alakeGL
2m temperature [K]	-0.0311499	-0.00983737	-0.0409873
Seasonal 2m temperature [K]			
DJF	0.00753999	-0.00163364	0.00590635
MAM	-0.0437235	-0.00220398	-0.0459275
JJA	-0.0736711	-0.0277953	-0.101466
SON	-0.0147457	-0.00771503	-0.0224608
Glacier depth	0.240802	0.0862742	0.327076

Table A.2: Global mean anomalies for the time period 2070-2099.

	alakeGLAC	alake13ka	plake
2m temperature [K]	283.549	283.518	283.508
Seasonal 2m temperature [K]			
DJF	281.586	281.593	281.592
MAM	283.532	283.488	283.486
JJA	285.479	285.405	285.377
SON	283.601	283.586	283.578

Table A.3: Specific global mean values for the time period 2070-2099.

A.3.2 Northern America

	alakeGLAC	alake13ka	plake
2m temperature [K]	258.827	258.535	258.503
corr. standard deviation [K]	12.5828	12.3475	12.062
Seasonal 2m temperature [K]			
DJF	243.83	243.741	244.166
MAM	256.712	256.118	256.128
JJA	275.03	274.194	273.872
SON	259.736	260.086	259.846
corr. standard deviation [K]			
DJF	3.80192	3.91752	3.76389
MAM	7.22136	7.09718	6.97709
JJA	2.39231	2.52324	2.39359
SON	7.85278	7.55867	7.50171
Total precipitation [mm/year]	540.932	538.377	527.136
corr. standard deviation [mm/year]	347.083	342.108	336.835
Seasonal precipitation [mm/month]			
DJF	33.2256	33.2979	32.6675
MAM	38.8432	38.4986	37.8544
JJA	58.8348	57.4099	55.7332
SON	49.4073	50.2525	49.4569
corr. standard deviation [mm/month]			
DJF	16.6377	17.4208	16.8311
MAM	20.1699	19.7501	19.0793
JJA	28.3148	28.0343	26.9163
SON	27.263	27.0542	27.7774

Table A.4: Mean values for the time period 2070-2099 above land surface of northern America, "corr" means corresponding.

	alake13-alakeGL	plake-alake13	plake-alakeGL
2m temperature [K]	-0.195302	-0.0142661	-0.209568
Seasonal 2m temperature [K]			
DJF	-0.0611014	0.336687	0.275586
MAM	-0.399559	-0.00919909	-0.408758
JJA	-0.566425	-0.212336	-0.778761
SON	0.245877	-0.172215	0.0736624

Table A.5: Mean anomalies for the time period 2070-2099 above land and sea surface of northern America.

	alake13-alakeGL	plake-alake13	plake-alakeGL
2m temperature [K]	-0.292207	-0.0317674	-0.323974
Seasonal 2m temperature [K]			
DJF	-0.0889363	0.425025	0.336089
MAM	-0.593651	0.0101451	-0.583506
JJA	-0.835915	-0.322658	-1.15857
SON	0.349674	-0.239581	0.110093

Table A.6: Mean anomalies for the time period 2070-2099 above land surface of northern America

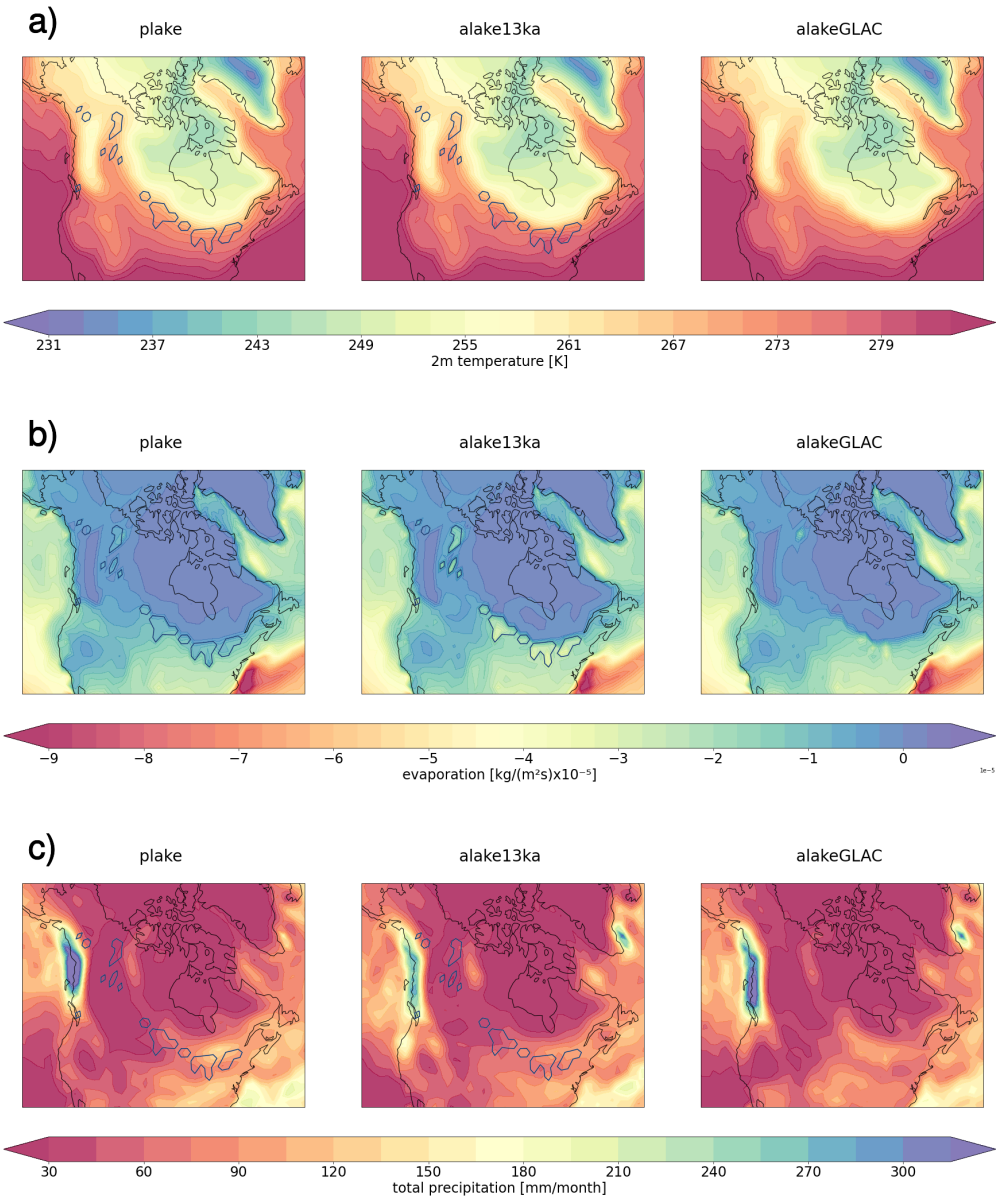

Figure A.3: Mean seasonal (JJA) surface variables for northern America.

A.3.3 Northern Europe

	alakeGLAC	alake13ka	plake
2m temperature [K]	267.926	267.381	266.92
corr. standard deviation [K]	10.2643	9.85494	9.84756
Seasonal 2m temperature [K]			
DJF	256.013	255.939	254.915
MAM	266.649	265.351	265.359
JJA	280.664	279.435	278.717
SON	268.38	268.799	268.688
corr. standard deviation [K]			
DJF	4.64862	4.49644	4.53149
MAM	6.42948	5.91086	5.77503
JJA	1.64414	1.93944	1.62179
SON	6.88388	6.4749	6.19414
Total precipitation [mm/year]	699.987	712.107	699.374
corr. standard deviation [mm/year]	358.888	361.533	355.26
Seasonal precipitation [mm/month]			
DJF	53.1081	53.3681	49.9023
MAM	54.3914	53.6355	53.0788
JJA	64.5237	64.6611	65.2223
SON	61.3059	65.7043	64.9214
corr. standard deviation [mm/month]			
DJF	24.0334	24.037	24.8179
MAM	26.0599	25.2307	24.2315
JJA	33.5753	31.4066	32.0199
SON	28.914	31.3444	28.3967

Table A.7: Mean values for the time period 2070-2099 above land surface of northern Europe.

	alake13-alakeGL	plake-alake13	plake-alakeGL
2m temperature [K]	-0.459141	-0.378421	-0.837562
Seasonal 2m temperature [K]			
DJF	-0.0861677	-0.898123	-0.984291
MAM	-1.07163	0.0184868	-1.05315
JJA	-0.972183	-0.593527	-1.56571
SON	0.293417	-0.0405165	0.2529

Table A.8: Mean anomalies for the time period 2070-2099 including land and sea surface of northern Europe.

	alake13-alakeGL	plake-alake13	plake-alakeGL
2m temperature [K]	-0.545401	-0.46119	-1.00659
Seasonal 2m temperature [K]			
DJF	-0.0738259	-1.02406	-1.09789
MAM	-1.29782	0.00775431	-1.29006
JJA	-1.2291	-0.717793	-1.94689
SON	0.419142	-0.110661	0.308481

Table A.9: Mean anomalies for the time period 2070-2099 above land surface of northern Europe.

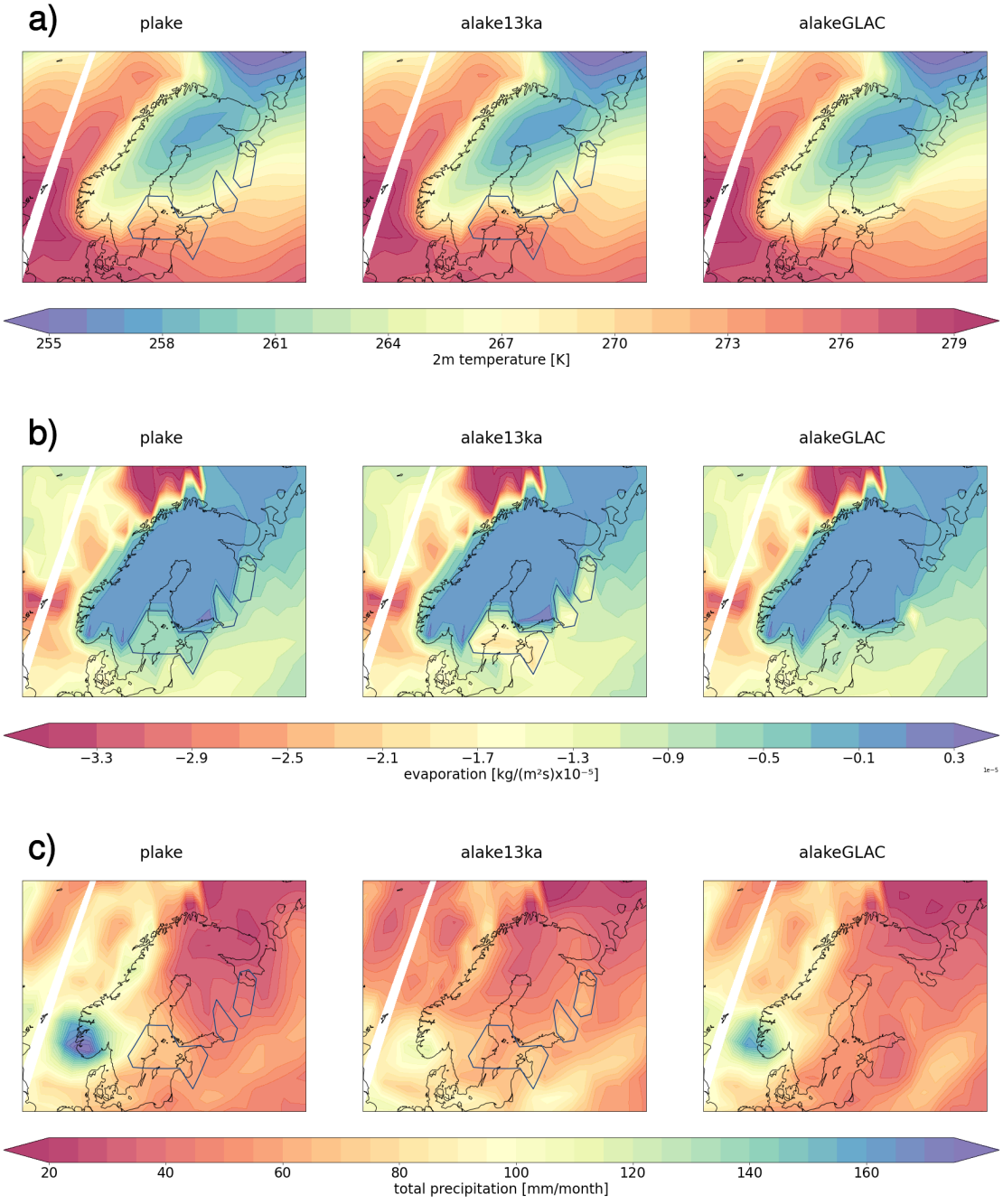

Figure A.4: Mean seasonal (JJA) surface variables for northern Europe.

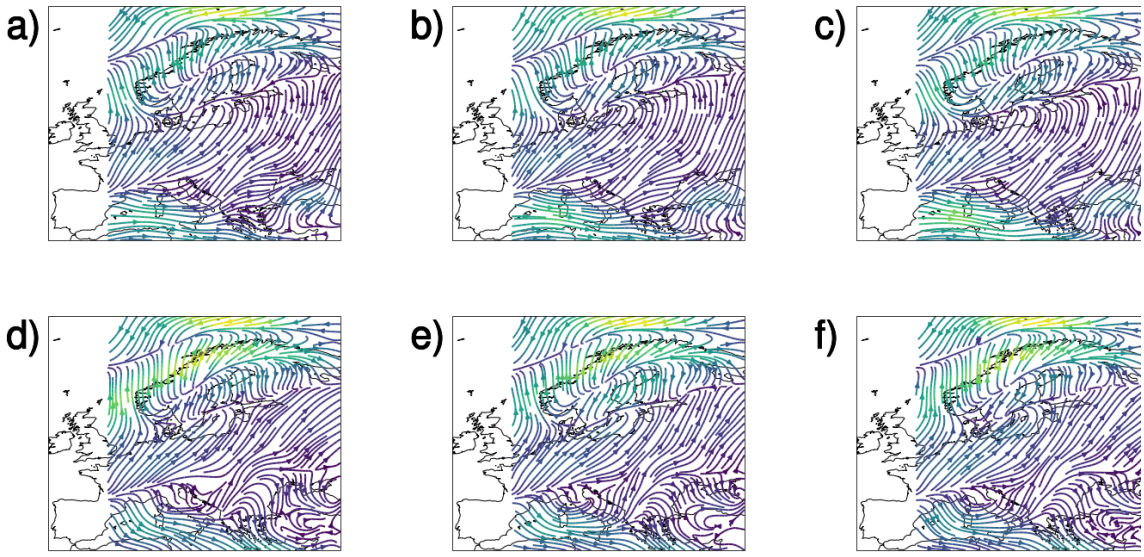

Figure A.5: General wind direction over northern Europe for a) to c) DJF and d) to e) JJA. First column refers to the alakeGLAC scenario, second column to alake13ka and the last to plake.

As indicated here, there was a problem with python calculating wind vectors beyond the 0 meridian. This problem could unfortunately not be solved up to this point, which is why this figure is missing for northern America. Not only is this missing in the appendix part for northern America, it is also knowingly not described in the thesis, since no substantiated statements could be made in this regard. Still, in case of northern Europe, this map gives a clearer notice of how wind patterns look like during two seasons.

A.3.4 Surface water temperature

	FIS lakes	LIS lakes
May	-	273.395
June	274.801	275.154
July	279.646	281.595
August	284.344	287.623
September	283.43	286.367
October	277.718	279.989
November	273.686	274.437
December	-	273.183

Table A.10: tsw values [K] for months of free water surface.

A.4 Calculations for dEBM outdata

A.4.1 LIS

	alakeGLAC	alake13ka	plake
Accumulation	524.34	510.412	500.155
Runoff	247.257	201.466	197.809

Table A.11: Mean accumulation and runoff in [mm/year] for LIS.

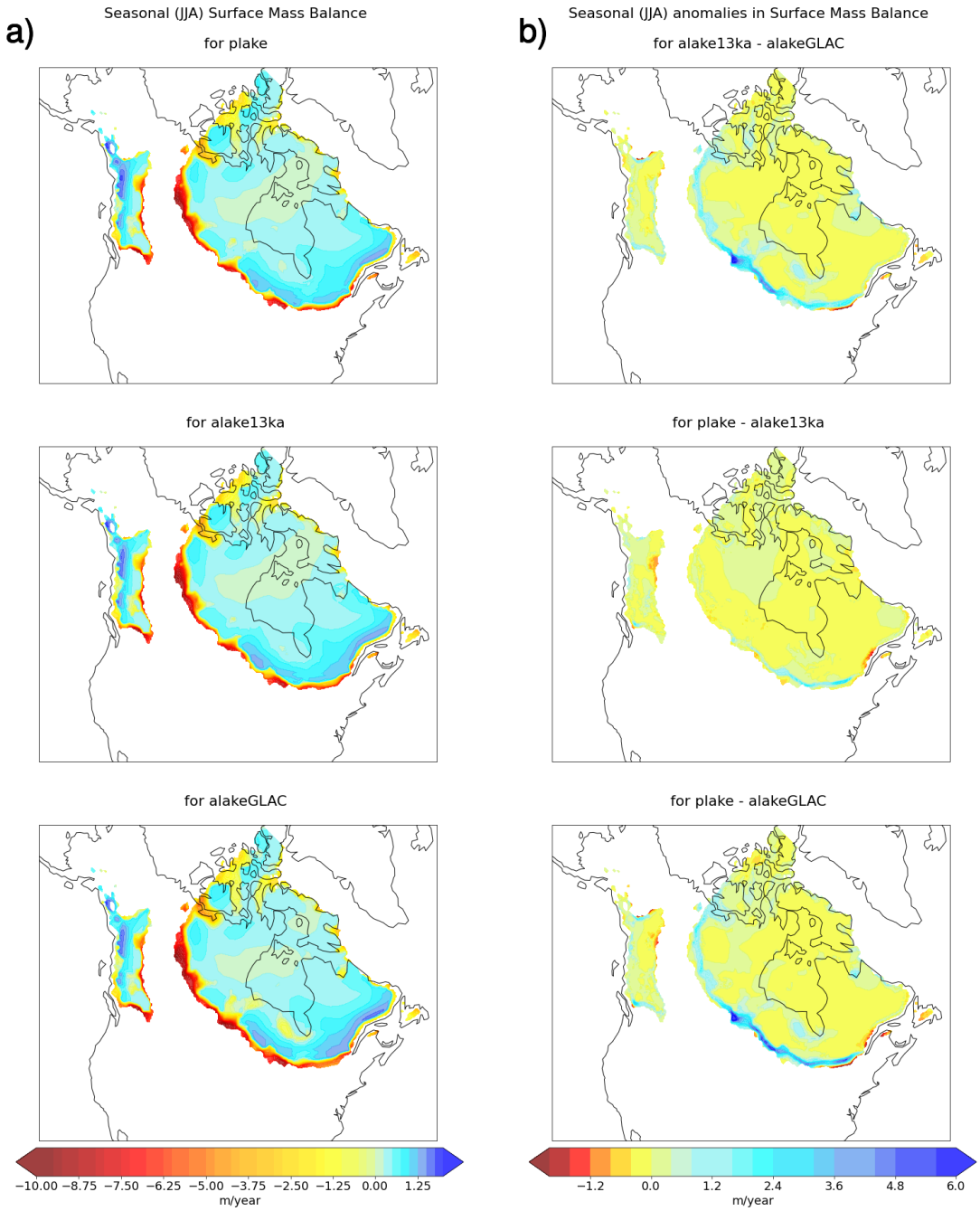

Figure A.6: Surface mass balance for the Laurentide ice sheet showing a) seasonal mean (JJA) and b) seasonal anomalies for JJA.

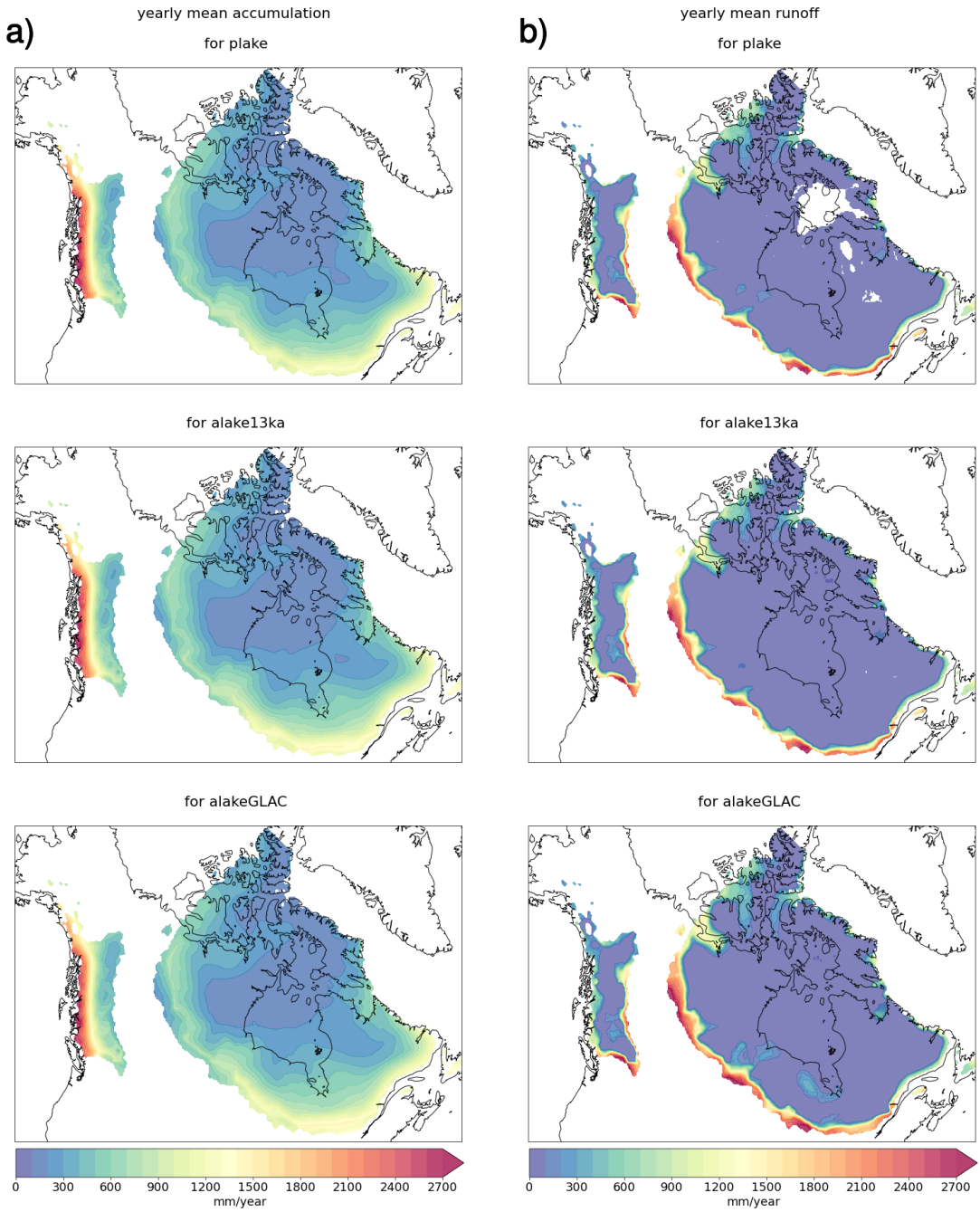

Figure A.7: Yearly mean accumulation and runoff for the Laurentide ice sheet showing a) accumulation and b) runoff for all three scenarios.

A.4.2 FIS

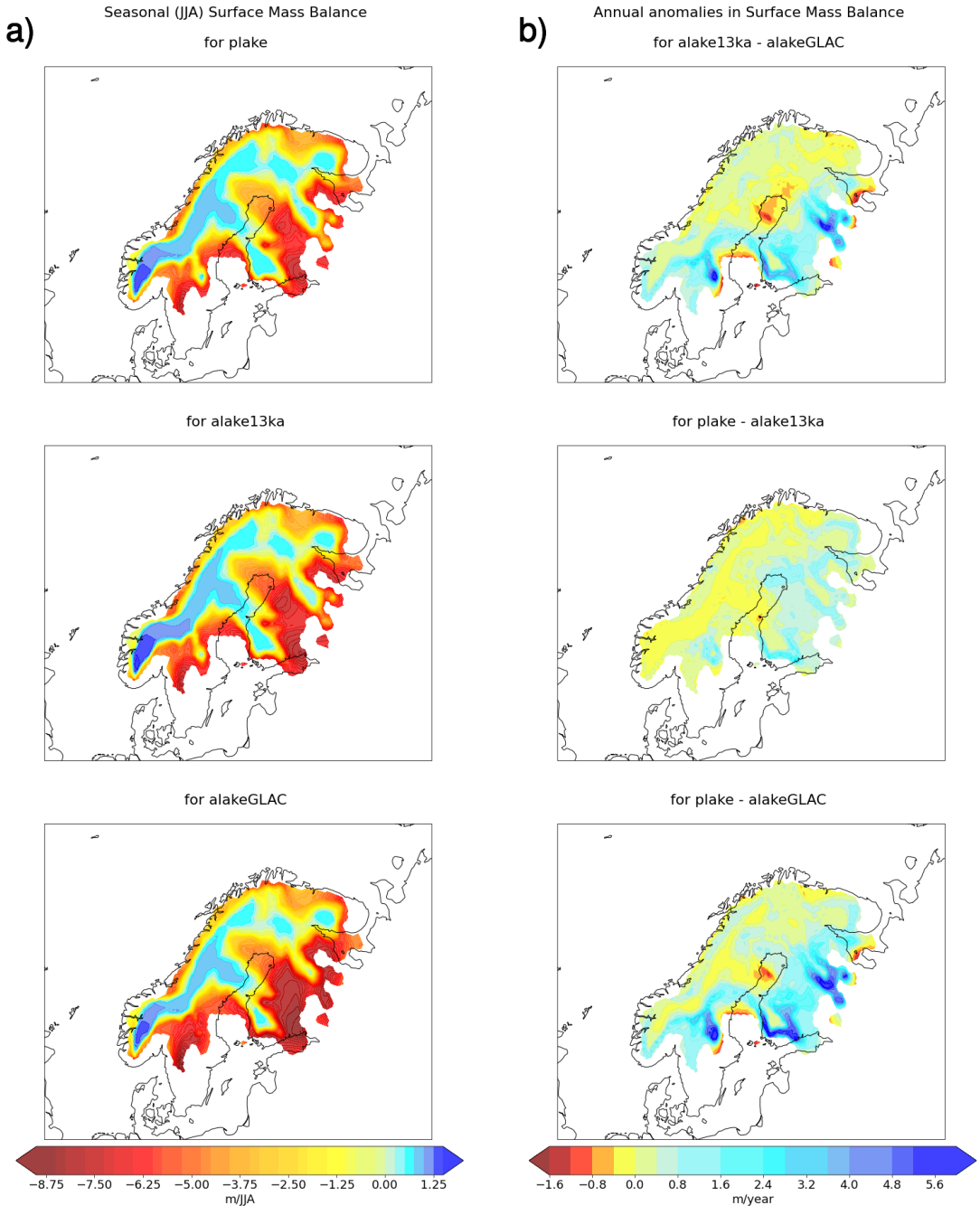

Figure A.8: Surface mass balance for the Fennoscandian ice sheet showing a) seasonal mean (JJA) and b) seasonal anomalies for JJA.

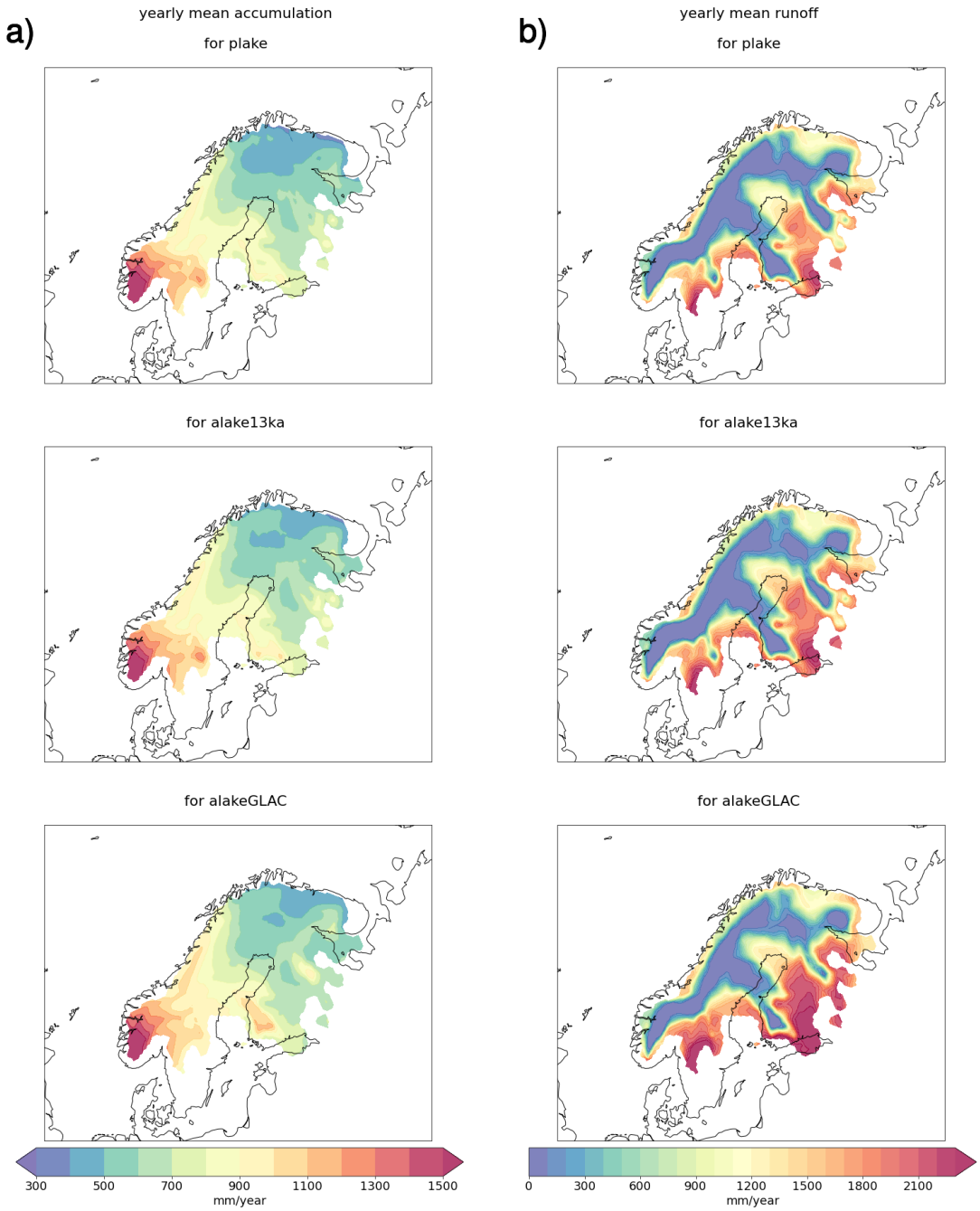

Figure A.9: Yearly mean accumulation and runoff for the Fennoscandian ice sheet showing a) accumulation and b) runoff for all three scenarios.

	alakeGLAC	alake13ka	plake
Accumulation	776.804	767.502	750.971
Runoff	1063.44	895.742	817.742

Table A.12: Mean accumulation and runoff in [mm/year] for FIS.

B Fortran source code

Unfortunately, it was not yet achieved to depict this Fortran90 code correctly in LateX. Nevertheless, this is the novel `temp_plake` subroutine, which only works on the `plake` branch with *plake* being defined throughout ECHAM6's source code.

```
SUBROUTINE s_lake(           &

[...]

  IF (lplake) THEN
          CALL temp_plake(kdim      , palake         &
                        , ptsw      , pplake         &
                        , pseaice   , psiced         &
                        , pahflw    , pahfsw         &
                        , ptrflw    , psoflw         &
                        , ptsi      , psni           &
                        , pcvsi     , pahfli         &
                        , pqres     , pfluxres)
  ELSE

[...]

END SUBROUTINE s_lake

SUBROUTINE temp_plake(   &
       kdim      , palake &
     , ptsw      , pplake &
     , pseaice   , psiced &
     , pahflw    , pahfsw &
     , ptrflw    , psoflw &
```

```
       , ptsi      , psni    &
       , pcvsi     , pahfli  &
       , pqres     , pfluxres)

    USE mo_physical_constants, ONLY: rhoilf, hcapmix, dmix,
&
                                     tmelt, tfreez, hcaprilf,
&
                                     dice, alice, snicecond,
&
                                     rilfhcap


    USE mo_control,         ONLY: lcolumn
    USE mo_time_control,    ONLY: delta_time


    INTEGER,        INTENT(in)    :: kdim
    REAL(wp),       INTENT(in)    :: palake(kdim)
    REAL(wp),       INTENT(inout):: ptsw(kdim)
    REAL(wp),       INTENT(in)    :: pplake(kdim)
    REAL(wp),       INTENT(inout):: pseaice(kdim), psiced(kdim)
    REAL(wp),       INTENT(in)    :: pahflw(kdim), pahfsw(kdim)
    REAL(wp),       INTENT(in)    :: ptrflw(kdim), psoflw(kdim)
    REAL(wp),       INTENT(inout):: pfluxres(kdim)
    REAL(wp),       INTENT(inout):: ptsi(kdim)
    REAL(wp),       INTENT(in)    :: psni(kdim)
    REAL(wp),       INTENT(in)    :: pcvsi(kdim)
    REAL(wp),       INTENT(in)    :: pahfli(kdim)
    REAL(wp),       INTENT(in)    :: pqres(kdim)
```

```
  REAL(wp)     :: zfluxw(kdim), zts(kdim), zfres(kdim), zconhflx(kdim)
  REAL(wp)     :: zdtime, zhcapdt, zdthcap, zdtrilf, zrilfdt
  REAL(wp)     :: zsubice(kdim), zhi(kdim)
  REAL(wp)     :: tplake(kdim) !! Proglacial lake surface temperature

! New constant for proglacial lake surface temperature calculation
  REAL(wp),       PARAMETER     :: tpmax = 277.15_wp    !! [K]
                                  !! maximum temperature proglacial lake
! Constants
  zdtime              = delta_time
  zdtrilf             = zdtime/rhoilf
  zrilfdt             = rhoilf/zdtime
  zdthcap             = zdtime/hcapmix
  zhcapdt             = hcapmix/zdtime
  IF(lcolumn .AND. nfor_ts(1) == 0) THEN  ! Use mixed layer depth from
     zdthcap = zdthcap*dmix/mld
     zhcapdt = zhcapdt*mld/dmix
  END IF


  WHERE ((palake(:).GE.0.5_wp .AND. pplake(:).LT.0.5_wp))
     WHERE (pseaice(:) .LT. 0.5_wp)       ! open water; for lakes, pse
        zfluxw(:) = pahflw(:) + pahfsw(:) + ptrflw(:) + psoflw(:)

        ! ----------- Lake Temperature ---------------- !
        zts          = ptsw(:) + zdthcap * (zfluxw(:) + pfluxres(:))
        ptsi(:)      = tmelt                                 ! ice surface
        pfluxres(:)  = 0._wp                                 ! No flux resi
        psiced(:)    = 0._wp                                 ! No ice
```

```
            WHERE (zts(:) .GE. tmelt)                          ! Still no ice
               ptsw(:)  = zts(:)
            ELSEWHERE                                          ! zts is below
               ptsw(:)  = tmelt                                ! water temp i
               zfres(:) = (zts(:) - tmelt) * zhcapdt           ! < 0.
               WHERE (zts(:) .LE. tmelt - tfreez)              ! ice formatio
                  psiced(:)   = hcaprilf * (tmelt - zts(:))
                  pseaice(:)  = 1._wp
               ELSEWHERE
                  pfluxres(:) = zfres(:)
               END WHERE
            END WHERE
         ELSEWHERE (psiced(:) .GE. dice)                       ! dice = min i
                                                               ! 0.05
            ! ----------- Ice thickness (psiced) -----------!
            zconhflx(:)   = alice * (ptsi(:) - tmelt) / (psiced(:) + snice
            zsubice(:)    = (1._wp - pcvsi(:)) * pahfli(:)
            zhi(:)        = psiced(:)-zdtrilf*(zconhflx(:)+pqres(:)+pfluxr
            ptsw(:)       = tmelt
            WHERE (zhi(:) .GE. dice)
               psiced(:)  = zhi(:)
               pseaice(:) = 1._wp
               pfluxres(:)= 0._wp
            ELSEWHERE (zhi(:) .LE. 0._wp)
! complete melting
               ptsw(:)       = tmelt - zhi(:) * rilfhcap
! ptsw > tmelt
               psiced(:)     = 0._wp
               pseaice(:)    = 0._wp
               pfluxres(:)   = 0._wp
```

```
          ELSEWHERE
! incomplete melting
             psiced(:)      = dice
             pseaice(:)     = 1._wp
             pfluxres(:)    = (dice - zhi(:)) * zrilfdt
! > 0
          END WHERE
       END WHERE


    ELSEWHERE (palake(:).GE.0.5_wp .AND. pplake(:).GE.0.5_wp)
       WHERE (pseaice(:) .LT. 0.5_wp)                    ! open water
          zfluxw(:)   = pahflw(:) + pahfsw(:) + ptrflw(:) + psoflw(:)

          !------------ Lake temperature -----------------!
          zts(:)      = ptsw(:) + zdthcap * (zfluxw(:) + pfluxres(:))
! zts is surface temp
          tplake(:)   = zts(:)
! proglacial lake temperature
                                                                    !
          ptsi(:)     = tmelt
! ice surface temp is 0C
          pfluxres(:) = 0._wp
! No flux residuum
          psiced(:)   = 0._wp
! No ice
          WHERE (tplake(:) .GE. tpmax)
! Temp can't be above 4C
             ptsw(:)  = tpmax
```

```
          ELSEWHERE (tplake(:).LT.tpmax .AND. tplake(:).GE.tmelt)
! Temp between 0 and 4C
             ptsw(:)   = tplake(:)
          ELSEWHERE
! check ice formation
             ptsw(:)   = tmelt
             zfres     = (zts(:) - tmelt) * zhcapdt
! zts can be used again for
             WHERE (zts(:) .LE. tmelt - tfreez)
! ice formation
                psiced(:)    = hcaprilf * (tmelt - zts(:))
! >= dice
                pseaice(:)   = 1._wp
             ELSEWHERE
                pfluxres(:)     = zfres(:)
             END WHERE
          END WHERE
       ELSEWHERE (psiced(:) .GE. dice)

          !------------ Ice thickness ----------------------!
          zconhflx(:)        = alice * (ptsi(:) - tmelt) / (psiced(:) + s
          zsubice(:)         = (1._wp - pcvsi(:)) * pahfli(:)
          zhi(:)             = psiced(:)-zdtrilf*(zconhflx(:)+pqres(:)+pf
          ptsw(:)            = tmelt
          WHERE (zhi(:) .GE. dice)
             psiced(:)       = zhi(:)
             pseaice(:)      = 1._wp
             pfluxres(:)     = 0._wp
          ELSEWHERE (zhi(:) .LE. 0._wp)
! complete melting
```

```
            ptsw(:)         = tmelt - zhi(:) * rilfhcap
! ptsw > tmelt
            psiced(:)       = 0._wp
            pseaice(:)      = 0._wp
            pfluxres(:)     = 0._wp
         ELSEWHERE
! incomplete melting
            psiced(:)       = dice
            pseaice(:)      = 1._wp
            pfluxres(:)     = (dice - zhi(:)) * zrilfdt
! > 0
         END WHERE
      END WHERE  ! open water or ice
   END WHERE     ! lakes

  END SUBROUTINE temp_plake
```